EVALUATION OF EROSION AND FRICTION WEAR OF DUCTILE MATERIAL

A Thesis Report Submitted
in partial fulfillment of the requirements for
the award of degree of

MASTER OF ENGINEERING
IN
PRODUCTION AND INDUSTRIAL ENGINEERING

Submitted by

Kapil Chawla
Roll No.: 801082018

Under the Guidance of

Dr. S.K. Mohapatra
Sr. Professor MED & Dean Academic Affair
Thapar University, Patiala

DEPARTMENT OF MECHANICAL ENGINEERING
THAPAR UNIVERSITY
PATIALA-147004, INDIA.

June 2012

DECLARATION

I hereby certify that the work which is being presented in the report entitled, **"EVALUATION OF EROSION AND FRICTION WEAR OF DUCTILE MATERIAL",** in partial fulfillment of the requirements for the award of degree of Master of Engineering in Mechanical Engineering with specialization in **PRODUCTION AND INDUSTRIAL ENGINEERING** submitted in **Mechanical Engineering Department** of Thapar University, Patiala, is an authentic record of my own work carried out under the supervision of **Dr. S.K. Mohapatra** and refers other researcher's works which are duly listed in the reference section.

The matter presented in this thesis has not been submitted for the award of any other degree of this or any other university.

Date: 17/07/12 **(Kapil Chawla)**

Place: Patiala

This is to certify that the above statement made by the candidate is correct and true to the best of my knowledge.

Supervisor:

Dr. S.K. Mohapatra

Sr. Prof. MED and Dean of Academic Affairs ,Thapar University,Patiala

Counter signed by

Dr. Ajay Batish
Professor & head
Mechanical Engineering Department
Thapar University, Patiala

Dr. S.K. Mohapatra
Dean of Academic Affairs
Thapar University,Patiala

ACKNOWLEDGEMENT

This thesis has been an inspiring, very challenging, but always interesting and exciting experience. In first place, I would like to express my sincere gratitude to my guide **Dr. S.K. Mohapatra, Sr. Professor, MED and Dean of Academic Affairs Thapar University, Patiala** for acting as my thesis supervisor and giving valuable guidance, for the patience, encouragement, many fruitful discussions, and never giving up on me.

It is my proud privilege to express regards and sincere thanks to **Dr. Ajay Batish, Professor and Head, Mechanical Engineering Department, Thapar University, Patiala** for giving me the opportunity of being a member of this project for the complete accomplishment of two years M.E. Course. I heartily thanks to Mr. Purshotam Kumar for his help in conducting the test on Spectro Electron Microscopy machine.

Finally, I thanks to entire faculty and staff of Department of Mechanical Engineering, Thapar University, Patiala for their help, Inspiration and moral support, which went a long way in successfully completion of my thesis.

Kapil Chawla

Abstract

Wear is the loss of material from a component due to a mechanical interaction with another object. Wear is one of the most common problem encountered in industries like thermal power plants, hydropower plants, mining industries, food-processing industries etc. in which solid liquid mixture is transported through pumps and pipes and also in the mechanical components which slides over another such as ball bearing, cylinder head and piston of the engine. Erosion wear is due to exposure to moving liquids and gases, which may or may not contain hard particulate. Effect of wear in slurry pumps, pipes, and in mechanical component is predominantly more as compared to corrosion. The service life of equipment of slurry transport system and several mechanical components is reduced by erosion caused by solid-liquid mixture following through the slurry transport system or friction caused by when one element slides over another element.

My present work is to study the wear behavior of ductile materials. Stainless steel 304 and grey cast iron taken for the study of erosion wear of pump and piping system with fly and bottom ash slurry. And same material are taken to calculate friction behavior as they used in steel 304 used in ball bearing and grey cast iron used in making cylinder head .To improve the wear resistance of stainless steel 304 and grey cast iron, chromium oxide powder coatings were done by electroplating coating method. The erosion wear evaluated with varying the parameters like concentration, speed and time using erosion pot tester TR-41. It is observe that both coatings shows better performance than uncoated steel and grey cast iron in all conditions in which erosion wear test was performed. Friction wear was calculated using pin on disc apparatus for both uncoated materials at different parameters such as speed, load, and time. The maximum erosion wear reported by stainless steel 304 as compared to grey cast iron and chromium oxide coating shows better wear resistance. But in friction wear grey cast iron shows better wear resistance as compared to the steel 304. Erosion wear of both coated and uncoated steel increases with increase in concentration, time and speed.

TABLE OF CONTENTS

LIST OF FIGURES

LIST OF TABLES

CHAPTER1

INTRODUCTION

Wear is defined as the removal of material from one or both of two solid surfaces in a solid-state contact. It occurs when solid surfaces are in a sliding, rolling, or impact motion relative to one another. Wear occurs through surface interactions at asperities, and components may need replacement after a relatively small amount of material has been removed or if the surface is unduly roughened.Wear acts as a natural consequence when two surfaces with a relative motion interact with each other. We know that one third of our global energy consumption is consumed wastefully in friction. Wear causes an enormous annual expenditure by industry and consumers. Most of this is replacing or repairing equipment that has worn to the extent that it no performs a useful function.

For many machine components this occurs after a very small percentage of the total volume has been worn away. For some industries, such as agriculture, as many of the components or equipment have failed by wear problem. So, the effective decrease and control of wear of metals are always desired.

Figure 1.1 Friction wear in ball bearing and erosion in slurry transportation pipe lines

Wear is one of the most common problems encountered in industries like thermal power plants, hydropower plants, mining industries, food processing industries etc. in which solid liquid mixture is transported through pumps and pipes. Many types of solids, liquids, and even high-velocity gases can remove material and change the physical dimensions and functionality of a part. Corrosion and erosion are the main causes of wear. Erosion wear is

due to exposure to moving liquids and gases, which may or may not contain hard particulate.Effect of erosion wear in slurry pumps and pipes is predominantly more as compared to the corrosion. So we can say that the removal of material from one or both solid surfaces in a sliding, rolling, or impact motion relative to one another is known as wear. The resistance to motion whenever one solid slide over another solid is known as friction wear.

1.1TYPES OF WEAR:

Wear may be defined as the progressive loss of material from contacting surface in relative motion. Wear includes mainly six types:

- Adhesive
- Abrasive
- Fatigue
- Impact by erosion or percussion
- Corrosive
- Electrical arc induced wear
- Erosion wear
- Friction/sliding wear

1.1.1Adhesive Wear

Adhesive wear occurs when two nominally flat solid bodies are in rubbing contact, whether lubricated or not. Adhesion (or bonding) occurs at the asperity contacts on the interface, and fragments are pulled off one surface to adhere to the other surface. Subsequently, these fragments may come off the surface on which they are formed and either be transferred back to the original surface or form loose wear particles. Severe types of adhesive wear are often called galling, scuffing, scoring, or smearing, although these terms are sometimes used loosely to describe other types of wear. Asperity contacts are sheared by sliding and a small fragment of either surface becomes attached to the other surface. As sliding continues, the fragment constitutes a new asperity that becomes attached once more to the original surface. This transfer element is repeatedly passed from one surface to the other and grows quickly to

a large size, absorbing many of the transfer elements so as to form a flake like particle from materials of both rubbing elements.

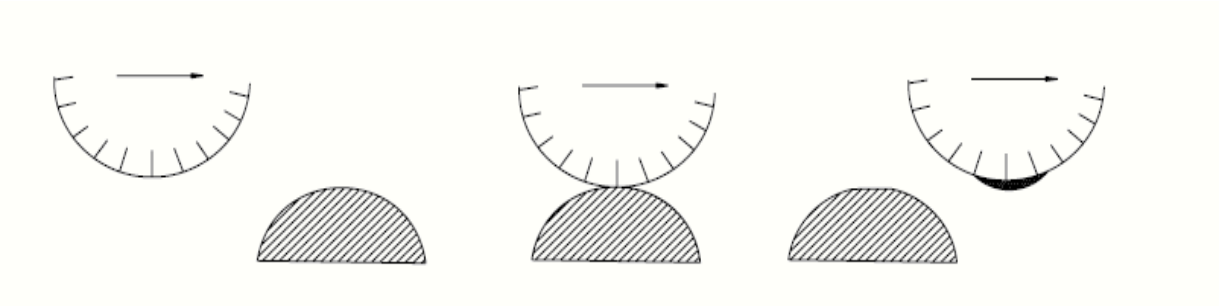

Figure 1.2 Adhesive wear

One of the significant things about adhesive wear is that at the interface, or the point where it touches another metal surface, it must be very hot in order for the micro welding to take place at all. That is what adhesive wear is — minute welding. The heat produced at the contact interface is very high — near the melting point of the two metals touching each other. This heat mostly comes from the stress of contact and not from the temperature of the environment.

1.1.2Abrasive wear

Abrasive wear occurs when a rough, hard surface slides on a softer surface and ploughs a series of grooves in it. The surface can be ploughed (plastically deformed) without removal of material. However, after the surface has been ploughed several times, material removal can occur by a low-cycle fatigue mechanism. Abrasive wear is also sometimes called ploughing, scratching, scoring, gouging, or cutting, depending on the degree of severity. There are two general situations for this type of wear. In the first case the hard surface is the harder of two rubbing surfaces (two-body abrasion), for example, in mechanical operations such as grinding, cutting, and machining. In the second case the hard surface is a third body, generally a small particle of grit or abrasive, caught between the two other surfaces and sufficiently harder that it is able to abrade either one or both of the mating surfaces (three-

body abrasion), for example, in lapping and polishing. In many cases the wear mechanism at the start is adhesive, which generates wear debris that gets trapped at the interface, resulting in a three-body abrasive wear.

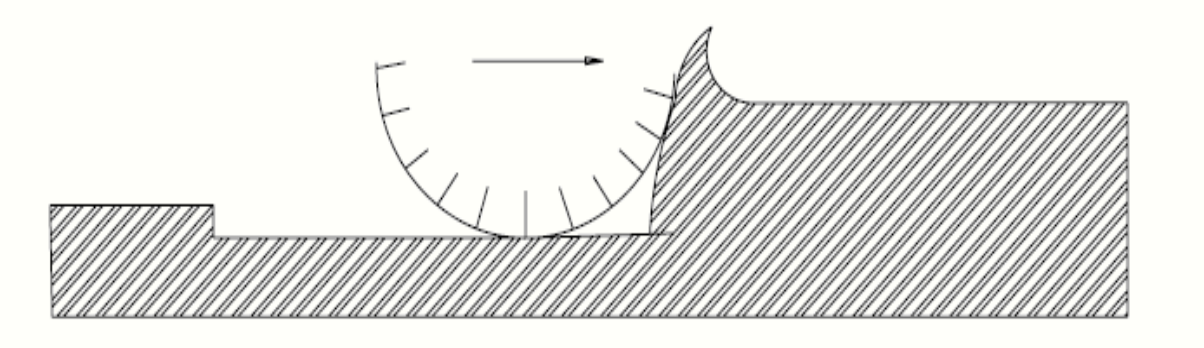

Figure 1.3 Abrasive wear

1.1.3 Fatigue Wear

Subsurface and surface fatigues are observed during repeated rolling and sliding, respectively. For pure rolling condition the maximum shear stress responsible for nucleation of cracks occurs some distance below the surface, and its location moves towards the surface with an application of the friction force at the interface. The repeated loading and unloading cycles to which the materials are exposed may induce the formation of subsurface or surface cracks, which eventually, after a critical number of cycles, will result in the breakup of the surface with the formation of large fragments, leaving large pits in the surface. Prior to this critical point, negligible wear takes place, which is in marked contrast to the wear caused by adhesive or abrasive mechanism, where wear causes a gradual deterioration from the start of running. Therefore, the amount of material removed by fatigue wear is not a useful parameter. Much more relevant is the useful life in terms of the number of revolutions or time before fatigue failure occurs. Time to fatigue failure is dependent on the amplitude of the reversed shear stresses, the interface lubrication conditions, and the fatigue properties of the rolling materials.

1.1.4 Impact Wear

Two broad types of wear phenomena belong in the category of impact wear: erosive and Percussive wear. Erosion can occur by jets and streams of solid particles, liquid droplets, and implosion of bubbles formed in the fluid. Percussion occurs from repetitive solid body impacts. Erosive wear by impingement of solid particles is a form of abrasion that is

generally treated rather differently because the contact stress arises from the kinetic energy of a particle flowing in an air or liquid stream as it encounters a surface. The particle velocity and impact angle combined with the size of the abrasive give a measure of the kinetic energy of the erosive stream. The volume of wear is proportional to the kinetic energy of the impinging particles, that is, to the square of the velocity. Wear rate dependence on the impact angle differs between ductile and brittle materials. When small drops of liquid strike the surface of a solid at high speeds (as low as 300 m/s), very high pressures are experienced, exceeding the yield strength of most materials. Thus, plastic deformation or fracture can result from a single impact, and repeated impact leads to pitting and erosive wear. Cavitations erosion arises when a solid and fluid are in relative motion and bubbles formed in the fluid become unstable and implode against the surface of the solid. Damage by this process is found in such components as ships' propellers and centrifugal pumps. Percussion is a repetitive solid body impact, such as experienced by print hammers in high-speed electromechanical applications and high asperities of the surfaces in a gas bearing (e.g., head-medium interface in magnetic storage systems). In most practical machine applications the impact is associated with sliding; that is, the relative approach of the contacting surfaces has both normal and tangential components known as compound impact.

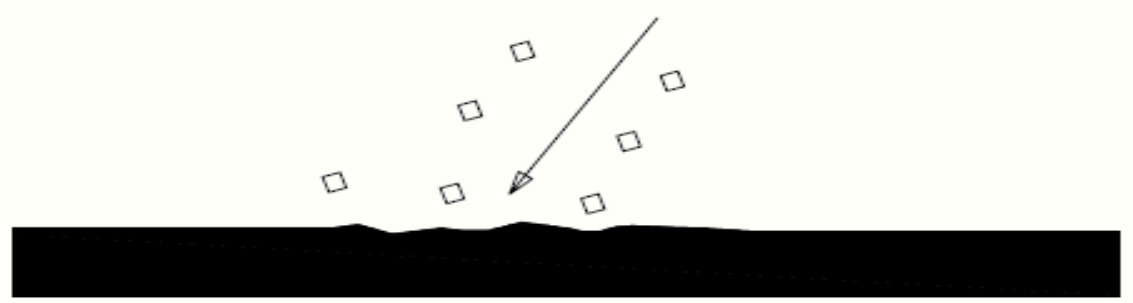

Figure 1.4 Impact wear

1.1.5 Corrosive Wear

Corrosive wear occurs when sliding takes place in a corrosive environment. In the absence of sliding, the products of the corrosion (e.g., oxides) would form a film typically less than a micrometer thick on the surfaces, which would tend to slow down or even arrest the corrosion, but the sliding action wears the film away, so that the corrosive attack can continue. Thus, corrosive wear requires both corrosion and rubbing. Machineries operating in

an industrial environment or near the coast generally corrode more rapidly than those operating in a clean environment. Corrosion can occur because of chemical or electrochemical interaction of the interface with the environment. Chemical corrosion occurs in a highly corrosive environment and in high temperature and high humidity environments. Electrochemical corrosion is a chemical reaction accompanied by the passage of an electric current, and for this to occur as potential difference must exist between two regions.

1.1.6 Electric arc induced Wear

When a high potential is present over a thin air film in a sliding process, a dielectric breakdown results that leads to arcing. During arcing, a relatively high-power density (on the order of 1 kW/mm^2) occurs over a very short period of time (on the order of 100 /s). The heat affected zone is usually very shallow (on the order of 50/m). Heating is caused by the Joule effect due to the high power density and by ion bombardment from the plasma above the surface. This heating results in considerable melting, corrosion, hardness changes, other phase changes, and even the direct ablation of material. Arcing causes large craters, and any sliding or oscillation after an arc either shears or fractures the lips, leading to abrasion, corrosion, surface fatigue, and fretting. Arcing can thus initiate several modes of wear, resulting in catastrophic failures in electrical machinery.

1.1.7 Erosion Wear

Erosion wear is a process of progressive removal of material from a target surface due to repeated impacts of solid particles. The particles suspended in the flow of solid liquid mixture erode the wetted passes limiting the service life of equipment used for slurry transportation system. Erosion wear caused by the kinetic energy transferred to target surface by impinging solid particles. Material loss of target material is higher for higher kinetic energy of impinging particle. So impact velocity largely affects the erosion wear of target material. Also erosion wear depends on the angle with which erodent strikes at target surface (impact angle), slurry concentration, erodent size, erodent shape etc. the extent of erosion wear changes material to material of target surface.

Erosion wear can be classified into three categories: solid particle erosion, liquid impact erosion and cavitations erosion. Solid particle erosion is the loss of material volume from target material due to continues impingement of solid particles present in the flowing fluid. The continues striking of liquid jet on material surface cause liquid impact erosion.

1.1.8 Friction / Sliding wear

The resistance to motion whenever one solid slide over another solid is known as friction wear. All engineering surfaces are rough on a micro scale. When two nominally flat surfaces are placed in contact under load, the contact takes place at the tips of the asperities and the load is supported by the deformation of contacting asperities, and the discrete contact spots (junctions) are formed. When these two surfaces move relative to each other, a lateral force is required to overcome adhesion. This force is referred to as adhesion friction .The adhesion strength depends upon the mechanical properties and the physical and chemical interaction of the contacting bodies. The adhesion strength is reduced by reducing surface interactions at the interface. For example, presence of contaminants or deliberately applied fluid film (e.g., air, water, or lubricant) would reduce the adhesion strength. Sliding between clean solid surfaces is generally characterized by a high coefficient of friction and severe wear due to the specific properties of the surfaces, such as low hardness, high surface energy, reactivity, and mutual solubility. Clean surfaces readily adsorb traces of foreign substances, such as organic compounds, from the environment. The newly formed surfaces generally have a much lower coefficient of friction and wear than the clean surfaces. The presence of a layer of foreign material at an interface cannot be guaranteed during a sliding process; therefore, lubricants are deliberately applied to produce low friction and wear. For example, a bearing operative at high loads low speeds and vice versa this leads to wear of the component that means sliding wear is taking place between two components.

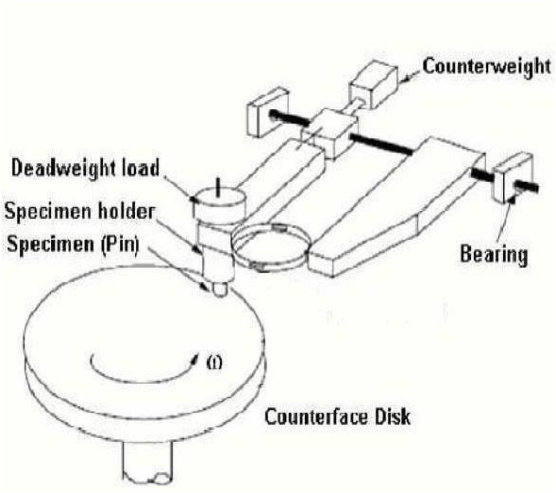

Figure 1.5 General view of sliding wear

1.2 DUCTILE MATERIALS

The property of a material that allows it to be bent, drawn out (as a wire), or otherwise deformed without breaking is known as ductility. Materials that offer such property are known as ductile materials. So we can define ductile materials "Materials that are malleable and will absorb impact loads without breaking."

.

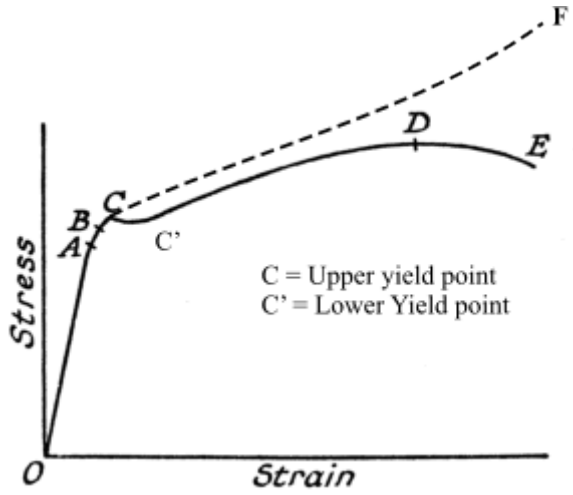

Figure 1.6 Stress – strain diagram for a ductile material

The stress strain relationship is a straight line between 0 and A. This region is called the Elastic region. Within this region if the load is removed the specimen would return to its original length. The slope of the curve in this region (stress/strain) is identified as Young's Modulus (E). The design of machines is based on component materials operating within this region. The region from A to the breaking point E /F the region is called the plastic region. The point A is called the Elastic/Proportional limit. Between A and B some plastic yielding takes place. Removal of the stress results in significant recovery of the initial length. At point C there is a definite extension with no increase in load. This is called the yield point and is primarily exhibited in ductile materials such as mild steel. The stress reduces at C and there are two yield stress values used to identify the yield value i.e. the upper yield point and the lower yield point. For materials exhibiting no clear yield point an value proof stress is identified as the point of onset of yielding e.g. a 0,2% proof stress is the point at with the material has yielded (non-recoverable extension) by 0,2%. Between C and D the specimen

continues to extend as the load increases the extension being primarily not recoverable the material is deforming plastically. Removing the load will result in recovery of only the strain between 0 and A. The material is actually becoming a little stronger in this region as a result of cold working .At point D the specimen will exhibit a significant reduction is section diameter within the calibration length. The specimen will start to neck. The reference ultimate /maximum tensile stress of a material is calculated by dividing the load by the original section area. In the region from C to D the diameter of the specimen is reducing as the linear strain increases this is a result of the Poisson effect. From D to E the cross section will reduce significantly as the specimen approaches failure. The true stress in the region from C to Fracture is shown as the dotted line and, is different to that recorded on the stress-strain curve. The true stress is shown on the diagram as the curve from C to F. From D to E the specimen will start to lengthen with no increase in load and the overall strain at point E is important as it identifies the ductility of the material and is listed in the material standards as the % elongation at rupture. The following table has some applications of ductile materials.

Table 1.1 Applications of ductile materials:

Steel 304	Waste water transportation, chimneys of thermal power plants, Ball bearings, springs, threaded Fasteners, Food processing plants (storage and hauling tanks).
Grey cast iron	Slurry transportation pipes, Cylinder heads, gear box, Cylinder blocks, Pump casing.
Copper	Natural gas piping system, plumbing, fire sprinklers ,
Brass	Architectural fascias, grillwork, jewellery, ornamental trim, vitreous enamel base, badges, door handles, escutcheons, marine hardware, munitions, primer caps, rotating bands, metallic bellows, pen, pencil and lipstick tubes etc.
Aluminum	Aircrafts, engine castings, wheels, radiators

	and used as foil for food wrapping.

1.3 PARAMETERS AFFECTING THE LIFE OF MECHANICAL COMOPNENTS:

The prominent parameters affecting the life of mechanical components are as under:

1.3.1 Impact angle

Impact angle is defined as the angle between the target surface and the direction striking velocity of the solid particle. The variation of erosion wear with the impact angle depends on the characteristics of the target surface material namely brittle or ductile type.

1.3.2 Velocity of solid particles

Velocity of solid particle strongly affects the erosion wear. As particle velocity increases there is significant increase in erosion rate. The erosion rate is generally related to the particle velocity using power law relationship in which the power index for velocity varies in the range of 2-4.

1.3.3 Hardness

Hardness is the characteristic of a solid material expressing its resistance to permanent deformation. Surface hardness as well as hardness of solid particles has profound effect on the erosion wear mechanism. Hardness ratio has been defined as the ratio of hardness of target material to the hardness of solid particles.

1.3.4 Particle shape and size

Particle size and shape is also one of the prominent parameter, which affect erosion wear. Many investigators have considered solid particle size important to erosion. The erosion wear increases with increase in particle size according to power law relationship. The effect of particle shape on the erosion is not very well established due to difficulties in defining the different shape features. Generally roundness factor is taken into consideration. If roundness factor is one then the particles are perfectly spheres and a lower values show the particle angularity.

1.3.5 Solid concentration

Concentration is amount of solid particles by weight or by volume in the fluid. As concentration of particle increases more particles strike the surface of impeller which increase the erosion rate, the concentration of slurries can vary from 2% to 50% depending upon the type of slurry. However, at very high concentrations particle interaction increases and this decreases the striking velocity of particle on the surface.

1.3.6 Load

Friction wear largely affected by load, more is the load more is the wear rate. As the load increase both thermal conductivity and friction coefficient increases this leads to mild severe wear during sliding.

1.3.7 Time

More is the sliding time more will be the wear rate. Wear rate increases linearly with the time. As the time increases more will be the sliding time between the pin and disc it will generate more heat due to which more fracture of the material will take place.

1.3.8 Sliding distance

Sliding distance is directly proportional to wear rate. After 5000m sliding distance wear rate becomes constant means seizure temperature and pressure will generate.

Sliding distance = sliding speed X Time

$$\frac{\pi DN}{60} \times t$$

Where D= Diameter of wheel track (60mm)

N= R.P.M

t= Time duration in seconds

π = 3.14

1.4 EROSION WEAR TESTING APPARATUS

The erosion wear can be determined by different test rigs. Following are the some test rigs that are commonly used to determine the erosion wear.

- Miller test apparatus

- Slurry pot tester
- Jet impingement tester (JIT)
- Falling jet apparatus
- Jet in slit apparatus
- Centrifugal erosion tester
- Coriolis erosion tester

1.4.1 Slurry pot tester

This test rig is small in size, simple in design, easy to operate, economical and can be used to generate experimental data at an accelerated rate. In this test rig, the wear specimens are rotated in a cylindrical pot containing solid-liquid mixture. The specimen is hold in a fixture connected to a rotating steel shaft. The propeller having two blades at the end connected to a rotating shaft keeps the solid particle suspended in a liquid. The relative motion between the wear specimen and the slurry causes erosion wear. Effect of various operating parameters like concentration, velocity and impact angle can be easily calculated.

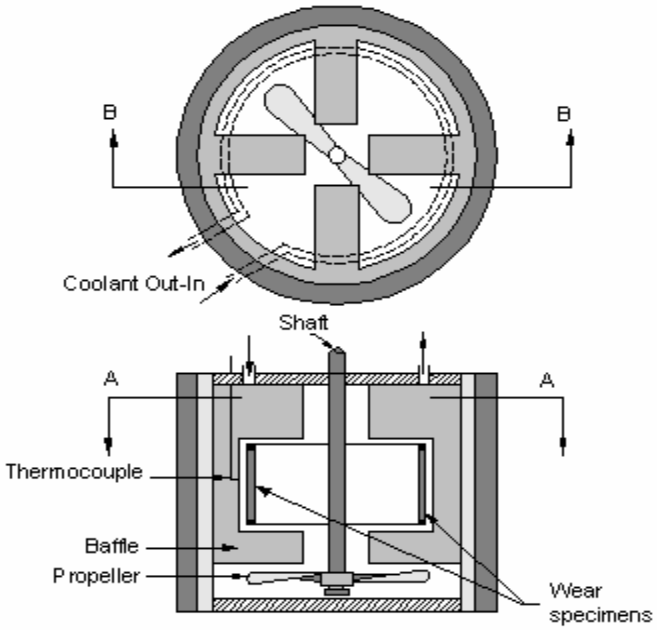

Figure 1.7 Slurry pot tester

1.4.2 Jet impingement tester (JIT)

In this type of test rig, a flat specimen can be oriented at different impact angles in the range of 0 to 90 degree. It comprises of a pump and an ejector to issue a jet through a nozzle. Jet

impingement tester simulates the wear for direct impact of solid particles in equipment such as pumps, bends, tee junctions, elbows, contractions etc. This type of tester provides very good control over various parameters of erosion wear.

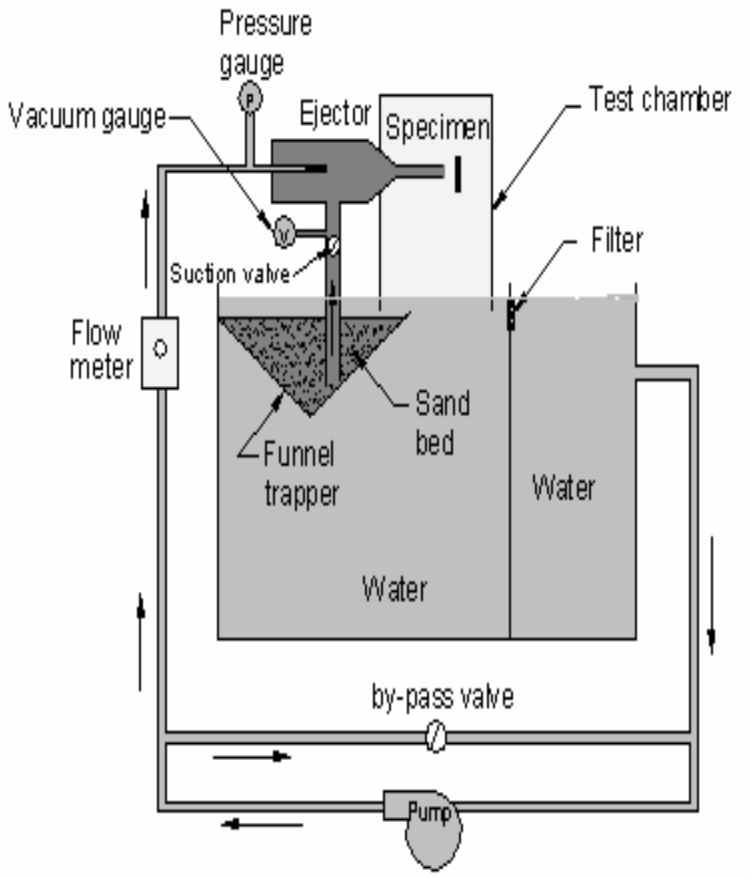

Figure 1.8 Jet Impingement Tester (JIT)

1.4.3 Coriolis erosion tester

In this test rig, the wear specimens are to be fixed on the channels. The slurry is accelerated centrifugally from a rotating bowl through two small radial channels located at 180º apart. The Coriolis force increases the slurry interaction with the back wall of the wear specimens.

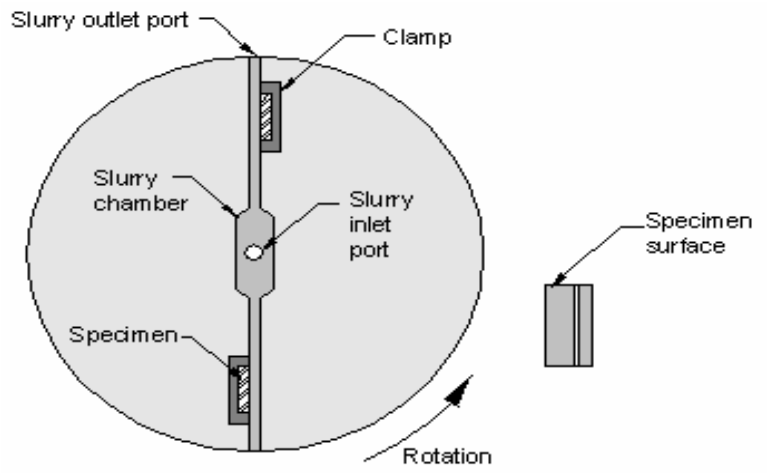

Figure 1.9 Coriolis erosion tester

1.5 SYMPOTON OF WEAR

A summary of the appearance and symptoms of different wear mechanism is indicated in the table 1.1 and same is the systematic approach to diagnose the wear mechanisms.

Table 1.2 Symptoms and appearance of different types of wears.

Type of wear	**Symptoms**	**Appearance of the worn out surface**
Abrasive	Presence of clean furrows cut out by abrasive particles	Grooves
Adhesive	Metal transfer is the prime symptom	Seizure, catering rough and turn out surfaces.
Erosion	Presence of abrasive in fast moving fluid and short abrasion furrows	Waves and Troughs
Corrosion	Presence of metal corrosion products	Rough pits and depression
Fatigue	Presence of subsurface and cracks accompanied by picks and spalls	Sharp and angular edges

1.6 MOTIVATION FOR THESIS WORK

As erosion of slurry transportation system, slurry pumps and friction wear of many automobile components such as ball bearing, cylinder head is a very serious problem. This wear rate reduces the life of mechanical components and their efficiency. So engineering interest is to determine the service life of equipment/ components subjected to erosion wear and how we can prevent erosion wear by coating application.

CHAPTER 2

LITERATURE REVIEW

2.1 LITERATURE REVIEW OF EROSION WEAR

Panayotova et al. [2000] studied the effect of deposition of Fe- C alloy on structural steel and cast iron by electroplating technique for the repair of worn machine parts. They have prepared steel sheets of dimensions 50X 30X 3mm and grey cast iron in cylindrical of dimensions internal diameter of 50 mm, height of 30 mm. They prepared baths of reagent-grade chemical and distilled water contained 1.15 M of $FeSO_4$ and $2X10^{-2}$M of organic acid. Before electroplated the specimen must be cleaned properly by etching, the outside surface of the cylindrical component was covered with metha methyl crylate based clay which remain stable while electroplating on the internal dia. of the cylindrical component. Anodes were inserted in the middle of the hollow cylindrical component and two plat anode strips were placed around the steel specimen for 5 min before imposing current. After imposing current for the time of 12 h Fe-C of thickness 520-590 µm was obtained. An increase of current efficiency helps in increasing pH value was observed for baths containing asparaginic acid as compared to the succinic acid. They found that these deposits exhibit good mechanical and corrosion properties for the both acids addition for both specimens.

Tian et al.[2005] evaluated erosion wear of soft ductile aluminium (A380 grade) alloys and hard brittle high chromium white iron using coriolis wear test with slurries of different solids and concentration. The dimension of test specimen was 63.5mm×19.1mm×6.4mm. The test slurries were made of commercial grades of silica sand of semi-rounded to semi-angular shapes and mix with clean water. Several particle sizes were used in the tests with mean diameter ranging from 22µm to 1428µm. Coriolis wear tests were carried out at ambient temperature with a bowl speed of 975 rpm. They observed that higher the solid volume fraction the more frequently and strongly the solids contact and react with the target material, and more wear results. It was conclude that when slurry concentration increase from 1.52 vol.% solids to 12.12vol.%, the wear rate increased 187 – 204% on high-Cr (sand cast) material and by 298 – 468% on the aluminium alloy. It was observed that larger solid

particles resulted in higher mass loss in all test materials. At slurry with 12.12 vol. % solids concentration and 15 gal/min flow rate, the wear rate increased about 20–28 times for the aluminium alloys and 42–45 times for the white iron materials as the mean diameter particle size increased from 22 μm to over 1400 μm. At 22μm (D50), the wear rate difference was only 4.3% between high-Cr (sand cast) and G75 white irons, and − 6.7% between aluminium alloys 380 and 6061T-6511. The wear rate difference grew to 10.3% between the white irons and to 29.9% between the aluminium alloys at the particle size of 1428 μm (D50). It was also found that the wear rate ratio between the aluminium alloy 380 and white iron G75 was about 40 with very fine particles (22 μm D50). The wear ratio value peaked at around 150 with particle size between 100–200 μm and it decreased to about 27 with very coarse particles around 1400 μm. During the test it was found that a higher slurry flow rate generates more erosion wear but the percentage increase of wear rate was not as high as the percentage increase in flow rate. They observed that the much harder and stronger high-Cr white irons showed a tremendous advantage in wear resistance (up to 150 times) over the test aluminium alloys under the test conditions. Because Among the test materials, the extruded aluminium alloy containing limited alloy elements has the highest elongation/ductility.

LI Xiao-yan et al. [2005] determined the corrosion failure of petrochemical pipe elbow. The pipe material he has used was 16 MnR steel of breaking stress 570 Mpa and of shear stress 345 Mpa. They have used EDTA (ethylene diamine tetra acetic acid) and NTA (nitrilo tri acetic acid), as organic chemicals that react with hardness minerals to form soluble chemical complexes so as to avoid the formation of scale on the inner surface of the pipe. The specimen was treated with 2% natal (volume fraction), the line type distributed pearlite was observed, showed the failure at the elbow of the pipe. They have used optical examination and SEM examination to indicate that the grain boundary failure was a major form of the corrosive attack occurred on the inner surface of the pipe elbow. In fact, the grain boundary decohesion and grain dissolution together with the multiple cracks were found on the inner surface of the failed elbow, indicating that the most likely cause of the failure is the grain boundary attack. For calculating how many mass has been lost from the elbow of the pipe it was found that mass fraction of C, O, S, Mn, Fe 7.94%, 19.77%.29%, .96%, 71.04% respectively.

K. Shimizu et al. [2006] evaluated the erosion wear of S50C steel, SK3 and high V–Cr–Ni stainless spheroidal carbides cast iron (SCI-VCrNi). They have used Spherical shaped

alumina ball with average diameter 1mm as erodent materials with a hardness of 9 Mohs the erodent particles were maintained at a temperature of 873 and 1073 k. Specimens of dimensions 50mm×50mm×10mm were used for the erosion test. The standoff distance between the work piece and the nozzle is 50mm. Erosion test duration was 300 s and the amount of erodent was 8 kg/test. The impingement angle was varied from0^0 to 90^0, respectively. They have used high temperature blast type erosion tester for conducting erosion test. Hot air was utilized as the carrier gas for the particles and the particle feed rate was approximately 26 g/s. They found that S50C and SK3were most eroded among them, and the erosion rates of SCI-VCrNi were the lowest at an impact angle of $90^{0.}$ It means that erosion wear resistance SCI-VCrNi is excellent as compared to other steels. They found that erosion rate of SS400 was 41.148×10^{-3} cm^3/kg, at 873K but when at the temperature to 1073K with no change of other testing conditions, the erosion rate reached to 61.854×10^{-3} cm/kg. This showed that erosion rate of SS400 increased 1.5 times by increasing the temperature of erodent particles from 873 to 1073K.

Manisekaran et al. [2006] studied the effect of particle size and impingement on 16Cr-5Ni stainless steels (as they are generally used for hydro turbines and water pumps) of dimension of 50×50 mm^2 by the slurry erosion test rig and the surface modifications were done by two methods namely laser hardening and pulsed-plasma nitriding. The slurry test rig having a conical of 10 L capacity used for mixing the slurry and water in the required proportion. They have used silica sand as a erodent material of particle size ranges (less than 150 and 150-300µm). They have followed following test conditions: the test duration was 2 h, impact angle used was 30, 45, and 60 and90° and the flow velocity was 12m/s. They observed that the amount of erosion with erodent size range 150-300µm was two times more than the amount of erosion with erodent size range less than 150 µm and pulsed plasma hardened steels showed more hardness than laser hardened steels at all impact angles. The removal was more at 60^0 as compared to 90^0 impingement. It was found that the surface hardness obtained with pulsed-plasma nitride steels was around 1500 HV. It was reported that the plasma nitriding of 13Cr-4Ni steels with continuous technique increased the hardness to merely 700 HV .They also observed that the material removal was due to extensive micro cutting as compared to repetitive plastic deformation.

Mann et al. [2006] determined erosion behaviour of WC10Co4Cr, Armcore 'M', Satellite 6 treated with 12 HVOF coatings and TiAlN PVD coatings. They have used mineral sand as

an erodent material of size 25000ppm. They maintained constant impact angle of 60° and velocity of 20m/s constant .the test was carried out using a water jet impingement erosion apparatus having 10litre water reservoir. A rectangular sample of size 50mm×50mm×6mm was kept in Front of a sand-laden water jet at an angle of 60^0. Sand laden water was circulated in a controlled manner by a variable speed pump controlled by a frequency inverter. They have maintained pressure in the range of 1.2–2 kg/$cm^2$and jet velocities in the range of 15–20 m/s. The slurry passed through a tungsten carbide 6mm diameter nozzle, providing a jet velocity of 18.2 m/s. They calculated the mass loss of the materials with or without coating was: WC10Co4Cr HVOF coated steel 0.4235, TiAlN PVD coated steel 0.846, Armcore 'M' HVOF coated steel 2.42, Stellite 6 HVOF coated steel 10.30, Stellite 12 HVOF coated steel 13.55, Satellite 6 weld deposited steel 14.90.They concluded that WC10Co4Cr HVOF coatings show best performance against slurry erosion, also found that WC10Co4Cr HVOF coating corroded significantly. WC10Co4Cr HVOF coatings have very good erosion resistance but not corrosion resistance.

Yıldızlı et al. [2006] determined the erosion mechanism of nodular and fine grey cast iron at 30, 60, 90^0impact angles with the help of erosion tester. They have used round specimen of diameter 15mm and angular steel as a erodent particle. The standoff distance between the work piece and erodent was 6mm and erodent particles were following at a velocity of 30m/sec at a exposure time of 720s. They used angular steel in the weight of 240, 480, 720, 58.2, 116.4, 174.6kg. As the weight of the erodent particle increases it leads to the plastic deformation of the fine grey cast iron as compared to the nodular grey cast iron. Because fine has week bonding strength this leads to the crack nucleation phenomena. They found that wear mechanism dependence of the mass loss of GCI has fairly affected by variation in the impingement angle. At oblique angles, severe surface damage by the erodent cluster occurs on the surface, associated with the changing of wear mechanism. The reason for this damage is that the material removing process was performed with the ploughing. The mechanism seen at 30^0has a more predominant ploughing effect than that in at an impact of 60^0. Therefore, the removed material from the surface, with respect to the effect of the mechanism, was more at 30^0.They found that weight loss by GCI after erosion wear was found out be 0.6mg/kg and of NCI was 0.30-0.50mg/kg.

Harpreet et al.[2007] evaluated the wear and oxidation behaviour of carbon steel of composition 0.4 C, 0.3 Mn, 0.1 Si, 0.04 P, 0.04 S and remaining Fe was used as substrate

steel coated with shrouded plasma sprayed fly ash . Fly ash with composition SiO_2 (60.27%), Al_20_3 (25.46%), Fe_2O_3 (6.02%), CaO (3.68%), MgO (1.06%) and SO_3 (0.12%) sprayed on these steel. These steels subjected to eroded and material loss was calculated after an interval of 5, 5, 10, 20, 40 and 60 min. They have performed the cyclic oxidation in air and molten salt (Na2SO4–60% V_2O_5) environment at 900^0C in furnace. It was concluded that Wear rate observed to be more in the initial stages of the cycles, which gradually deceases to steady state in the latter stages of the study for both coated and bared steels. They concluded that the wear rate for fly ash coated steel was more than that of similar type of uncoated steel, which might be ascribed to the coarse grain size of fly ash particles. They also concluded that the fly ash coating was found to be very effective in increasing the oxidation and salt corrosion resistance of the given carbon steel at 900^oC.

Gandhi et al .[2008] evaluated the erosion wear of ductile material under normal impact conditions (solid concentration of 10 % wt, velocity 3m/s and particle size of 550µm). They have conducted test was on seven different materials namely aluminium alloy (AA6063), copper, brass, mild steel, AISI 304L stainless steel, AISI 316L stainless steel, and turbine blade steel. Solid particles of slurry were mixture of quartz, alumina and silicon carbide. They used slurry pot tester for calculating the erosion wear in this specimen can be varied from $0\text{-}90^{0.}$ But they fixed the angle for all these materials at the 90^0. They have used pot tester of capacity 7 litre whose shafts were rotating by 0.75 KW dc motor through V- Belt pulleys. They evaluated that erosion of target material is dependent on ratio of hardness of solid particles to hardness of target material and independent of hardness of target material and hardness of slurry particles. They also found that AA6063, copper, brass and mild steel, depict mass loss rate with quartz particles as 1.18, 1.05, 1.18 and 1.20 mg/h, respectively. The mass loss rate for AISI 304L, AISI 316L and turbine blade steel are lower than that for these four target materials. The minimum and maximum mass loss rate is depicted by AISI 304L and mild steel, respectively, for all the three erodent. They formulated an empirical formula for erosion rate at normal condition: $E_{w= KV}{}^{\beta}d^{\gamma}C^{\phi}f(\alpha)$ Where *Ew* is the erosion rat *V* the velocity, *d* the particle size ,*C* the solid concentration ,*K*, β, γ and ϕ are constants.

Noui-Mehidi et al. [2008] determined the effect of paint layers on stainless steel specimen in a slurry-mixing tank in which 10 painted samples mounted on a shaft were rotated at constant speed for a certain interval of time. They have used different type of paints such as

Gloss Enamel paint, Epoxy Enamel, Standocryl 527 two-pack paint etc were applied on steel specimen by spray guns operated with compressed air slurry was a mixture of tap water and alumina particles with a concentration of 15% (v/v). They have used test rig consisting of a 390mmdiameter tank with a 1mheight. Four diametrically opposed vertical baffles of 32mm width were placed in the tank. Ten arms of 140mm length each were mounted on the shaft. Were rotated by a 1.1kW motor at the speed of 250 rpm. The angle of impact was varied from 0^0 to 90^oat an increment of 10^0. The flow rate maintained was 18.1l/min and paint thickness was 0.7mm on all the work pieces, They found that in the slurry medium, most soft paints, such as "Enamel" type have similar erosion maps to ductile materials with a maximum wear rate at around 30^0. Metallic paints and styrene type paints have shown slightly higher erosion at an angle of 40^0.

Mishra et al. [2009] determined the parameters affecting the erosion wear using jet erosion tester on fly ash-quartz coating using Taguchii approach. They have deposited fly ash – quartz coating on the metal substrate using plasma spray technique. They have used dry silica sand of particle size 150, 260 and 360 μm as erodent materials. The eroded coating at the impact angle of 30, 60, 90^0 .the coating was made at the power of 18 KW. They have maintained a pressure of 6MPa and moving velocity of 58m/s. eroded time for different impact angles was 20min. they found that at the impact angle of 30^o chipping of layers take place and more cavities were formed, at the impact angle of 90^0 sharp grooves were formed known as extruded lips or indentations due to the perpendicular impingement of erodent particles on the surface. By varying different parameters they evaluated that impact angle is the most significant factor influencing the erosion wear of fly ash-quartz coating. They also evaluated that maximum erosion takes place at impact angle of 90°.

Dube et al. [2009] evaluated the effect of slurry turbulence on wear with a counter rotating double disc erosion tester developed by DUCOM. In this experiment they use two discs (dia 160mm and thickness 2mm) of aluminium and stainless steel (SS-304) placed co-axially and rotates at equal rate in opposite direction with the help of two induction motors. The discs are fixed at the end of each of motor shaft were rotated at the speed of 1500rpm for the duration of 1 hour. The distance between discs was varied to generate the turbulence in slurry chamber. They have used silica and alumina as an erodent for making slurry of concentration varied from 14% to 55%. During test they founded that the wear on stainless steel disc (SS-304) is less compared to aluminium in all the three parameters; time (0.5-3h), angular speed

(1000-3000rpm) and concentration (14- 55%). This is because of high yield strength of the stainless steel than aluminium.. Alumina slurry shows a slight decrease in wear of stainless steel between 0.25 to 0.35 concentrations. At the concentration of 40% and angular speed of 1000-3000rpm they observed that increased in the angular rate increases the turbulence and hence increase in the weight loss of discs. The effect of wear is higher in alumina slurry over the range of angular speed. They found that wear increase with increase in particle concentration (wt. fraction) the result shows that wear increases linearly with particle concentration in all cases except wear on stainless steel by alumina. The alumina slurry causes the higher volume loss then silica slurry identical testes conditions because alumina is harder than silica particles.

Keshavamurthy et al. [2011] determined the erosion behaviour of mild steel of dimensions25 mm×25 mm×8 mm and thermally sprayed Inconel-718 both were coated with the APS coating technique. They have conducted test in a slurry erosion tester having six spindles connected to an electronic motor with the maximum speed of 1500 rpm using a belt drive. All the samples were dipped into slurry pot made of stainless steel. Slurry was prepared by mixing 3.5% sodium chloride and silica sand with distilled water at different concentration of 5-15 % by wt. carried out at a speed of (500-1500 rpm). They observed that a reduction of 120% and 200% in mass loss when compared with mild steel at slurry concentrations of 50 and 150 g/l. They also observed that increased sand particle size leads to increased mass loss for both uncoated and Inconel-718 coated mild steel large sized sand particles are more effective and are capable to apply their mass and energy in direct contact to the surface of target material with few interactions whereas smaller sized particles possess lower impact stresses and also tends to deviate near the surface of target material leading to reduced weight loss .increased speed of slurry rotation results in marginal increased mass loss for both uncoated and Inconel-718 coated mild steel because of the localized attacks leads to crack formation. However the developed coatings exhibited a significantly reduced mass loss when compared with mild steel. They also reported that an increase in slurry rotation results in increase mass loss and maximum material loss is encountered at a very high speed of 1500 rpm.

Jha et al. [2011] evaluated the erosion wear of aluminium (grade 1900) of hardness HV 40 with the help of DUCOM made slurry tester. They have used Quartz silica sand as the erodent of concentration 40%bty wt. whose particle size varied from 200 to 300 μm.

Specimens were positioned at angles of 0°, 30°, 45° and 90° with respect to its rotating direction. The rotation per minute (r/min) maintained was 300, 400, 500, 600 and 700. They found that difference in the wear rate of the specimen positioned at 0° and those positioned at higher angles (30°, 45° and 90°) tested at maximum rotation speed. The wear rate of specimen positioned at 0^o was found to be in the range of $(1\text{-}5)\times10^{-12}$ m^3/m, whereas, the wear rate of the other samples was found to be in the range from 20×10^{-12} to 25×10^{-12} m^3/m at higher speed. They also developed a formula to calculate the volume loss

$V= ku^n$ Where where *k* is a constant; *n* is the velocity exponent generally in a range of 2-4.and u is the velocity.

Harsha et al. [2011] investigated various unreinforced thermoplastic polymers (epoxy, PA 6, and PPS, PEEK) using a rubber wheel abrasion test (RWAT) rig. Wear studies have been carried out using angular silica sand granular particles of size ranging between 150 and 250 µm and used as dry and loose abrasives and at a constant velocity (v = 2.4 m/s) of rubber wheel. Before using silica as a erodent it was preheated to remove the moisture content from it. They developed few relations to calculate wear volume (ΔV), wear rate (w_r), and specific wear rate (K_o). $\Delta V = \frac{\Delta m}{\rho}\ mm^3$, $K_0 = \frac{\Delta v}{M_a}\frac{m^3}{g}$

Where Δm is the mass loss, ρ is the density of the material, L the load in Newton and d the sliding distance in meters, M_a is the mass of the abrasive in the grams, Δv is the volume loss in the mm^3. The results showed that abrasive wear rates were strongly influenced by the applied load and type of polymeric material. They have observed that polymeric materials tested PEEK showed lowest wear rate whereas an epoxy, PA 6, and PPS showed highest wear rate PA 6 was having higher ductility among the selected polymers showed poor abrasion resistance as compared to other thermoplastic polymers.

Partap et al. [2011] evaluated erosion and sliding wear behaviour of stainless steel 304 coated with nanostructure alumina coatings (NC) and conventional alumina coatings (CC) coated with plasma sprayed technique. For erosion wear they have used erosion pot tester and for sliding wear they have used pin on disc. They have uses stainless steel in the form of blocks and pins of dimensions of 20 X15 X $5mm^3$ were used for slurry erosion testing and cylindrical pins of 8 mm diameter and 30 mm length were used for sliding wear against the counter surface of EN32 steel disc. For plasma sprayed deposition they have used two coating powders one was CC of size 40µm and NC of 80 µm. In sliding wear they have used

sliding speed of 0.5m/sec at the load of 30 N, 40 N, 50 N, 60 N, 70 N and 80 N for the maximum duration of 80 min. For erosion wear they have used two different concentrations of Al_2O_3 and SiO_2 of 10%, 20% by wt. in water, erosion wear was performed for 10h at the constant speed of 800rpm. They found that at the load of higher end loads of 50 N, 60 N, 70 N, and 80 N there was gradual increase in the difference between the weight loss of NC and CC coatings for the same sliding distance. At 80 N loads, the wear resistance exhibited by the NC is almost 1.5 times that of CC because of presence of finer wear debris between mating parts. In the case of erosion wear they found that at 20 % concentration exhibit faster rate of weight loss compared to 15% concentration by wt. For both the concentrations, CC exhibit more weight loss as compared to NC. The difference in the weight losses of NC and CC was quite significant in 20% concentration as compared to 15%. They found that erosion increases with the increase in abrasive particle concentration. .

N. Krishnamurthy et al. [2012] determined erosion of Al-6061 which was plasma sprayed coated and uncoated with the help of erosion rig. They have used alumina and calcia-stabilized zirconia coatings silica as erodent material of size 150-300 µm, at a velocity of 40 m/s. the standoff distance was 10mm and impact angle was 15, $45,90^0$. The overall density values of alumina coatings on Al-6061 and cast iron substrates vary between 2.49 and 2.67 g/ cm^3 and it was between 6.37 and 6.96 g /cm^3 in case of ZrO $_2$5CaO coatings. With the help of the XRD technique they found that Al2O3 particles are not completely transferred into soften γ-Al2O3 phase after the plasma spray process in case of alumina. Because of the good result from the tribological behaviour of coatings. The hardness of Al_2O_3 coating is lower than that of bulk alumina which was due to the intrinsically lower hardness of γ-Al $_2$O $_3$ they observed that the volume loss is more at 45◦ angle of impact. The volume erosion loss of Al-6061 substrate decreases with increase in angle of impact. The volume erosion loss of these substrates is less than that of all coating systems. Although the cumulative mass loss of $ZrO_2$5CaO coatings is more than that of alumina coatings, because the volume erosion loss of these coatings is higher.

Geng et al. [2012] determined the effect of composite Fe-Co-Ni coated by electroplating on stainless steel .They cut steel pieces in the dimension of 15x10x1 mm with the help of electric discharge machining and a drill of 1.5mm dia. was made in the centre of the specimen each piece was finished with the acetone prior to electroplate. They used stainless steel substrate as a cathode and nickel plate as a anode. They made a solution for

electroplating contains 40 g/L $NiSO_4 \cdot 6H_2O$, 10 g/L $NiCl_2 \cdot 6H_2O$, 10 g/L $FeSO_4 \cdot 7H_2O$, 10 g/L $CoSO_4 \cdot 7H_2O$ and 15 /L H_3BO_3. Fe-Co-Ni coating was electroplated at 55°C under a cathode current density of 27 mA/cm^2 for 5 minutes. Thickness of coating was 3-4 µm to provide goods bonding prevents from oxidation. The mass gain of the steel with Fe-Co-Ni coating was much higher than that of the bare steel. They found that after the first-week rapid oxidation has been started, the mass gain of the steel with the electroplated coating increased insignificantly with oxidation time, and its oxidation rate was similar to that of the bare steel, which implied that a protective oxide layer has been formed on the steel after coating. After three weeks when both substrates coated and uncoated exposed in air at 800^0c. They found that in the case of coated steel its outer layer was rich in Fe, Co and Ni, and no Cr was detected and inner layer having Cr-rich oxide with small amount of Mn. In the case of uncoated steel an oxide layer has formed. $(Fe,Co,Ni)_3O_4$spinel outer layer not only suppressed the evaporation of the Cr2O3 inner layer, but also reduced the growth rate of the Cr2O3 inner layer and improved the electrical performance of the whole surface.

Caicedo et al. [2012] evaluated the erosion behaviour of AISI D3 steel, 304 stainless steel and CrN/AlN coatings. They have used AISI D3 steel, 304 stainless steel of specification 10 mm in diameter and 7 mm in height. 50bilayerCrN/AlN coating was deposited on above materials. They used a gas mixture of Ar (92%) + N2 (8%) as an erodent material stored in gas chamber at a pressure of $2x10^{-3}$ mbar. Erosion behaviour of these materials was calculated with the help of testing system consisting of a tribometer with a glass container for erosive-corrosive storage, one reference and one counter electrode, an acrylic, sample holder and electrodes, a impeller of High Ultra Molecular Weight Polyethylene (HUMWPE) which rests on the Teflon shaft that was attached to the main motor shaft that provides fluid motion. The fluid movement was controlled by shaft driver of the motor which rotates erosive particles at a fixed speed of 11.12 m/s at an impact angle of 30 and 90^0. It was found that for the erosion wear of AISID3 steel show significant wear rate as compared to AISI 3304 for the first two hours but after some time it becomes stabilize because plastic hardening of material takes place due to erosive effect. They found that erosion at impact angles of 30° and 90° AISI D3 coated by CrN/AlN multilayer showed lower wear rate as compared to AISI 304. The mass loss between AISI D3 coated and uncoated was 35% whereas for AISI 304 it was around 65%.

2.2 LITERATURE REVIEW OF FRICTION WEAR

Hung-Kuk Oh et al. [1999] determined the effect of humidity on carbon steel 1020, 1041, 1045 used in making tools and dies. They have used pin on disc to determine the wear behaviour of above mentioned steels. The disc was 50 mm diameter and 5 mm thickness, while the pin was 6 mm diameter and 70 mm long, both being annealed and then washed in alcohol before being located in the tester. The roughness of the contact-area plane between the pin and the disk was value of 0.03 mm. a linear velocity was maintained between 18.3 to 20.9 cm/s (70±80 rpm) to avoid frictional heating. At the end of each 10 000m rotation/step, the disc and pin were disassembled from the tester and the debris was removed by ultrasonic water cleaning, the weight being measured by means of an electronic scale. They found that when the humidity increased, a transition of wear rate changed depending on carbon concentration in steels. The indicated points of transition increased with decrease of the carbon concentration of the steel. The abrupt decrease of wear rate occurred at about 45% humidity for 1020 steel. However, big drops for 1041 steel and 1045 steel were observed at almost the same relative humidity of 50%, but slightly higher for 1041 steel. The wear rate shown by 1045 steel was more, 1041 steel shows intermediate and 1020 steel shows smallest.

Fernandez et al. [2005] evaluated the wear behaviour of grey cast iron coated with NiCrBSi as a coating material using laser cladding technique. They made substrate of the specification 15.75x10x6.35mm and its wear behaviour was calculated at the load of 30- 100 N and at the sliding speed of 0.65-2.6m/sec. for coating the used Ar as the carrier gas, Optimum process conditions were established at a power density of 54W/mm^2 per piece, at a beam scanning speed of 200 mm/min and with a powder feed flow of 9 g/min. AISI 1043 steel ring, with an outer diameter of 50 mm, an average roughness of 0.9µm and an average hardness of 820 HV. They found that at the constant load of 30N and at the varying sliding speed the oxide layer of the coating material seems to break up faster than it can form, thereby, leaving new material at the surface which can then oxidize and wear away. They concluded that more Ni, Cr and Si contents present in the coating material more will adhering to the wear track of the counter body as the load increased. This suggests that there was some adhesive wear mechanism combined with the oxidation process observed for the lowest load.

Bateni et al. [2006] determined the sliding behaviour of steel 304 with the help of pin on disc wear tester. They annealed steel at 875±25^{0}C for an hour for decreasing and relieving internal

stresses. The harness of stainless steel 304 was obtained 163 HB after annealing respectively. They have used pin-on-disk tribometer to perform wear tests having AISI 3Cr12 steel Pins (220 HB) were used of dimension 6mm×12mm×40 mm. They conducted Wear tests under different loads of 9.6, 32, 54 and 71N velocity of 0.53 m/s and sliding distance of 160mm.They found that with the increasing of loads specific wear rates started to decrease and approach to constant value.. At higher loads, a hard surface layer is formed, most likely martens tic formation on surfaces of the steel, as the load increased, the oxide layer broke down and metallic contact was created between two surfaces. The breakdown of the oxide layer and metallic contact are main reasons for the existence of adhesion wear. The wear rate of steel was found out of the order of $10^{-3}mm^3/Nm$.

Grzesik et al. [2006] evaluated the sliding wear behaviour of PVD coated carbide against AISI steel 304 and grey cast iron counter parts, at a sliding distance of 2000m for normal loads of 1o, 20, 30 N, and the pin sliding velocity of 0.5, 1.0,1.5 m/s. They made round specimen of dia. 25.4mm coated with PVD-TiALN powder. The coating was deposited by the plasma assisted arc evaporation (PA PVD-arc) technique, known also as cathodic arc evaporation technique; this technique depends upon metallurgical effects. They found that when steel used as counterpart the coefficient of friction increases up to its maximum value and remains stable until end of the test. When the cast iron disc was used as a counter body the coefficient of friction usually reached about 90% of its final value just after the test started and further it slightly increases during the rest of the test duration. For the loads of 10 and 20 N, after the sliding distance of 250 m, no wear of the TiAlN coating was observed, despite the fact that built-up layers with the height of 1–2 μm were formed; the brown colour iron oxides were produced for the lowest load of 10N due to oxidative wear. On the other hand, for the higher load of 20N the adhesive transfer of steel layer mainly occurs, but also a tribo-oxidation takes place. The wear scars produced under the load of 30N are about 2–3μm deep. They found that When the sliding wear test was carried using an austenitic steel grade a severe adhesive wear of both the TiAlN coating and the steel surface was found to be predominant. In this case the protective layer was removed and the substrate material was pulled out from the specimen even under the lowest load and sliding speed applied, and when the cast iron was used as the counter specimen only a very mild abrasion of the TiAlN coating occurred.

Zandrahimi et al. [2007] determined the friction wear behaviour of austenitic stainless steel 304 using a pin on disc tribometer. AISI 52100 steel pins (60HRC hardness) of 5mm in diameter and 50mm in length. Were employed as the counter face. AISI 304 stainless steel of 50mm in diameter and 5mm in thickness were used. Wear tests were carried out under different loads of 100, 200, and 300 N. wear test at 200N load presence of martensite and austenite and an average grain size of about 20 microns was observed. With the increasing of the load from 100 to 300 N the plastic deformation takes place this plastic deformation leads to the formation of martensitic structure. They found that In AISI 304 stainless steel samples, abrasive wear was predominant wear mechanism, where the abrasion wear could be due to the higher hardness of counter face surface than the substrate. In AISI 52100 pins delamination was the predominant wear mechanism cause pulling out and delamination of detached layers.

Hua et al. [2008] determined the friction wear behaviour of SUS 304 austenitic stainless steel (ASS) disc against Al_2O_3 ceramic ball and GCr15 bearing steel ball, respectively, were studied using a Cameron-Plint TE67 tester. The tests were performed under 5–50N loads and 0.06–0.19 m/s sliding speed. The specimen they were used were SUS 304 and GCr15 bearing ball were cut in dimension of 70mm diameter×5mm thickness. Hardness of both specimens was 129 and 800 HV. Tribological tests were performed at a room temperature with a load of 5, 10, 30 and 50 N, applied on the stationary ball pressing against the disc specimen immerged in a Shell oil lubricant. The Turbo N46 oil has specific density 0.872, and viscosity 0.046 and 0.0066 Pa at 40 and 100^0C, respectively. For each individual tribological test, a pair of fresh ball-disc mating assembly was slid at a relative sliding speed of 0.06, 0.13 and 0.19 m/s. they have made some observations regarding both materials they found that (1) the friction coefficient at low pressure was low and the values were exhibiting relatively stable within the testing condition; (2) the friction coefficient increased sharply when the applied force was beyond 30N and the system mated with either ceramic balls or GCr15 steel balls. They also found that (i) 50 N–0.19 m/s–5 min was generally higher than that of (ii) 50 N–0.13 m/s–30 min although their structure may be similar, whilst that of (iii) 50 N–0.06 m/s–2 min was higher than that of (iv) 10 N–0.06 m/s–30 min although their structure was similar. They developed a relation to find out the specific wear rate $K = \frac{WvH}{LD}$ where H is hardness of the material, K is then specific wear rate, D is the sliding distance, W_v is the wear volume, H is the constant =1.

Taktak et al. [2008] evaluated the wear and friction behaviour of bearing steel (AISI 52100 and 8620). The bearing steels were used in a dimension of 25mm in diameter and 6 mm in thickness and abraded and polished up to 1 µm Al_2O_3 powder. TRD carbide coatings were performed by pack method in the powder mixture consisting of 40 wt. %ferro-chromium powder, 15 wt. % ammonia chloride activator and 45 wt. % filler (alumina powder) in a double stainless steel box at 1000 °C for 5 h in an electrical resistance furnace. Tribological properties of the duplex treated bearing steels were examined using a pin-on-disc test device. It has movable flat surface was the treated steel and upper fixed surface was the Al_2O_3 ball with diameter of 8 mm. The ball was fixed and the disk sample was rotated at the speed of 300 rpm (0.3 m/s). Applied load on the fixed ball was 5 and 20 N and the sliding time was 60 min. Wear tests were carried out in the un lubricated condition at room temperature and 500°C in open air. Wear volume of the disk specimen was determined from the cross-sectional area of the wear track obtained perpendicularly to the sliding direction. They found that at the steady state coefficient of friction of chromized (TRD) AISI 8620 and 52100 bearing steels for loads of 5 and 20 N was in order of 0.63– 0.75 at R.T. When sliding occurred at 500 °C, friction coefficient values dropped to 0.43–0.53 for chromized steels. The steady state friction coefficient of duplex treated bearing steels for loads of 5 and 20 N was in order of 0.55–0.41 at R.T. whereas friction coefficient dropped to in order of 0.47– 0.38 at temperature of 500 °C. They also found that Plasma nitriding process decreased the coefficient of friction values of chromized steels at room temperature and at 500 °C and the coefficient of friction coefficient values at 500 °C are lower than that of at R.T. for all the samples.

Cruzado et al. [2010] determined the friction wear of thin steel wire 0.45 mm dia. and of tensile strength 2800 MPa and a hardness of 659±81 HV0.05. The surface average roughness (Ra) of these wires along its axis was 0.35 and 0.70µm in perpendicular direction. Fretting wear tests were carried out on a tribometer designed to operate under oscillating motion with small amplitudes (10–200µm) and small loads (0.1–10 N) and speed for the revolutions was between 20,000–50,000 cycles. They found that for 1N 65µm and 200,000 cycles the dissipated energy is about 15.8 J, for 2Nand 65µm it is about 32 J and for 3Nand 65µm it is about 49.3 J. for 0.5N the coefficient f wear is 9.49×10-6mm^3/Nm and for 3N the coefficient of wear is 20.74×10-6mm^3/Nm and for 65m the coefficient of wear is 9.65×10-6mm^3/Nm and for 130m the coefficient of wear is 20.74×10-6mm^3/N m. the results show that the wear

coefficient increases with normal load and stroke, the wear produced was higher when the load and/or stroke is increased.

Rathod et al. [2010] evaluated sliding wear behaviour of foundry prepared of cast iron with oil suspended with lead particles. They have prepared two samples of cast iron one for microstructure testing (15mm thickness, 20mm diameter) and another sample for wear testing (53mm in length and 8mm in diameter). They used pin on disc having sliding disc AISI 4340 and had hardness of318 HV, and they have used of SAE40 oil (density 11.34g/cc.) mixed with lead particles of the size range 5–75 μm. the suspension mixture must be stirred properly so as to avoid segregation of the lead particles. The pin and disc surfaces were polished and cleaned well with nital solution prior to and after conducting the wear tests. The test conditions that they were used for the test were sliding speed of 4.2m/s and sliding distance of 2500m, load of 1, 5, 7, 9MPa, and lead content added in the proportion of 3, 5, 7, 10% by wt. in the oil. They found that the wear rate decreased with increasing lead content initially and attained the minimum in the oil lubricant mixture containing 5% lead, while the maximum was delineated in the lubricant mixture containing 10% lead. Higher wear rate and frictional heating led to more severe surface damage and less effective formation of lubricant film. With the increase in the load temperature will increase leads to the more wear rate, more debris will formed, more debris formation leads to the abrasion.

Masanta et al. [2011] determined the tribological behaviour of AISI steel 304 and AISI 1020 coated with composite substrate TiB_2–TiC–Al_2O_3. Coating was done with the help of laser cladding technique. They have used argon as a shroud gas at a pressure of 1 bar. The specimen they have used of the specification 100X 50X 8 mm polished with emery paper of grit size 220. They have used 10mm/s and 15mm/sec laser scan speed for coating they found that at a lower speed some cracks were found in the AISI 1021 steel .but as scan speed increased no cracks or dendrites were found in the AISI 1020. WC–Co ball (WC – 94.5% Co – 5.5%) of 5 mm diameter was employed as the counter body, rotating with a track diameter of 5 mm and at a load of 9.8-39.2 N at a constant speed of 0.104m/sec. They found that with lower applied normal loads, the substrate materials have not been exposed due to wear. However with higher applied normal loads, partial removal of coating were observed causing exposure of substrate material. They also found that wear resistance of the coating increases with increase in laser scan speed and decreases with increase in applied normal load during

tribological test. Average wear rate (for same applied normal load) of the coatings developed on AISI 304 steel was higher than that of the coatings developed on AISI 304 steel.

Prasad et al. [2011] evaluated the dry and lubricated sliding wear of grey cast iron using pin on disc. They have conducted test on the following conditions for both dry and oil lubricated conditions, sliding speed: 500 and 1500 rpm ,sliding distance: 500 and 2500 min dry and oil lubricated conditions , load :1kg. For carrying out oil lubricated tests, the disc was immersed in SAE40 oil lubricant and allowed to Rotate at a speed of 2.08m/s for 5s prior to conducting the tests. They showed that in the case of dry friction wear rate first increase and in the end it starts decreasing. But the presence of oil leads to decrease the wear rate as compared to the dry friction condition. They found that main reason behind the wear rate was the adhesion (i.e. presence of machining chips in the debris and deep groves on the wear surface.) and the wear temperature as the sliding speed increase temperature increase it will leads to more material loss The friction coefficient decreased with increasing load also, increasing sliding speed caused the friction coefficient to decrease during dry sliding while it produced a mixed effect on the property in the presence of the oil lubricant.

Wang et al. [2011] evaluated the sliding wear of Cr–Mo–Cu alloy cast irons with and without nano-additives against the Gr15 steel balls at constant load (10N) and rotating velocity (1.4m/min) for 110min. They have prepared three samples namely : Cr–Mo–Cu alloy cast iron without nano-additives , as-cast Cr–Mo–Cu alloy cast iron with nano-additives (CG alloy cast iron), and heat treated Cr–Mo–Cu alloy cast iron with nano-additives (VG alloy cast iron) respectively. They have made Cr–Mo–Cu alloy cast irons (DISK) whose dimensions were 20 mm× 20 mm × 5 mm wear against GCr15 steel ball (BALL) with diameter of 5 mm and hardness of HRC64. The average diameter and sliding distance of wear track were 7.074 mm and 490 m. The hardness of VG and CG alloy cast irons is higher than that of the non additive alloy cast iron, so the wear resistance also increased considerably. The worn area of GCr15 steel ball worn against with VG alloy cast iron was obviously larger than that of worn against with FG and CG alloy cast irons, which showed the grinding efficient of VG alloy cast iron was better than that of FG and CG alloy cast irons. The groove left on the worn surface of GCr15 steel balls which wore against with CG and VG alloy cast irons was relatively narrow. The worn surface of steel ball wore against with FG alloy cast iron was rough, and the degree of wear (plough and adhesion) was higher than that of steel ball wore against with CG and VG alloy cast irons.

Coronado et al. [2011] determined the effect of load and orientation effect of carbides on cast iron. The cast iron they have used was solidified at the temperature of 15^0c. With the help of wire electro-discharge machining, they cut wear samples in the dimensions of 20mm of length and 3mm of diameter. They have used PLINT TE79 type wear tester to carry out wear out using fixed alumina abrasive grains at the parameters : fixed rotational speed of 66rpm and loads of 2N, 4.6 N, 8N, 10Nand 15N. They have used alumina as an abrasive feed in both longitudinal and transversal direction. They found that in the longitudinal direction at 15 N some cracks in the carbides forming at an angle of about 45^0 with the scratches were generated from the grooves and continuous microchips (wear debris) and alumina abrasive gets penetrate in the surface. But in the transverse direction no wear debris seen in the microstructure as cementite is very hard.

Balamurugan et al. [2012] determined the tribological behaviour of austenitic steel 304 coated with WC-CO and hard chromium. They have conducted the experiment with the help of pin on disc having EN 24 medium carbon steel pin at the room temperature of 100, 200, 300^0c at a load of 50 N and at a sliding speed of 1m/s. They found that Mass loss of the chromium and plasma coated specimen increased up to 100 ^{0}C due to softening of the intermetallic. The wear resistance of WC–Co coatings has been increased at 200^0C due to the prow formations and frequent ploughing which leads to more material loss. Wear resistance considerably increased from 200^0C to 300^0C, due to the formation of oxides, which showed the reduced severity of material loss. They found that Coefficient of friction (CoF) for the chrome coated discs in all the temperatures varied between 0.39 and 0.96. Whereas, for plasma WC–12%Co coated discs the CoF in all the temperatures was found to be lesser than that of chrome coated discs and it varies from 0.17 to 0.62. The reason was due to dry sliding which leads to high local pressure between contacting asperities, resulting in plastic deformation, adhesion and the consequent formation of local junctions. They developed formula to calculate the wear rate:

$$\text{Volume loss } (mm^3) = \frac{\text{Mass loss}}{\text{Density}} \times 100$$

$$\text{Wear rate } (mm^3/m) = \frac{\text{Volume loss}}{\text{Sliding distance}}$$

Wei et al. [2012] evaluated the wear behaviour of both carbon steel and grey cast iron with the help of pin on disc wear tester. Both materials were made in the specification of 6 mm

diameter and 12 mm length, and D2 steel was choose as counter-surfaces of 70 mm diameter and 8 mm thickness. Wear tests was performed at a distance of 1.2×10^{3}m at a velocity of 1 m/s within an ambient temperature range of 25–400^{o}C and a load range of 50–200 N. During sliding, they suggested that the graphite in the spheroidal graphite cast iron was gradually exposed. Graphite as a strong reducer would cause the following reactions during elevated-temperature wear .These reactions could occur during sliding, i.e. graphite powder reacts first with oxygen to produce carbon monoxide, which then reduces the tribo-oxides generated on the worn surface. They found that the wear rate of the carbon steel at 25 ^{0}C increased approximately linearly with increasing load. At 200 ^{0}C, the wear rate abruptly decreased as the load was raised from 50 to 100 N, and then increased again slightly with further increasing load. The wear rate at 400 ^{0}C increased gradually at first with increasing load, then started to rise rapidly once the load surpassed 125 N. grey cast iron showed same wear rate but at 400^{0} C.

CHAPTER 3

PROPERTIES OF DUCTILE MATERIAL AND SLURRY

3.1 STUDY DIFFERENT PROPERTIES OF DUCTILE MATERIALS

Ductility is more commonly defined as the ability of a material to deform easily upon the application of a tensile force, or as the ability of a material to withstand plastic deformation without rupture. Ductility may also be thought of in terms of bend ability and crushability. Ductile materials show large deformation before fracture. The lack of ductility is often termed brittleness. Usually, if two materials have the same strength and hardness, the one that has the higher ductility is more desirable. The ductility of many metals can change if conditions are altered. An increase in temperature will increase ductility. A decrease in temperature will cause a decrease in ductility and a change from ductile to brittle behaviour. A no. of ductile materials are available they are aluminium, steel 304, grey cast iron, copper, brass. But we have used only steel 304 and grey cast iron as they have used many industrial components making as we have mentioned above.

Stainless steel 304 is ductile in nature and also does not require post-weld annealing, so is extensively used in heavy gauge components (over about 6mm). It is used for a wide variety of home and commercial applications, this is one of the most familiar and most frequently used alloys in the stainless steel family. Typical applications include tanks and containers for a large variety of liquids and solids. It is highly suitable and applied in dairy equipment such as milking machines, containers, homogenizers, sterilizers, and storage and hauling tanks, including piping, valves, milk trucks and railroad cars. Very common in the brewing industry where it is used in pipelines, yeast pans, fermentation vats, ball and bearings, storage and railway cars, etc.

Grey cast iron and stainless steel 304 samples are used for estimation of erosion wear as they both are ductile materials. Basically grey cast iron is a type of cast iron that has a graphitic microstructure. It is named after the grey colour of the fracture it forms, which is due to the presence of graphite. It is the most common cast iron and the most widely used cast material based on weight. It is used for housings where tensile strength is non-critical, such as internal combustion engine cylinder blocks, pump housings, valve bodies, electrical boxes, and decorative castings. Grey cast iron‘s high thermal conductivity and specific heat capacity are often exploited to make cast iron cookware and disc brake rotors**.**

Before conducting the experiments, various properties of grey cast iron and stainless steel 304 needs to be determined. These properties are chemical composition, some mechanical properties and micro hardness.

3.1.1 Chemical composition

The chemical composition of grey cast iron and stainless steel 304 samples were determined by the spectrometer analysis as shown in figure 3.1. A spectrometer (also known as spectrophotometer, spectrograph or spectroscope) is a device that used to measure the chemical composition of ferrous materials.

Figure 3.1 Spectrometer

The chemical composition is measured by the light intensity produced by arc. A spectrometer is used in spectroscopy for producing spectral lines and measuring their wavelengths and intensities. Spectrometer instruments operate over a very wide range of wavelengths, from gamma rays and X-rays into the far infrared. Figure 3.1, showing the spectrometer.

A composition of both ductile materials (Stainless steel 304 and Grey cast iron) is shown in the table below:

Table 3.1 Chemical composition of steel 304 and grey cast iron

Name of the element (%)	Percentage average of steel 304	Percentage average of grey cast iron
Fe%	69.4	55.7
C %	.225	2.46
Si %	.439	7.00
Mn %	1.73	1.47
P %	0.0165	0.800
S %	0.0121	0.154
Cr %	19	0.116
Ni %	0.106	0.164
Al %	0.38	5.75
Co %	0.0416	0.0687
Cu %	0.116	0.698
Mb %	0.318	4.64
Ti %	0.0044	0.181
V %	0.0168	0.211

3.1.2 Basic mechanical properties of ductile materials

Grey cast iron is characterized by its graphitic microstructure, which causes fractures of the material to have a grey appearance. It is the most commonly used cast iron and the most widely used cast material based on weight. Grey cast iron has less tensile strength and shock resistance than steel, but its compressive strength is comparable to low and medium carbon steel.

Steel 304, the low carbon version does not require post-weld annealing and so is extensively used in heavy gauge components. Grade 304 is the standard "18/8" stainless; it is the most versatile and most widely used stainless steel, available in a wider range of products, finishes than any other.

Table 3.2 Mechanical properties of ductile materials

Property	Steel 304	Grey cast iron
Density	8000kg/m^3	7000kg/m^3
Tensile strength	515 Mpa	_
Yield strength	205Mpa	50Mpa
Elongation percentage	40%	0.5

3.1.3 Micro hardness

Micro hardness testing shown in fig 3.2 is used for measuring the hardness of a material on a microscopic scale. A precision diamond indenter is impressed into the material at loads from a few grams to 1 kilogram and we have taken load of 100gm. The impression length, measured microscopically, and the test load are used to calculate a hardness value. The hardness values obtained are useful indicators of a material's properties.

The indentations are typically made using either a square-based pyramid indenter (Vickers Hardness scale) or an elongated, rhombohedra-shaped indenter (Knops hardness scale). The tester applies the selected test load using dead weights. The length of the hardness impressions are precisely measured with a light microscope using either a filar eyepiece or a video image and computer software. A hardness number is then calculated using the test load, the impression length, and a shape factor for the indenter type used for the test and the test specimen.

The micro hardness of uncoated grey cast iron and uncoated stainless steel 304 is shown in the table.

Table 3.3 Micro hardness of ductile materials

Material	Micro hardness (VHN) at a load of 100 gm.
Stainless steel 304	107 Vickers Hardness number
Grey cast iron	111 Vickers Hardness number

Figure 3.2 Micro hardness

.

The following figures showing the indent of both ductile materials.

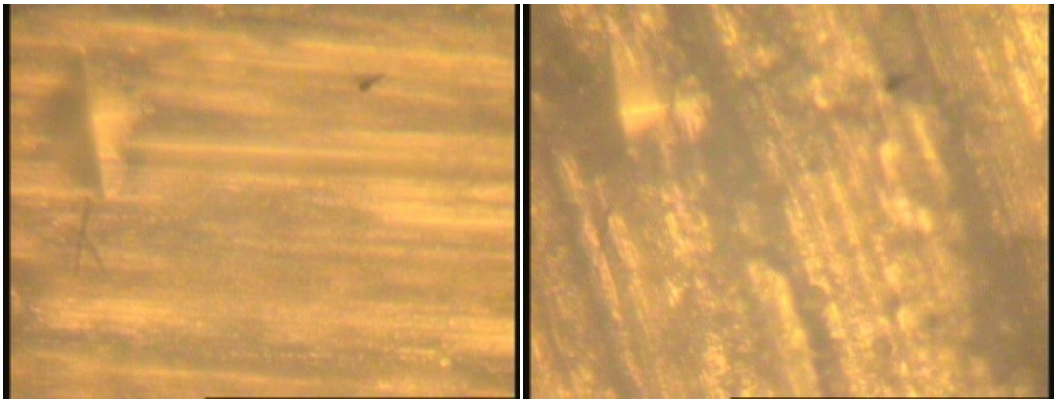

Figure 3.3 Indent mark on steel 304 **Figure 3.4 Indent mark on grey cast iron**

3.2 FLY AND BOTTOM ASH

In an industrial context, fly ash usually refers to ash produced during combustion of coal. Fly ash is generally captured from the chimneys of coal-fired power plants, and together with bottom ash removed from the bottom of the furnace, jointly known as coal ash. Fly ash includes substantial amounts of silicon dioxide (SiO_2) (both amorphous and crystalline) and calcium oxide (CaO). Fly ash is one of the residues generated in combustion, and comprises the fine particles that rise with the flue gases as shown in the figure 3.6.The fly ash may contain higher levels of contaminants than the bottom ash. Toxic constituents depend upon the specific coal bed makeup. Bottom ash is residue of coal, burning in thermal power plants.

Bottom ash being heavier in size cant escapes up the chimney along with the fumes to the atmosphere whereas fly ash escapes up the chimney along with the fumes to the atmosphere. Bottom ash is coarser than fly ash with grain size spanning from fine sand to fine gravel as shown in figure 3.5 and fig. 3.6. Before studying different properties of fly and bottom ash like particle size distribution, static settled concentration, specific gravity and rheological behaviour.

Figure 3.5 Fly ash

Figure 3.6 Bottom ash

We must know the chemical composition of both fly and bottom ash. The following tables will show the chemical composition. Chemical composition was measured by SEM.

Table 3.4 Fly ash composition

Element	Weight%	Atomic%	Compound%	Formula
C K	2.83	4.90	10.38	CO_2
Mg K	0.26	0.22	0.44	MgO
Al K	14.06	10.82	26.57	Al_2O_3
Si K	21.12	15.61	45.18	SiO_2
P K	0.45	0.30	1.02	P_2O_5
K K	1.27	0.67	1.53	K_2O
Ca K	1.40	0.72	1.96	CaO
Ti K	1.17	0.51	1.95	TiO_2
Fe K	3.87	1.44	4.98	FeO
Cu K	2.37	0.77	2.97	CuO
Zn K	2.43	0.77	3.03	ZnO
O	48.77	63.27		
Totals	100.00			

Table 3.5 Chemical composition of bottom ash

Element	Weight%	Atomic%	Compound%	Formula
C K	13.20	19.33	48.38	CO_2
Mg K	0.13	0.09	0.21	MgO
Al K	8.01	5.22	15.14	Al_2O_3
Si K	12.93	8.09	27.66	SiO_2
K K	0.51	0.23	0.62	K_2O
Ca K	0.28	0.12	0.39	CaO
Ti K	0.97	0.36	1.62	TiO_2
Fe K	3.13	0.98	4.02	FeO
Cu K	0.83	0.23	1.03	CuO
Zn K	0.74	0.20	0.92	ZnO
O	59.27	65.14		
Totals	100.00			

3.2.1 pH value

pH is a measure of the activity of the (solvated) hydrogen ion which measures the hydrogen ion concentration. Pure water has a pH very close to 7 at 25°C. Solutions with a pH less than 7 are said to be acidic and solutions with a pH greater than 7 are basic or alkaline. pH meter was used to determine pH value of fly and bottom ash slurry for any given solid concentration. The electrode of the pH meter was cleaned by rinsing vigorously with distilled water and then immersed in the slurry sample whose pH value was to be determined. The pH meter will digital display unit when equilibrium value was reached. Before calculating new pH value electrode must be cleaned with water. From the pH meter we found that pH value of both fly and bottom ash lies between 6 to 7.5 this shows that both are non reactive in nature.

3.2.2 Static settled concentration

The static settled concentration decides the highest limit of solid concentration, which can be achieved by gravitational settling. The experiment will be performed according to procedure discussed below.

The fly and bottom ash of known amount of concentration 20% by weight was taken in the measuring and cylinder and remaining cylinder was filled with water. Mix both ash and water properly with the stirrer so that no ash will settle down. Then leave the jar for 2 minute note how much ash was settled down. Repeat this experiment for 30, 45, 60, 90, 120, 180, 240, 360, upto 480min. Note the settled weight carefully after a fixed interval. After some time a time will come when settled weight comes out be constant. By following this procedure we found that as initial concentration of both fly and bottom ash was 20% by weight, final settled concentration after 5 hours comes out was 58.5%.

3.2.3 Specific gravity

Specific gravity is the ratio of the density (mass of a unit volume) of a substance to the density (mass of the same unit volume) of a reference substance. Apparent specific gravity is the ratio of the weight of a volume of the substance to the weight of an equal volume of the reference substance. The reference substance is nearly always water for liquids or air for gases. The following procedure must be followed for conducting the experiment.

The pyknometer of capacity 50 ml is cleaned and kept in an oven up to 2 hours and cooled down and weighted (W_b) to remove all moisture particles. After that dried ash is put in pyknometer and weighted (W_{bs}) put small amount of water is poured in it and shake properly for minute. It should be ensure that pyknometer is closed with thumb and there should be no air bubble in it. After 2 hours weight pyknometer having water and sand mixture (W_{bsw}). Now empty the pyknometer, dry it, and fill it with distilled water and weight it (W_{bw}). Then specific gravity of both ash can be calculated by the following formula:

$$\text{Specific gravity} = \frac{(Wbs - Wb)}{\{(Wbw - Wbsw) + (Wbs - Wb)\}}$$

Figure 3.7 Pyknometer & Oven

3.2.4 Particle size distribution (PSD)

Sieve analysis is used for determination of the distribution of particle size of fly and bottom ash. To determine the PSD of fly and bottom ash, a known weight of both ashes (100gm) were measured and put in the upper sieve. Sieve must be arranged in the order of 2000µm - 53µm, and close tightly so that it may not vibrate. Set time to shake it properly at least for 10min. after completion of time shaker will stop automatically then take the particles of ash from each sieve one by one may weigh them.

Table 3.6 Particle size distribution of bottom ash

Sieve opening(µm)	Sample Retained	Cumulative	Percentage of finer
2000	0.22	0.22	99.78
1700	0.16	0.38	99.62
1000	0.23	0.61	99.39
710	1.07	1.68	98.32
500	2.57	4.25	95.75
355	2.10	6.35	93.65
250	16.88	23.23	76.77
150	37.84	61.07	39.93
106	10.04	71.11	28.89
75	5.63	76.74	23.26
53	5.05	81.79	18.21
Pan weight.	18.21	100.00	0

Table 3.7 Particle size distribution of fly ash

Sieve opening(µm)	Sample Retained	Cumulative	Percentage of finer
500	0.30	0.30	99.70
355	1.77	2.07	97.93
250	6.06	8.13	91.83
150	9.98	18.11	81.89
106	16.91	35.02	64.98
75	20.84	55.86	44.14
53	29.75	85.61	14.39
Pan weight.	14.39	100.00	0

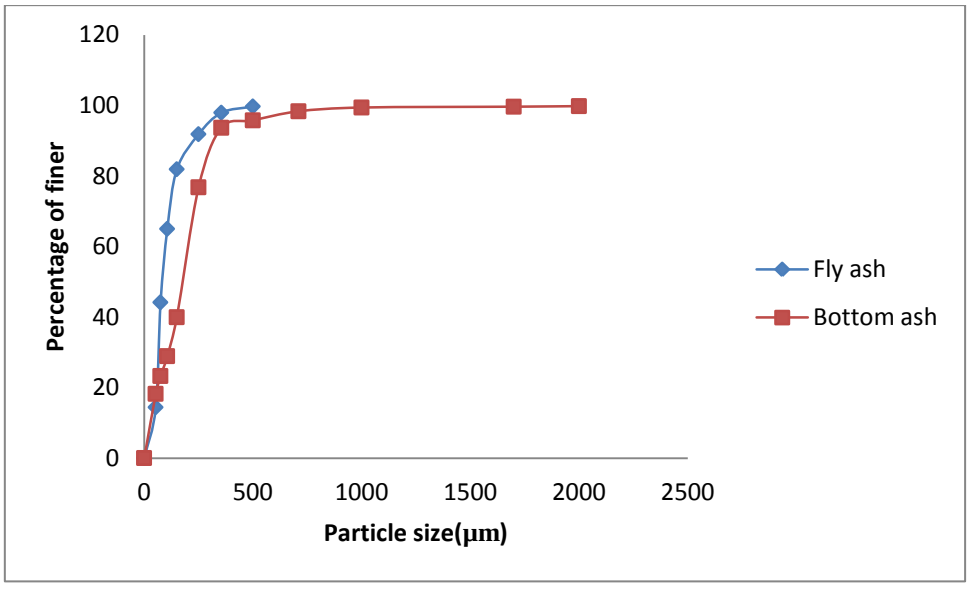

Figure 3.8 Particle size distributions of Fly and Bottom ash

3.3 VISCOSITY MEASUREMENT OF FLY AND BOTTOM ASH

Study of the flow behaviour and deformation of a fluid or a semisolid when subjected to forces is Rehology. The shear stress-shear rate relationship for fly and bottom ash slurry can

be determined by using bob and cup geometry, stirrer and bob geometry (in figure 3.09) of rheometer (make Anton paar). The geometry consists of a fixed cylinder (bob) and a rotating cylinder (cup). Viscosity plays important role in the estimation of energy required for transporting slurry through pipelines. The solid particles, which are present in a carrier fluid, alter its viscosity. To establish the Rheology of fly and bottom ash-water mixture, the variation of shear stress with shear rate has been obtained over a range of concentrations varying from 10 to 50% (by weight). Ash in a fixed quantity was mixed with water and shake properly so that ash will not settle down. Then put this mixture in the geometry that is between the bob and cup. When it will rotate it will generate torque due to torque shear stress and shear strain will generate. It will automatically generate graph between them. In this way we can vary concentration and measure the viscosity of the ash.

Figure 3.9(a) Rheometer (Anton Paar)

Figure 3.09(b) cylindrical cup and rotating Bob

Table 3.8 Rheological Properties of fly ash

Concentration (Cw) %	Yield stress(Pascal)	Slurry viscosity (Pascal/sec.)	Shear rate 1/s	Flow behaviour
10	0	0.002436	381.5	Newtonian
20	0	.00694	381.5	Newtonian
30	0	0.007806	381.5	Newtonian
40	0	.01178	381.5	Newtonian
50	0	.03481	381.5	Newtonian

Table 3.9 Rheological Properties of Bottom ash

Concentration (Cw) %	Yield stress (Pascal)	Slurry viscosity (Pascal/sec.)	Shear rate 1/s	Flow behaviour
10	0	0.020194	681.59	Newtonian
20	0	0.02356	681.59	Newtonian
30	0	.033031	681.59	Newtonian
40	0	.074631	681.59	Non-Newtonian
50	0	.6478	681.59	Non-Newtonian

CHAPTER 4

EVALUATION OF EROSION WEAR OF DUTILE MATERIAL

4.1 SLURRY POT TESTER

The slurry pot tester TR-41 is designed to determine the resistance of metallic materials to mass loss under slurry. The test data produced will reproducibly rank materials in their mass loss under a specified set of conditions.

This test is versatile with wide operating range and control systems.

- Test rig consists of frame, single, station slurry vessel, drive and control system.
- The main component of the test rig is installed in the frame. The frame is relatively rigid to avoid disturbing deformations and vibrations. The test chamber is sufficiently wide for placing slurry vessel dipped inside cooling jacket with circulating water through inlet and outlet ports. The water jacket with slurry vessel is lifted upwards to submerge specimen inside slurry.
- The drive system consists of an Ac motor speed controlled by a variable frequency drive.
- The control system controls the main operations of the rig.

  The cooling water jacket is a hollow cylinder shaped vessel made of stainless steel material with inlet & outlet ports for circulating water, it has a locator bush at bottom to centralize slurry vessel all around sufficient gap to circulate cooling water for carry away heat generated during erosion test. The water jacket is tightened to the base of a mechanical jacket prevents slurry spillage. Slurry vessel is made up of stainless steel material having outer dia. 120mm and height 120mm is placed inside the cooling jacket, for centralize for specimen to rotate without fouling during specimen rotation, the fins are fitted with replaceable rubber. The specimen for test is tightened to bottom of the spindle with a stirrer to agitate slurry during spindle rotation.

  Slurry is mixed in correct proportion is mixed inside slurry tank is filled till 15 mm above the specimen top or 60mm depth from the top face.
- The specimen for the test is rotated by AC motor , it is clamped between across flat on the face of the spindle is tightened to motor shaft, below specimen a stirrer is

Figure 4.1 Slurry pot tester TR-41

tightened to spindle by screw to rotate along with it slurry vessel is centralized to specimen centre to immerse it completely inside slurry.

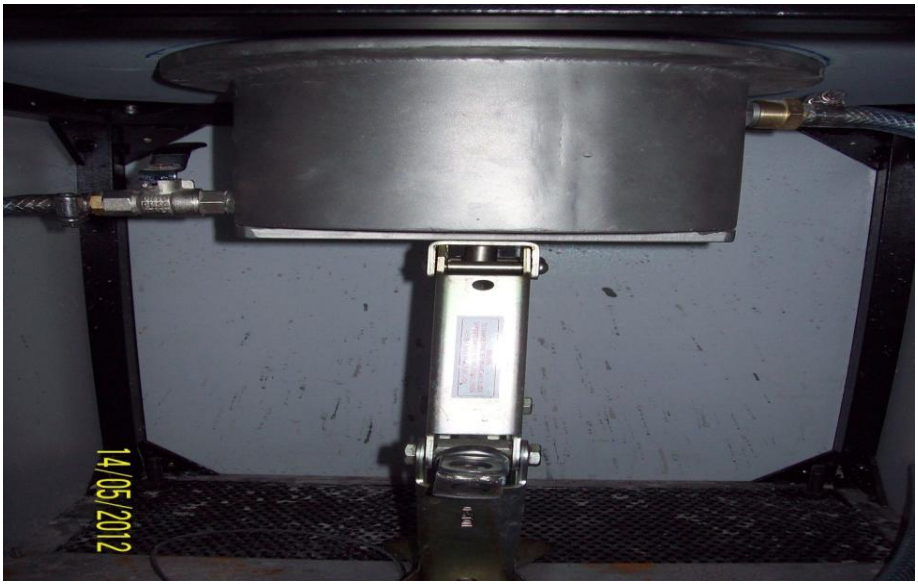

Figure 4.2 Internal view of pot tester

4.1.1Proximity sensor

Above motor end cover a bush it tightened to motor shaft with a flat edge, a proximity sensor is fitted facing the flat surface bush signal is generated when a flat surface approaches the sensor. This sensor functions in contact is less fashion and do not require any sensing mechanisms.

An inductive proximity sensor is used as it has excellent means of detecting the presence of wide range of metallic targets. This detection is accomplished without contacting target and its mechanically wear free. It is comprised of a high frequency oscillator circuit followed by level detector, a post amplification signal circuit and drives a buffered solid state output.

In effect when the sensor disc is brought within effective range of the estimated field of the oscillator a damping action results which reduces the amplitude of oscillator. This amplitude shift is converted to digital signal by the level detector which drives a buffer stage. When the object is removed the oscillator digital output is turned to its former state.

4.1.2 Controller

The operation of the machine is from the operator panel, fixed at a convenient height for the operation on the front panel of frame. Test speed is set by rotating the potentiometer knob in the clockwise direction till the required speed is noticed on the display above; the test duration is set by entering the values in to the timer module using the soft keys. By pressing the start or stop push buttons test begins, or ends.

4.1.3 Operation

The wear depends on abrasive particle size, shape and hardness and the frequency of contact of specimen with the abrasives. These conditions are standardized to develop a uniform condition of wear, the tests conducted does not to duplicate all the process conditions, it should only be used to predicting the exact resistance to of a give material in a specified environment. This test can be used to rank material in a relative order or merits as would occur in an abrasive environment.

4.1.4 Preparation of the slurry

Slurry pot tester is prepared on each slurry vessel, usually quartz, sand, ash and coal is preferred.

- Clean thoroughly slurry vessel.
- Weight and pour 600gms of sand in each vessel
- Fill each vessel with 600gms of water.

Figure 4.3 Slurry tank

4.1.5 Specimen preparation

Typical specimen is rectangular shape 25.4×76mm, 6.35 thicknesses. The specimen should be smooth, flat, and free of scale, machined and ground to size with a central hole for clamping.

- Remove all the dirt or foreign matter from the specimen.
- Clean the specimen with a solvent or cleaner or dry to remove all the traces of solvent.

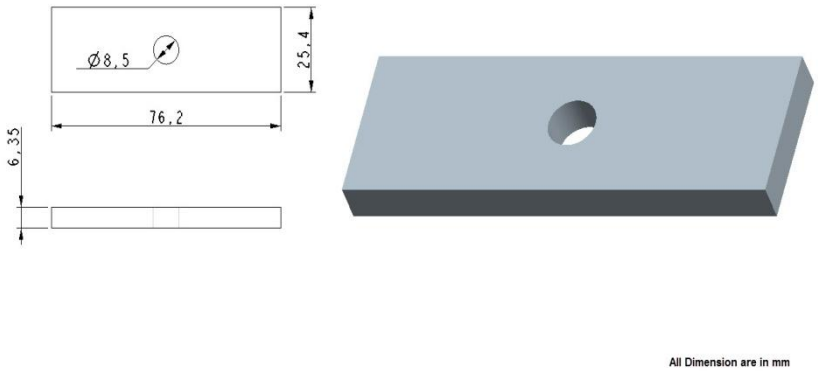

Figure 4.4 Sample Drawing

4.1.6 Procedure for performing test

- Thoroughly clean and rinse the slurry chamber to remove the remnants of slurry from the previous test.
- Weight 600 gm of abrasive (sand, alumina, ash, sand) and fill inside the slurry vessel.
- Fill vessel with 600gm of water.
- Weight specimen to the nearest 0.0001gm and record the value.
- Locate specimen on the slot of each spindle and tighten with stirrer.
- Connect inlet port to water source and outlet to drain.
- Switch "ON" MCB to supply power to tester to allow 1 min for stabilizing the circuits.
- Press start button on control panel and slowly rotate the SET RPM knob till the speed display module show 100 rpm.
- Press STOP to assets spindle rotation, but retain the position of SET RPM knob.
- Place the slurry vessel inside the water jacket.
- Clean the top surface of vessel and base plate with cloth.
- Slowly rotate the handle to raise the water jacket till it presses the base plate with sufficient pressure to prevent leakage of the slurry.
- Set the test duration to 3hrs to shut off automatically after completion of time,
- Press START switch to begins specimen rotation
- Specimen rotates, the direction or rotation is clockwise the stirrer agitates slurry, the slurry rotates along the direction of rotation, the slurry rotation is arrested by vertical fins to propel it towards specimen.
- The motor will be switched OFF automatically after the elapse of the preset revolution.
- Clean the surface of each specimen with cloth to remove slurry.
- Allow the specimen to cool, to room temperature and remove from specimen holder.
- Rinse to clean and dry the specimen.
- Weight each specimen and compute mass loss.

  Volume loss (mm^3) $= \frac{\text{Mass loss (gm)}}{\text{Density (gm/cm}^2\text{)}} . \times 100$

  Following parameters were taken while performing erosion wear on ductile materials with or without coating.

Speed: 700, 1000, 1400 rpm

Concentration: 20, 40, 60% by wt.

Time: 60, 90, 120,150min.

Ash: Bottom and fly both

4.2 EROSION WEAR OF STAINLESS STEEL 304

Erosion of steel 304 can be calculated by varying speed, time, and concentration. The amount of erodent material is calculated by calculating the weight loss after calculating the initial weight using weighing machine of least count 0.0001mg. The weight loss at different parameters is shown in figure 4.5- 4.10. It is observed that erosion wear rate (weight loss) increase with respect to time. Figures show that with the increase of time, speed and concentration o both bottom and fly ash the erosion wear rate increases. As the speed increases the kinetic energy of solid particles of erodent also increases which results in more weight loss. The weight loss of bottom ash as compared to the fly ash is more.

4.2.1 Effect of time, speed and concentration

From figure 4.5-4.7 observed that erosion wear of steel 304 increases with time of operation 60 to 150 minutes and between 120 to 150 minute rate of erosion wear increases very slowly as compared to time of operation between 60 to 120 minutes. It is also observed that rate of erosion wear increases with the changing the concentration of bottom ash and with the changing the speed.

From figure 4.5 noted that at 700 rpm speed rate of erosion wear in the terms of weight loss increase 57.99% from 60 minutes to 150 minutes of the operation for handling 20% bottom ash, similarly weight loss increases 40.35% for handling 40% bottom ash and similarly weight loss increases 28.48% for handling 60% bottom ash.

From figure 4.6 noted that at 1000 rpm speed rate of erosion wear in the terms of weight loss increase 65% from 60 minutes to 150 minutes of the operation for handling 20% bottom ash, similarly weight loss increases 43.99% for handling 40% bottom ash and similarly weight loss increases 41.66% for handling 60% bottom ash.

From figure 4.5 observed that at 1400 rpm speed rate of erosion wear in the terms of weight loss increase 48.43% from 60 minutes to 150 minutes of the operation for handling 20% bottom ash, similarly weight loss increases 34.69% for handling 40% bottom ash and similarly weight loss increases 27.61% for handling 60% bottom ash.

The results reveal that at lower concentration with variation of time of the operation more weight loss occurring as compared to higher concentration.

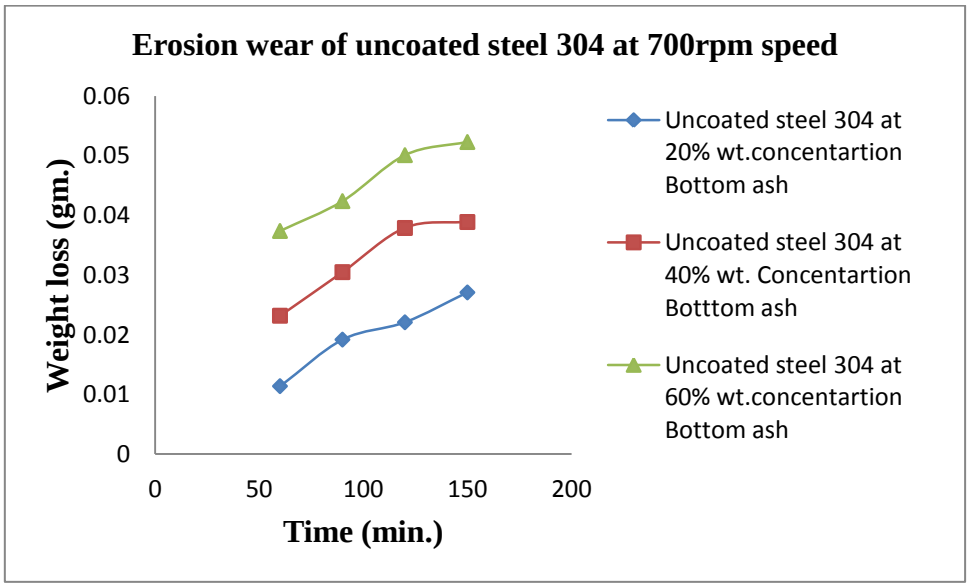

Figure 4.5 Erosion wear of uncoated steel 304 at 700 rpm speed

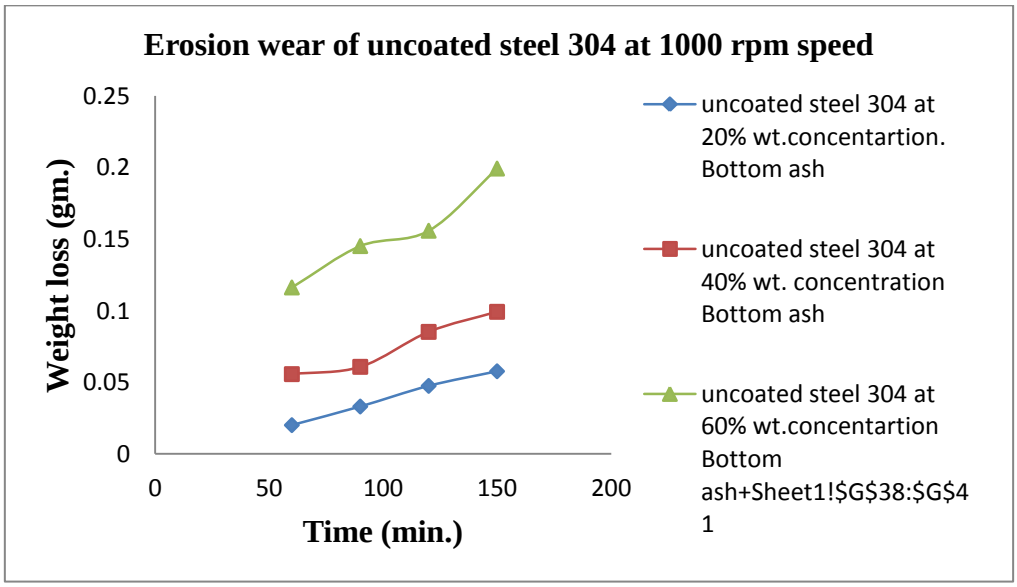

Figure 4.6 Erosion wear of uncoated steel 304 at 1000 rpm speed

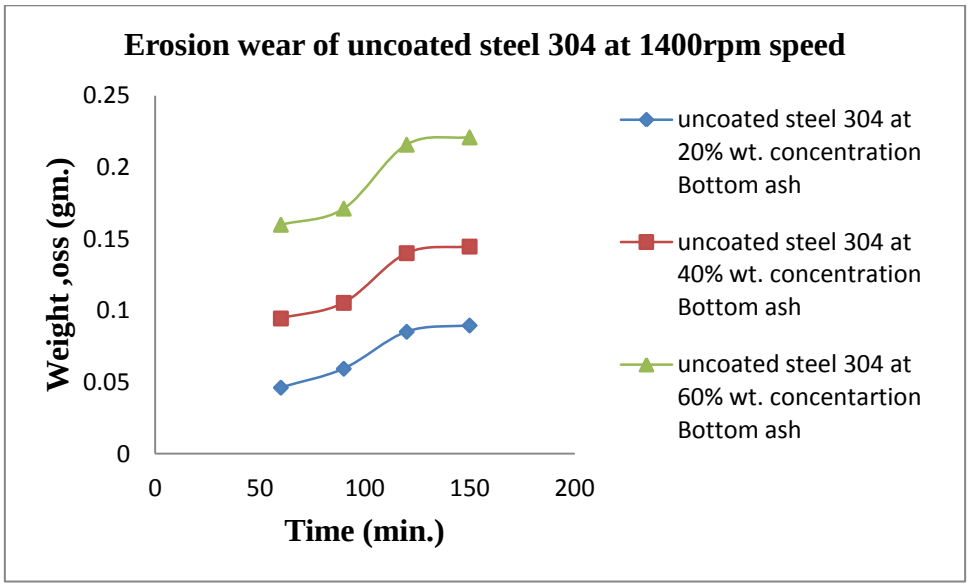

Figure 4.7 Erosion wear of uncoated steel 304 at 1400 rpm speed

From figure 4.8-4.10 observed that erosion wear of steel 304 increases with time of operation 60 to 150 minutes and between 120 to 150 minute rate of erosion wear increases very slowly as compared to time of operation between 60 to 120 minutes. It is also observed that rate of erosion wear increases with the changing the concentration of fly ash and with the changing the speed.

From figure 4.8 seen that at 700 rpm speed rate of erosion wear in the terms of weight loss increase 55.19% from 60 minutes to 150 minutes of the operation for handling 20% fly ash, similarly weight loss increases 48.96% for handling 40% fly ash and similarly weight loss increases 35.05% for handling 60% fly ash.

From figure 4.9 noted that at 1000 rpm speed rate of erosion wear in the terms of weight loss increase 31.69% from 60 minutes to 150 minutes of the operation for handling 20% fly ash, similarly weight loss increases 30.95% for handling 40% fly ash and similarly weight loss increases 17.88% for handling 60% fly ash.

From figure 4.10 observed that at 1400 rpm speed rate of erosion wear in the terms of weight loss increase 45.33% from 60 minutes to 150 minutes of the operation for handling 20% fly ash, similarly weight loss increases 51.14% for handling 40% fly ash and similarly weight loss increases 35.50% for handling 60% fly ash.

The results reveal that at lower concentration with variation of time of the operation more weight loss occurring as compared to higher concentration.

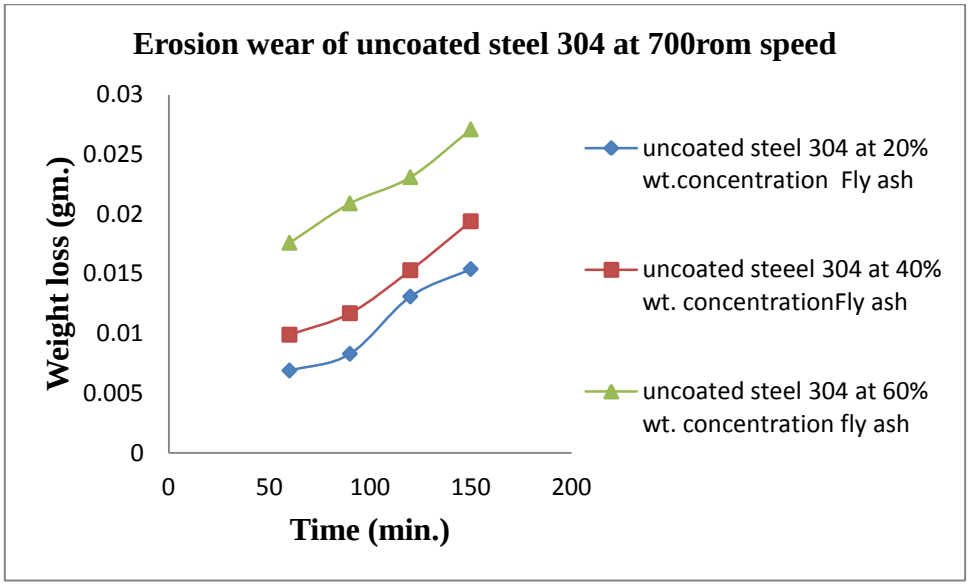

Figure 4.8 Erosion wear of uncoated steel 304 at 700 rpm speed

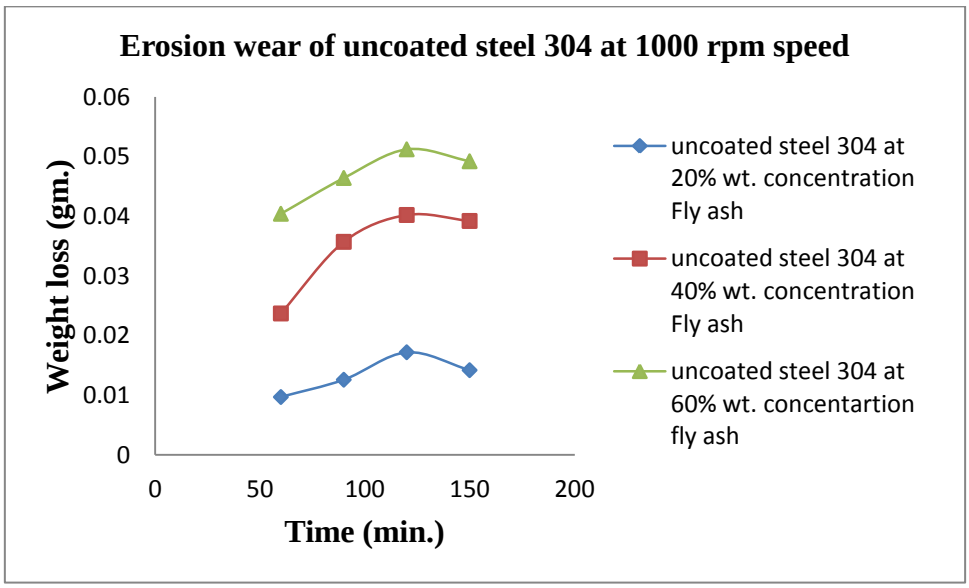

Figure 4.9 Erosion wear of uncoated steel 304 at 1000 rpm speed

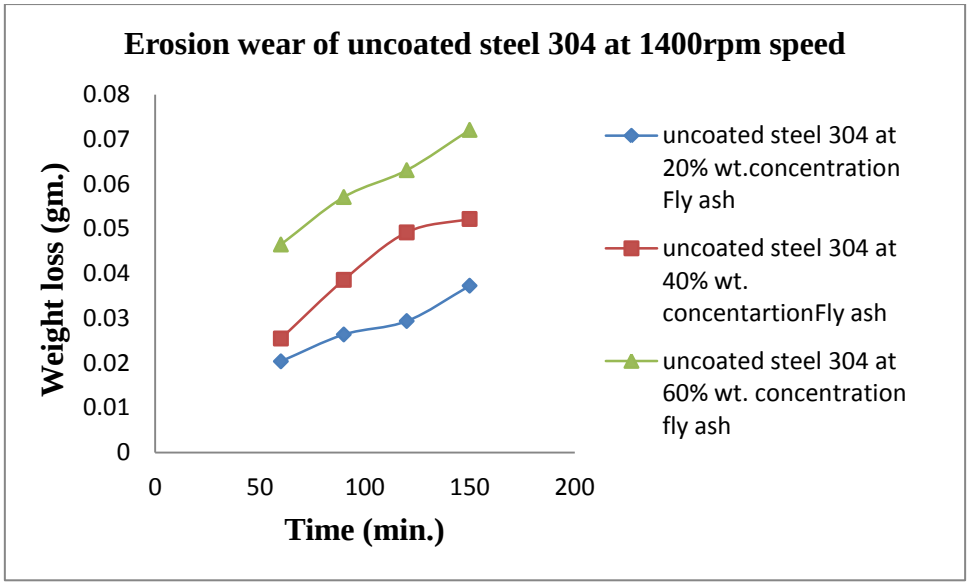

Figure 4.10 Erosion wear of uncoated steel 304 at 1400 rpm speed

4.2.2 SEM of steel 304 without coating

Figure 4.11- 4.13 shows the SEM of steel 304 before and after wear at 1400 rpm speed 60% bottom and fly ash. From figure 4.12 observed some creators in the form of black hole along the edges of the surface indicate the loss of material. Similarly from Figure 4.13 observed some white spots shows the area from where the material has removed.

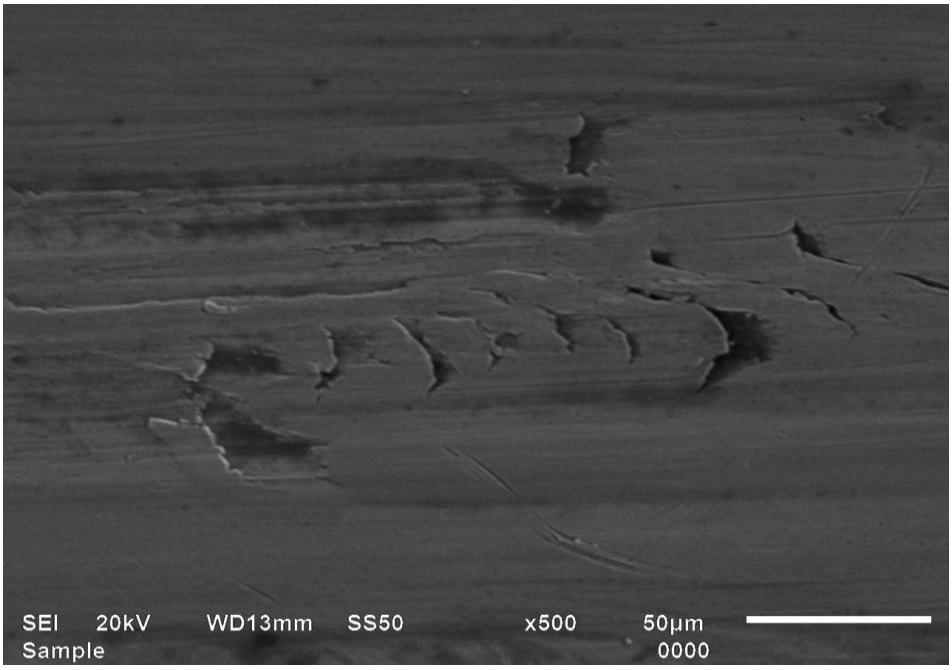

Figure 4.11 SEM of uncoated steel 304 before wear

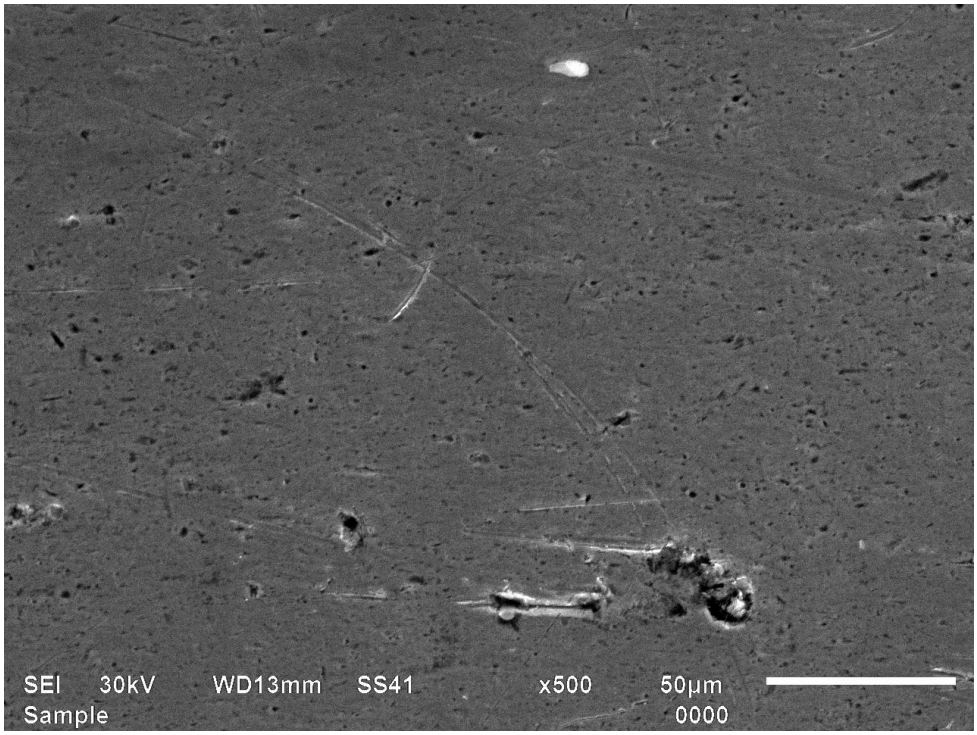

Figure 4.12 SEM of uncoated steel 304 after wear at 1400 rpm speed 60% bottom ash

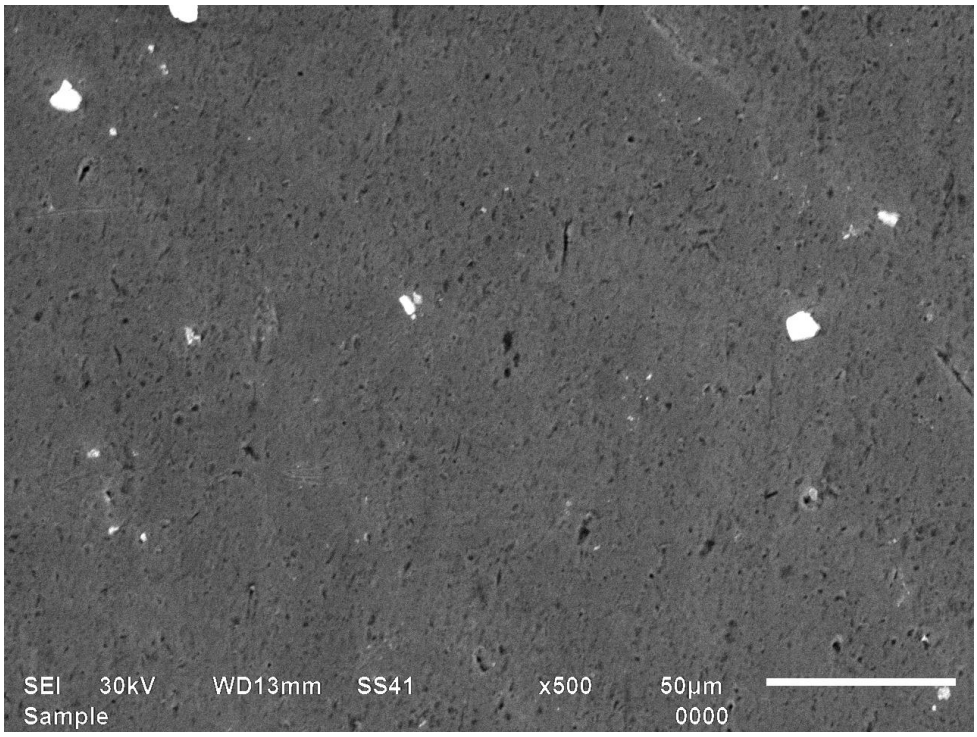

Figure 4.13 SEM of uncoated steel 304 after wear at 1400 rpm speed 60% fly ash

4.3 EROSION WEAR OF GREY CAST IRON

Erosion of grey cast iron can be calculated by varying speed, time, and concentration. The amount of erodent material is calculated by calculating the weight loss after calculating the initial weight using weighing machine of least count 0.0001mg. The weight loss at different parameters is shown in figure 4.14- 4.19. It is observed that erosion wear rate (weight loss) increase with respect to time. Figures show that with the increase of time, speed and concentration o both bottom and fly ash the erosion wear rate increases. As the speed increases the kinetic energy of solid particles of erodent also increases which results in more weight loss. The weight loss of bottom ash as compared to the fly ash is little bit more.

4.3.1 Effect of time, speed and concentration

From figure 4.14- 4.16 observed that erosion wear of grey cast iron increases with time of operation 60 to 150 minutes and between 120 to 150 minute rate of erosion wear increases very slowly as compared to time of operation between 60 to 120 minutes. It is also observed that rate of erosion wear increases with the changing the concentration of fly ash and with the changing the speed.

From figure 4.14 noted that at 700 rpm speed rate of erosion wear in the terms of weight loss increase 54.05% from 60 minutes to 150 minutes of the operation for handling 20% fly ash, similarly weight loss increases 40.44% for handling 40% fly ash and similarly weight loss increases 40.44% for handling 60% fly ash.

From figure 4.15 observed that at 1000 rpm speed rate of erosion wear in the terms of weight loss increase 32.00% from 60 minutes to 150 minutes of the operation for handling 20% fly ash, similarly weight loss increases 29.00% for handling 40% fly ash and similarly weight loss increases 21.82% for handling 60% fly ash.

From figure 4.16 seen that at 1400 rpm speed rate of erosion wear in the terms of weight loss increase 16.35% from 60 minutes to 150 minutes of the operation for handling 20% fly ash, similarly weight loss increases 21.82% for handling 40% fly ash and similarly weight loss increases 19.7% for handling 60% fly ash.

The results reveal that at lower concentration with variation of time of the operation more weight loss occurring as compared to higher concentration.

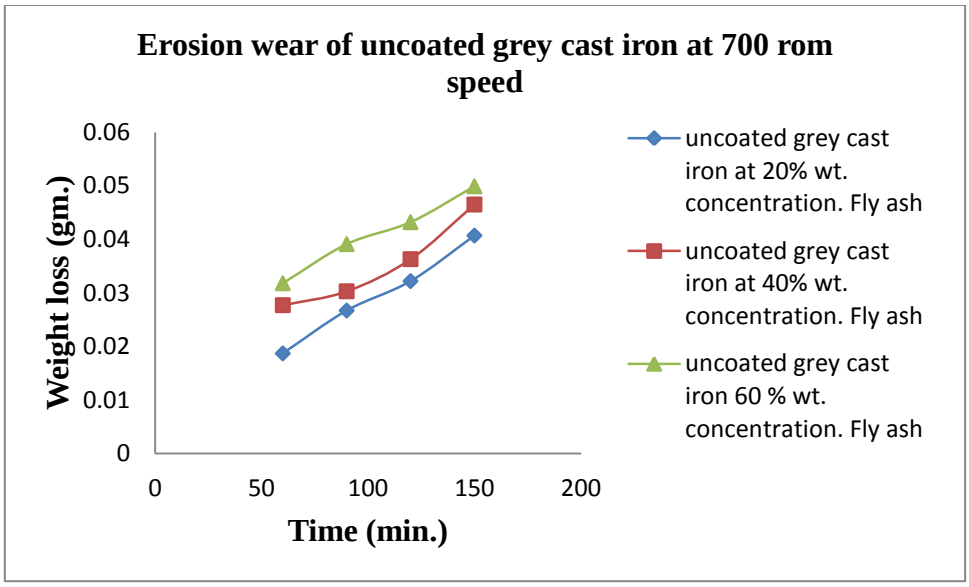

Figure 4.14 Erosion wear of uncoated grey cast iron at 700 rpm speed

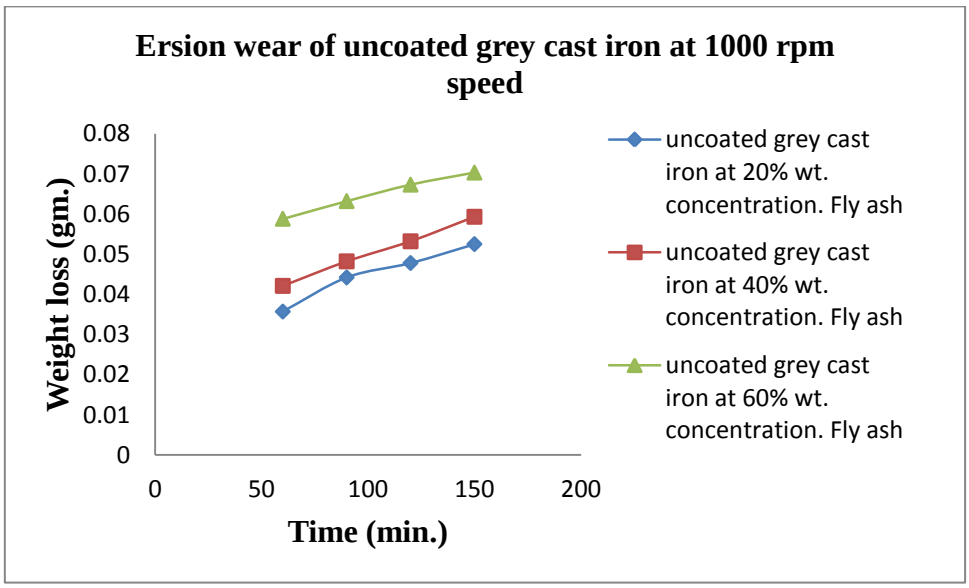

Figure 4.15 Erosion wear of uncoated grey cast iron at 1000 rpm speed

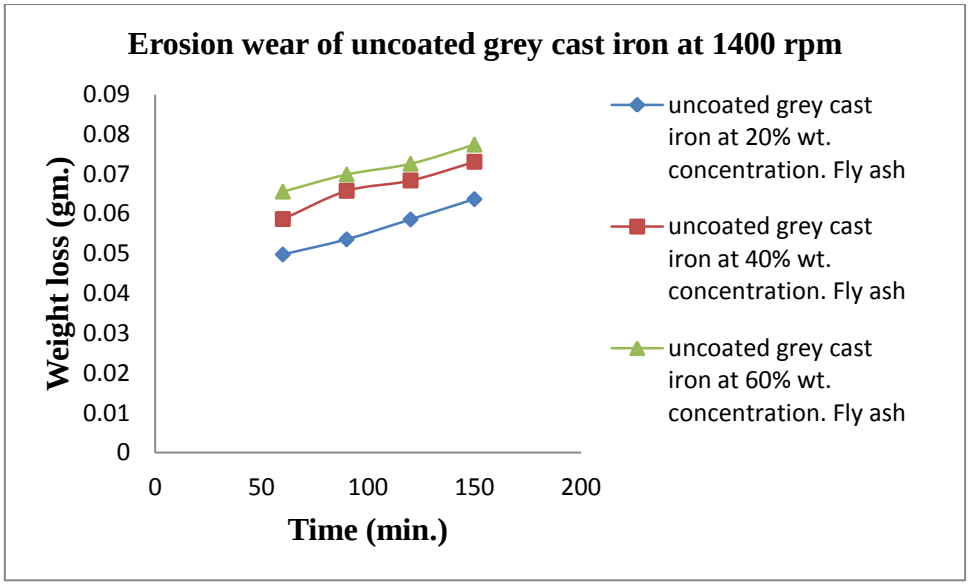

Figure 4.16 Erosion wear of uncoated grey cast iron at 1400 rpm speed

From figure 4.17- 4.19 observed that erosion wear of grey cast iron increases with time of operation 60 to 150 minutes and between 120 to 150 minute rate of erosion wear increases very slowly as compared to time of operation between 60 to 120 minutes. It is also observed that rate of erosion wear increases with the changing the concentration of bottom ash and with the changing the speed.

From figure 4.17 seen that at 700 rpm speed rate of erosion wear in the terms of weight loss increase 15.25% from 60 minutes to 150 minutes of the operation for handling 20% bottom ash, similarly weight loss increases 38.46% for handling 40% bottom ash and similarly weight loss increases 42.44% for handling 60% bottom ash. The result reveals that weight loss increases with the concentration.

From figure 4.18 observed that at 1000 rpm speed rate of erosion wear in the terms of weight loss increase 43.14% from 60 minutes to 150 minutes of the operation for handling 20% bottom ash, similarly weight loss increases 35.25% for handling 40% bottom ash and similarly weight loss increases 39.3% for handling 60% bottom ash.

From figure 4.19 seen that at 1400 rpm speed rate of erosion wear in the terms of weight loss increase 39.36% from 60 minutes to 150 minutes of the operation for handling 20% bottom ash, similarly weight loss increases 15.85% for handling 40% bottom ash and similarly weight loss increases 14.18% for handling 60% fly ash.

The results reveal that at lower concentration with variation of time of the operation more weight loss occurring as compared to higher concentration.

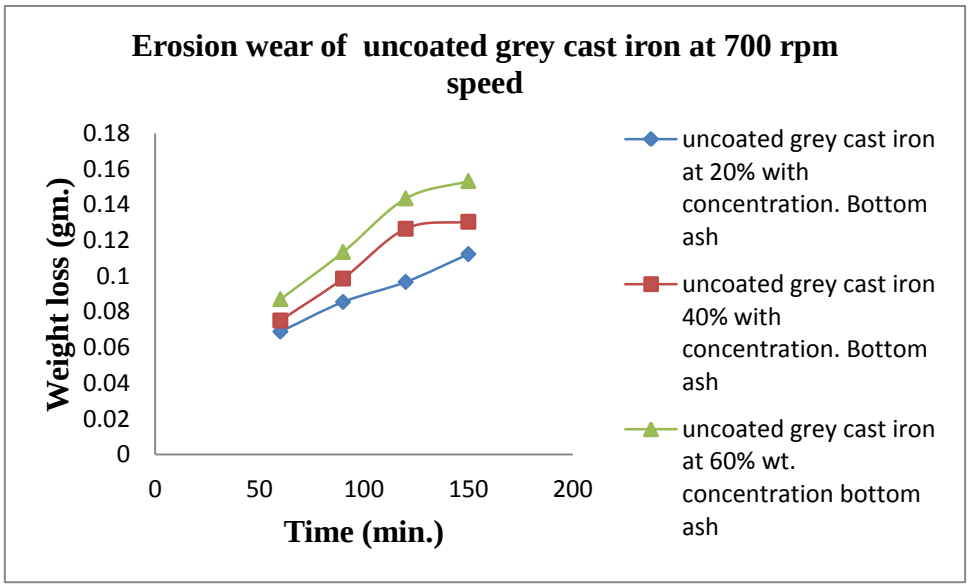

Figure 4.17 Erosion wear of uncoated grey cast iron at 700 rpm speed

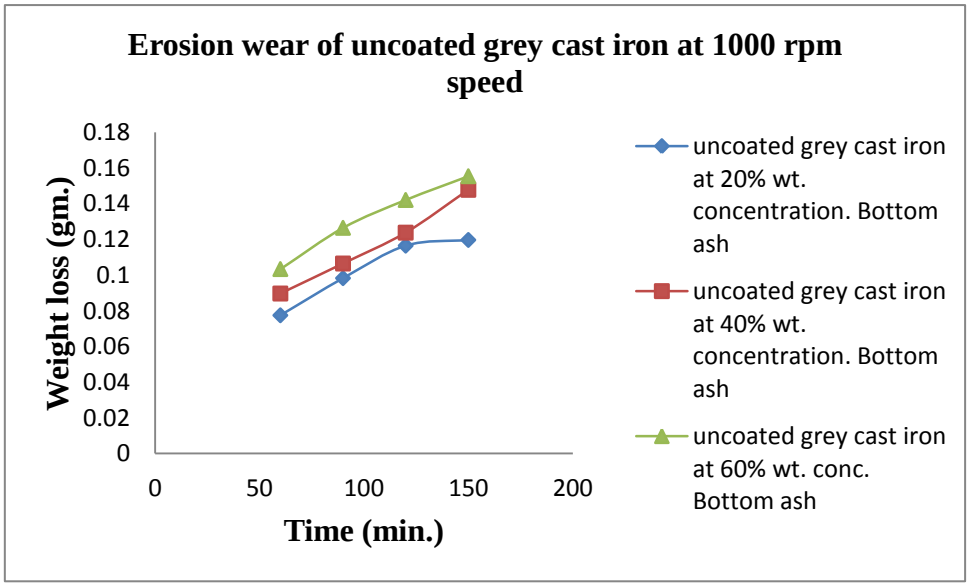

Figure 4.18 Erosion wear of uncoated grey cast iron at 1000 rpm speed

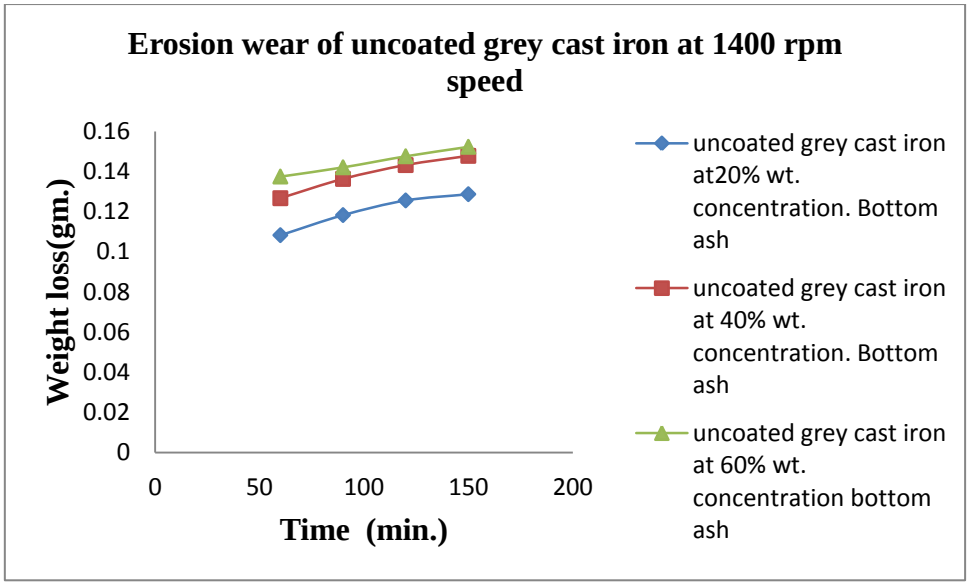

Figure 4.19 Erosion wear of uncoated grey cast iron at 1400 rpm speed

4.3.2Sem of uncoated grey cast iron

Figure 4.20-4.22 shows the SEM of grey cast iron at 1000X before and after wear. From figure 4.20 observed that before wear graphite structure of grey cast iron is clearly visible. From Figure 4.21 observed that at 1400 rpm speed bottom ash sticks along the edges of the graphite, indicates removal of graphite from the edges. Similarly from figure 4.22 observed that less fly ash particles stick along the graphite edges which leads to less wear rate.

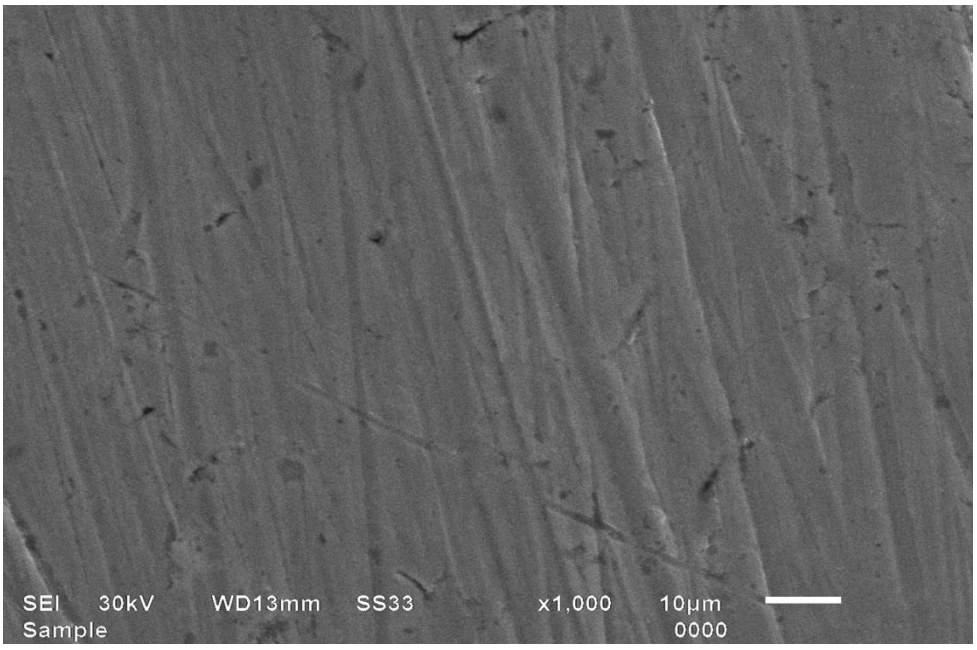

Figure 4.20 SEM of uncoated grey cast iron before wear

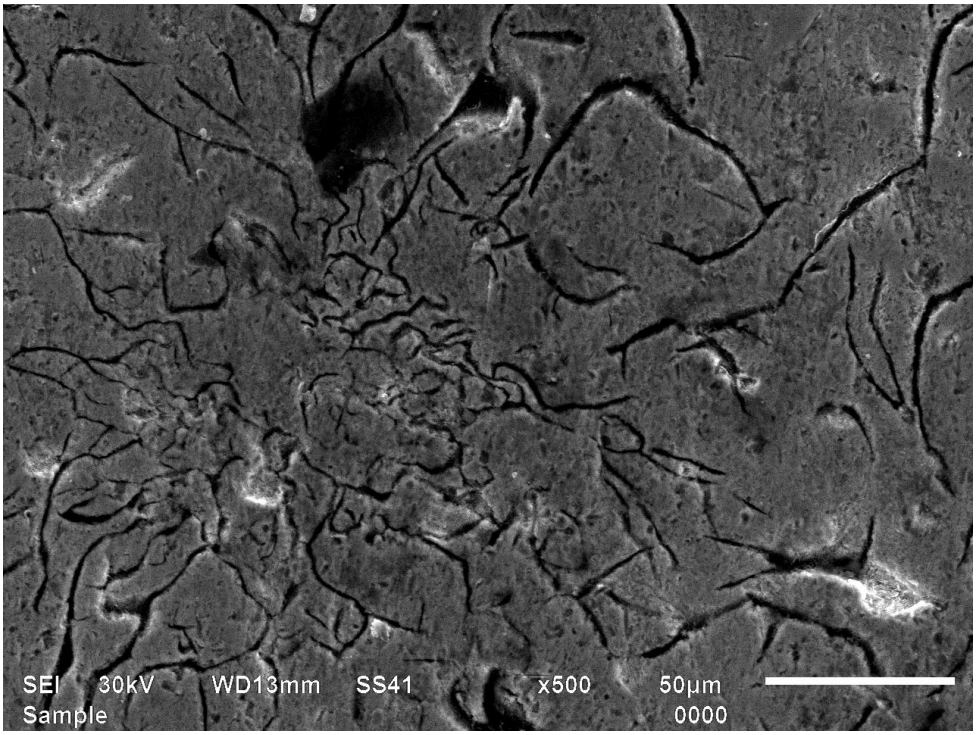

Figure 4.21 SEM of uncoated grey cast iron after wear at 1400 rpm speed 60% bottom ash

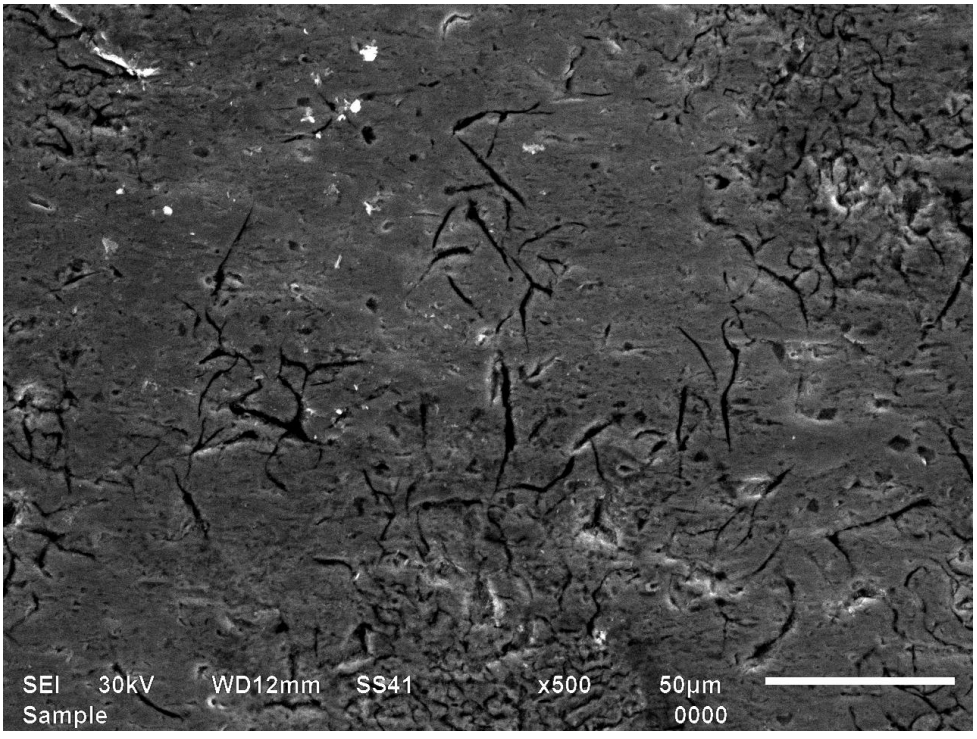

Figure 4.22 SEM of uncoated grey cast iron after wear at 1400 rpm speed 60% fly ash

.

4.4COATING TECGNIQUE FOR DUCTILE MATERIAL (ELECTROPLATING)

Electroplating is primarily used for depositing a layer of material to bestow a desired property (e.g., abrasion and wear resistance, corrosion protection, lubricity, aesthetic qualities, etc.) to a surface of the material. The anode and cathode in the electroplating cell are both connected to an external supply of direct current — a battery or, more commonly, a rectifier. The anode is connected to the positive terminal of the supply, and the cathode (article to be plated) is connected to the negative terminal .Electroplating can be defined as a plating process in which metal ions in a solution are moved by an electric field to coat an electrode. The process uses electrical current to reduce cations of a desired material from a solution and coat a conductive object with a thin layer of the material, such as a metal.

When the external power supply is switched on, the metal at the anode is oxidized from the zero valence state to form cations with a positive charge. These cations associate with the anions in the solution. The cations are reduced at the cathode to deposit in the metallic, zero valence state.

In this process, chromium plate is placed at anode and cast iron and steel 304 samples at cathode in a bath of chromium sulphate one by one. Chromic acid as sold is not truly chromic acid it actually chromium trioxide or chromium anhydride and is not an acid until it dissolved in water. Chromium trioxide dissolved in water and form chromic acid. As shown in figure 4.10**,** chromium is oxidized at the anode to Cr^{2+} by losing two electrons. The Cr^{2+} associates with the anion SO_4^{2-} in the solution to form. At the cathode, the Cr^{2+} is reduced to metallic chromium by gaining two electrons. The result is the effective transfer of chromium from the anode source to a grey cast iron and stainless steel 304 plates covering the cathode. Electroplating is also called electrode deposition. The electroplated plating metal is most normally a single metallic element, not an alloy. However, some alloys can be electro deposited.

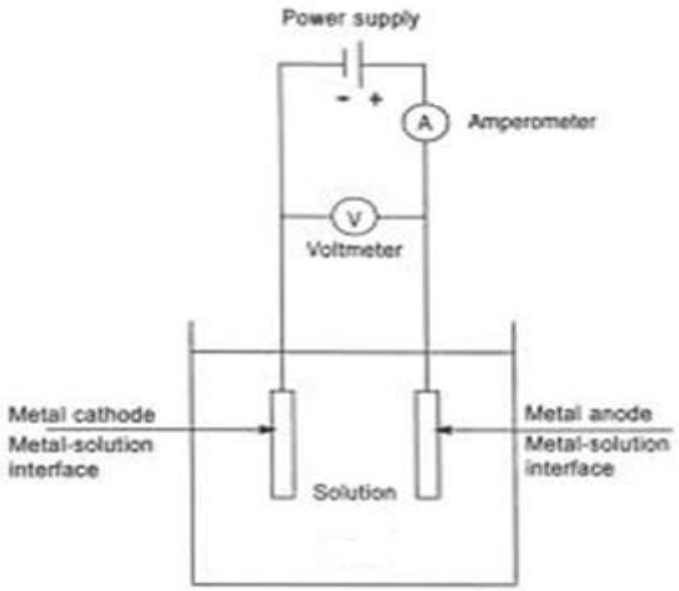

Figure 4.23 Schematic diagram of electroplating

4.4.1 Application of electroplating

Electroplating is used in many industries for function, corrosion control and/or decorative purposes. Chrome-plating of steel parts on automobiles and motorcycles is a common application of electroplating.

Other examples of electroplating applications are:

- Steel parts such as camshafts, crankshafts, and hand tools resists wear better when they are electroplated with chromium.
- Steel or aluminium parts in light fixtures are often electroplated with nickel and followed by chromium or brass.
- Common steel bolts, nuts, and washers are electroplated with a coating of zinc.
- Electroplating may deposit silver, copper or brass onto electrical connectors.

4.4.2 Electroplating caution

Not properly applying electroplating process and acid cleaning of springs, without proper baking treatment, can cause spring steels to become brittle, called "Hydrogen embrittlement " Nonferrous springs are immune do not share the same problem. In general, all electroplated

parts 1200 Mpa or higher should be baked at 190C for three hours or more within four hours after electroplating, to ensure Hydrogen embrittlement relief.

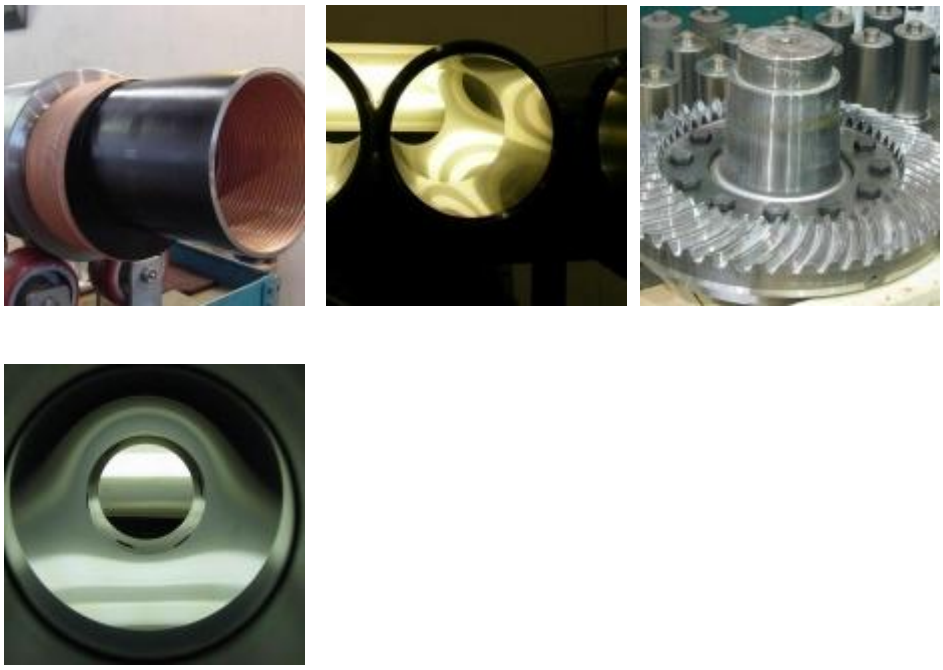

Figure 4.24 Electroplating done on internal surface of pipes and teeth's of the gear.

4.4.3 Effect of time, speed and concentration on coated grey cast iron and steel 304

Figure 4.25- 4.27 observed that erosion wear of coated steel 304 increases with time of operation 60 to 150 minutes and between 120 to 150 minute rate of erosion wear increases very slowly as compared to time of operation between 60 to 120 minutes. It is also observed that rate of erosion wear increases with the changing the concentration of bottom ash and with the changing the speed.

From figure 4.25 noted that at 700 rpm speed rate of erosion wear in the terms of weight loss increase 50.10% from 60 minutes to 150 minutes of the operation for handling 20% bottom ash, similarly weight loss increases 41.9% for handling 40% bottom ash and similarly weight loss increases 30.5% for handling 60% bottom ash.

From figure 4.26 noted that at 1000 rpm speed rate of erosion wear in the terms of weight loss increase36.16% from 60 minutes to 150 minutes of the operation for handling 20% bottom ash, similarly weight loss increases 29.19% for handling 40% bottom ash and similarly weight loss increases 14.44% for handling 60% bottom ash.

From figure 4.27 noted that at 1400 rpm speed rate of erosion wear in the terms of weight loss increase 32% from 60 minutes to 150 minutes of the operation for handling 20% bottom ash, similarly weight loss increases 16.68% for handling 40% bottom ash and similarly weight loss increases 14.92% for handling 60% bottom ash.

The results reveal that at lower concentration with variation of time of the operation more weight loss occurring as compared to higher concentration.

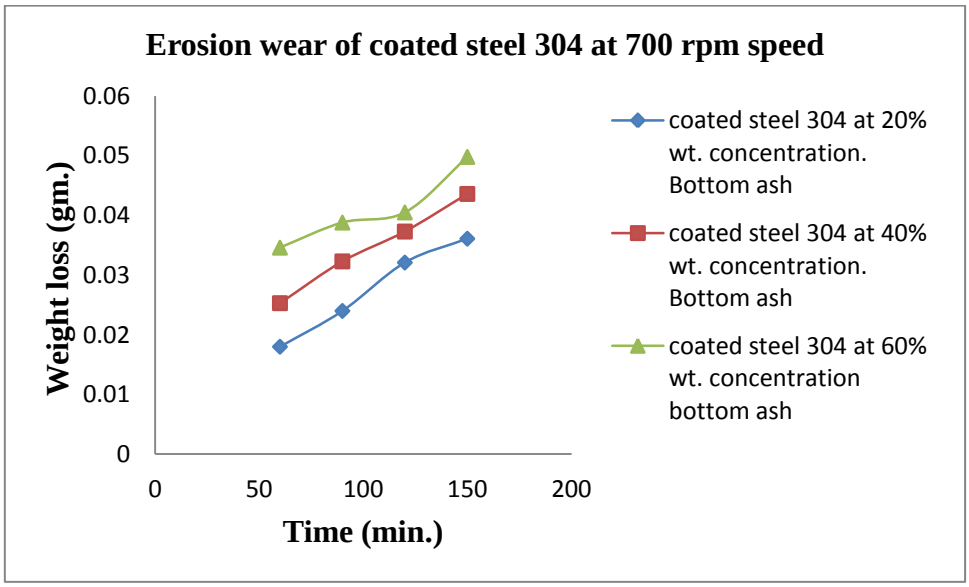

Figure 4.25 Erosion wear of coated steel 304 at 700 rpm speed

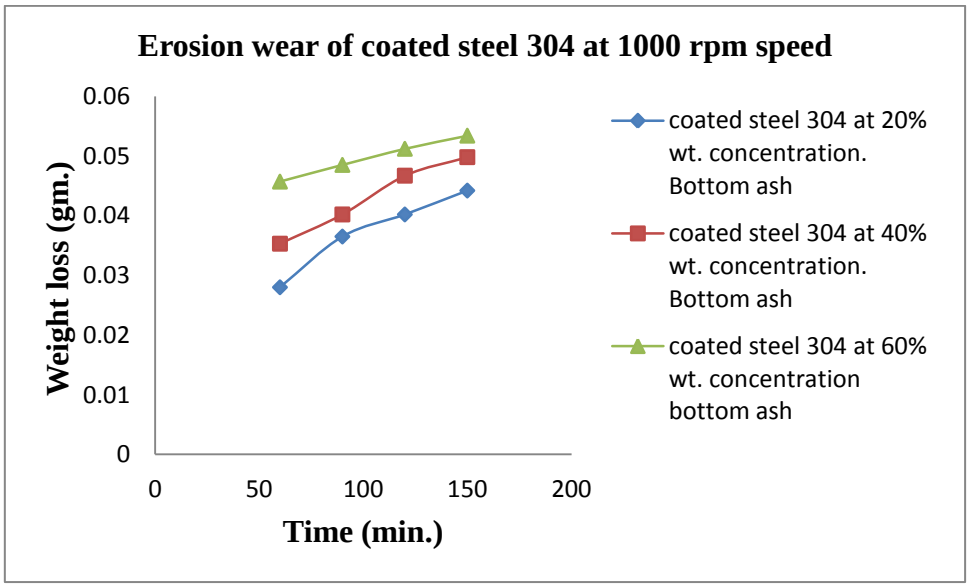

Figure 4.26 Erosion wear of coated steel 304 at 1000 rpm speed

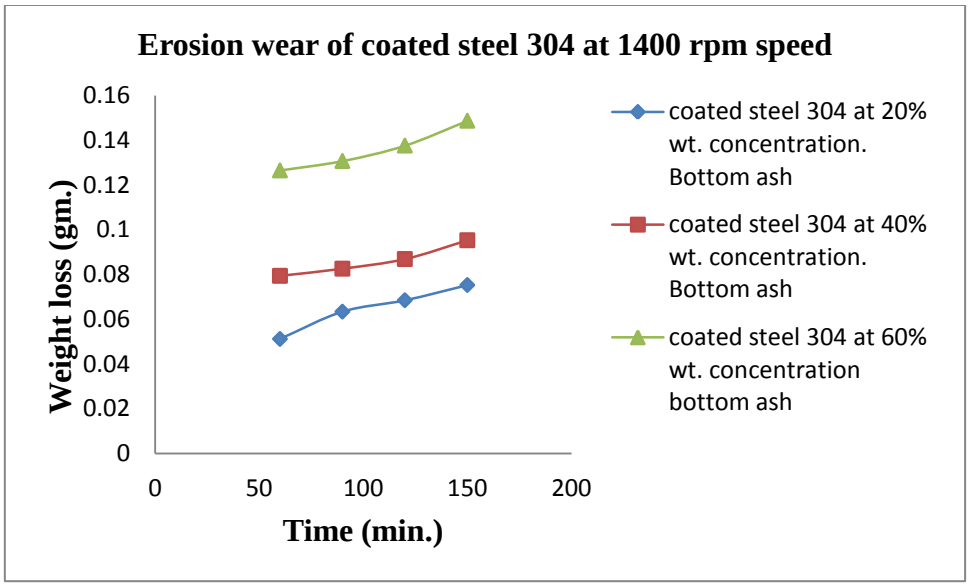

Figure 4.27 Erosion wear of coated steel 304 at 1400 rpm speed

Figure 4.28- 4.30 observed that erosion wear of coated grey cast iron increases with time of operation 60 to 150 minutes and between 120 to 150 minute rate of erosion wear increases very slowly as compared to time of operation between 60 to 120 minutes. It is also observed that rate of erosion wear increases with the changing the concentration of bottom ash and with the changing the speed.

From figure 4.28 seen that at 700 rpm speed rate of erosion wear in the terms of weight loss increase 76.28% from 60 minutes to 150 minutes of the operation for handling 20% bottom ash, similarly weight loss increases 61.7% for handling 40% bottom ash and similarly weight loss increases 60% for handling 60% bottom ash.

From figure 4.29 observed that at 1000 rpm speed rate of erosion wear in the terms of weight loss increase 56% from 60 minutes to 150 minutes of the operation for handling 20% bottom ash, similarly weight loss increases 55% for handling 40% bottom ash and similarly weight loss increases 45% for handling 60% bottom ash.

From figure 4.30 noted that at 1400 rpm speed rate of erosion wear in the terms of weight loss increase 48% from 60 minutes to 150 minutes of the operation for handling 20%

bottom ash, similarly weight loss increases 35% for handling 40% bottom ash and similarly weight loss increases 39% for handling 60% bottom ash.

The results reveal that at lower concentration with variation of time of the operation more weight loss occurring as compared to higher concentration

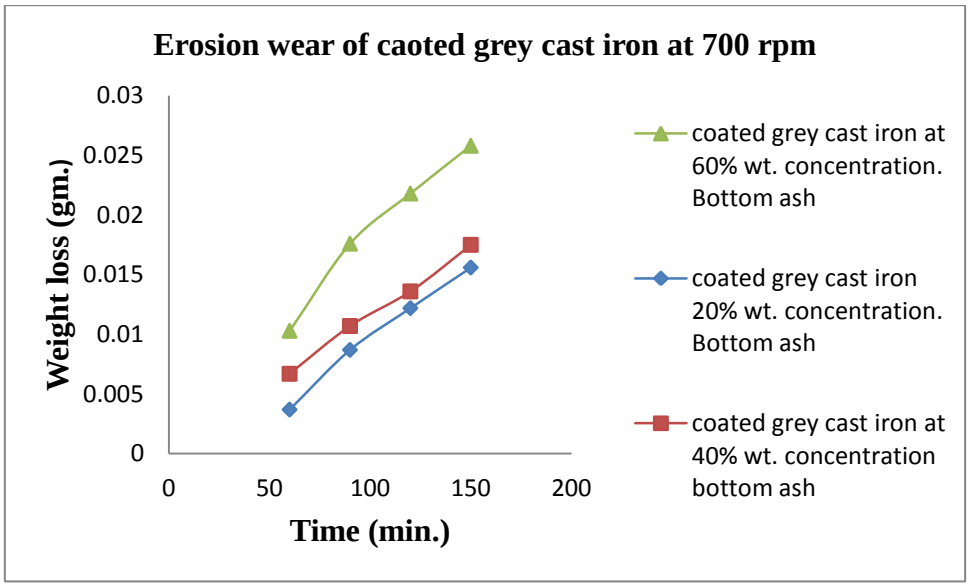

Figure 4.28 Erosion wear of coated grey cast iron 304 at 700 rpm speed

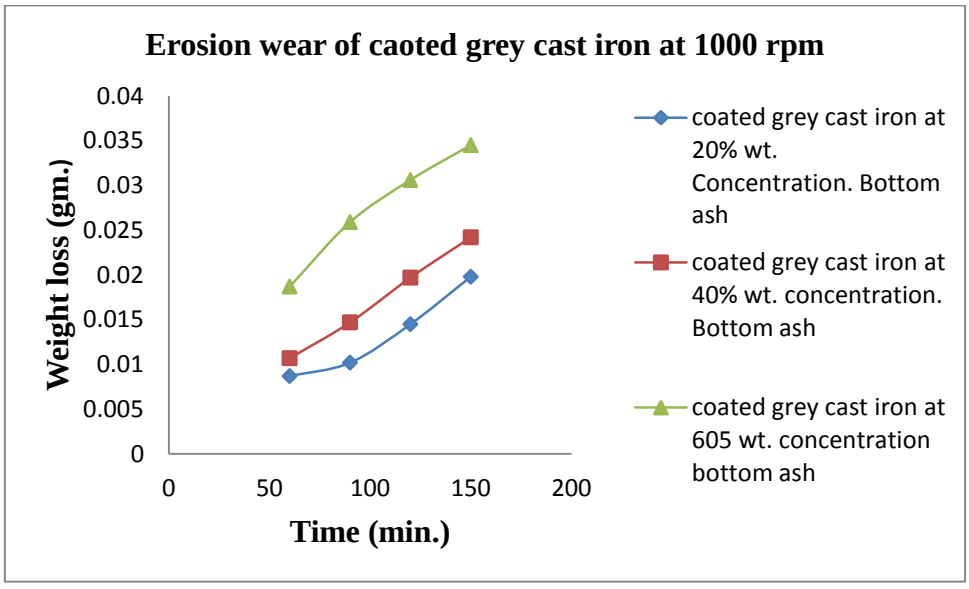

4.29 Erosion wear of coated grey cast iron 304 at 1000 rpm speed

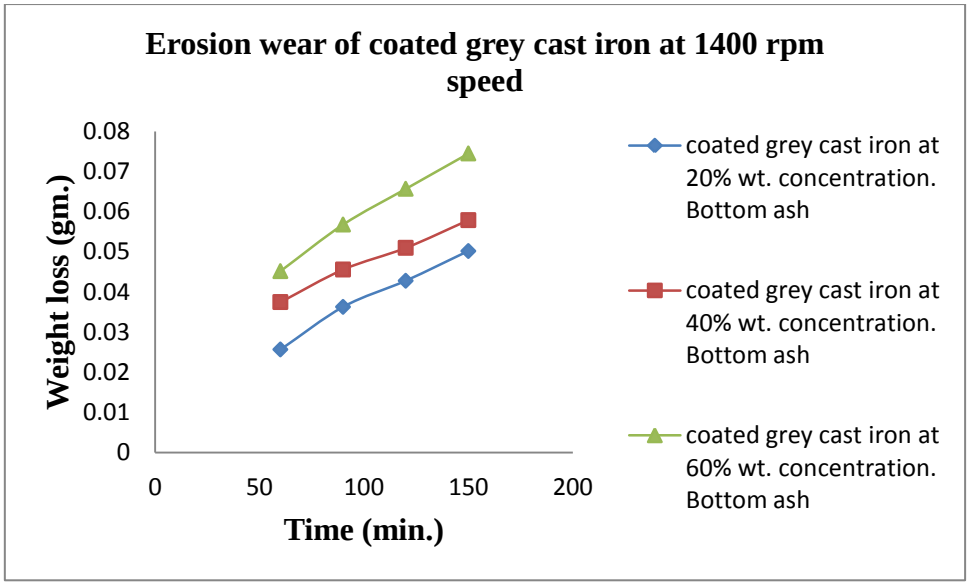

Figure 4.30 Erosion wear of coated grey cast iron 304 at 1400 rpm speed

4.4.4 SEM of coated steel 304 and grey cast iron

From figure 4.31 -4.34 observed clearly coating on the surface of grey cast iron and steel 304 before wear after wear there is an indication of some white spots as shown in the figure 4.33 it indicates removal of bottom ash from the surface due to the attack of bottom ash. Similarly from figure 4.34 observed large creators indicates removal coating layer due to the attack of bottom ash on the surface.

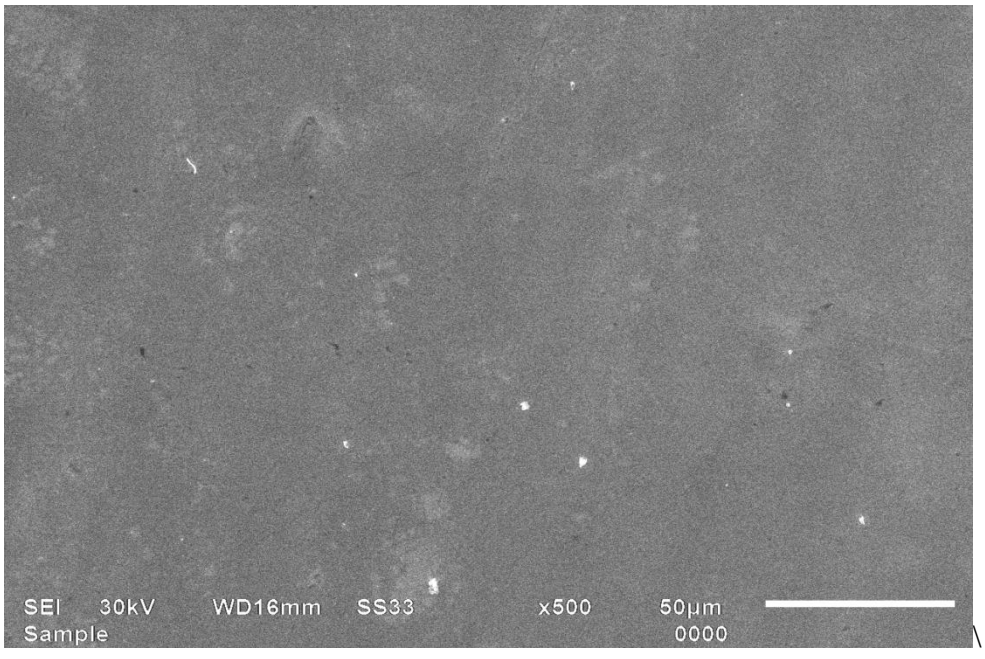

Figure 4.31 SEM of coated grey cast iron before wear

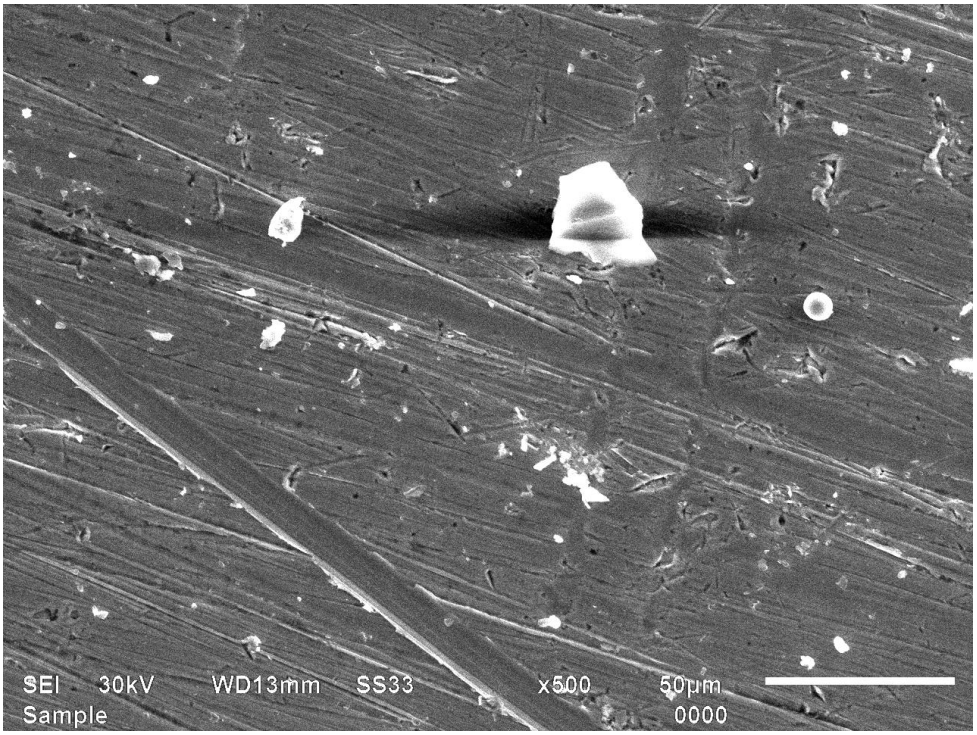

Figure 4.32 SEM of coated grey cast iron after wear

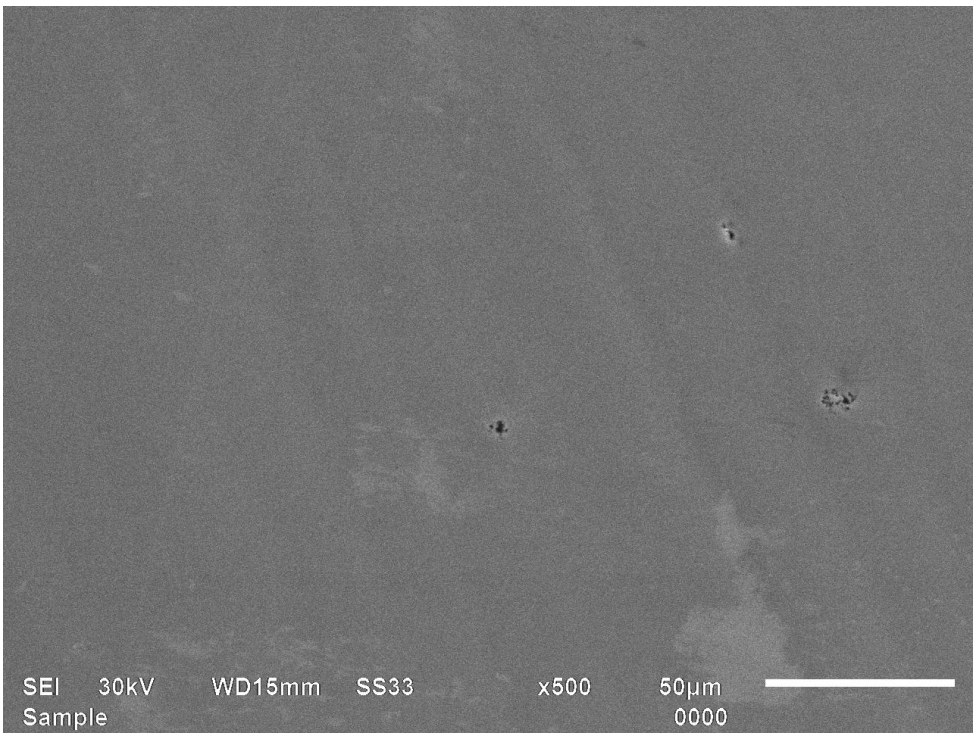

Figure 4.33 SEM of coated steel 304 before wear

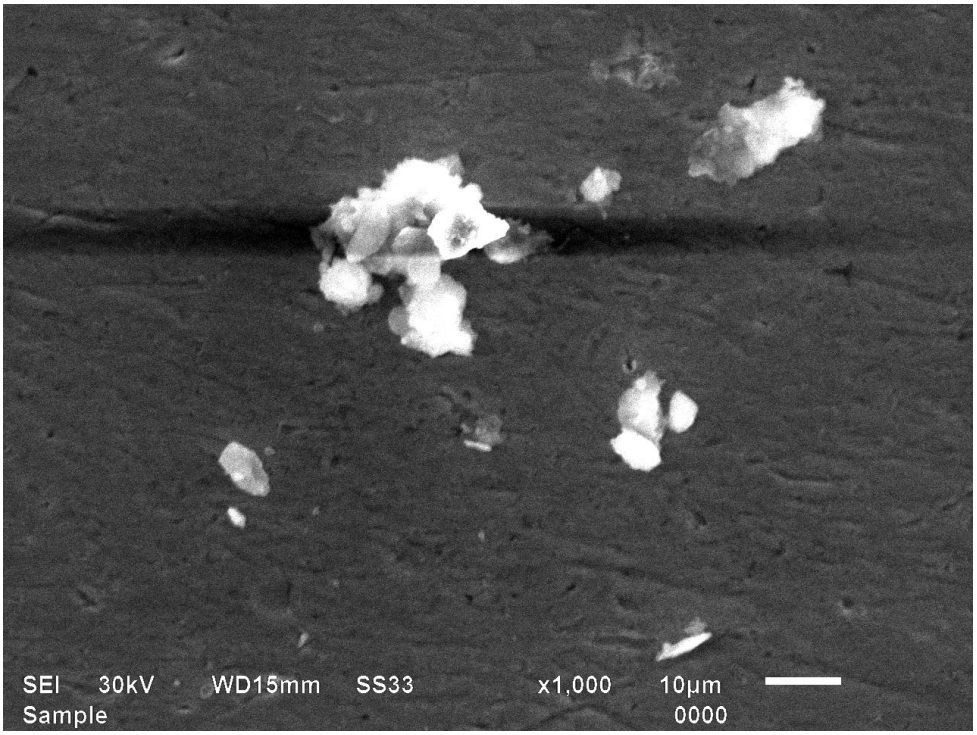

Figure 4.34 SEM of coated steel 304 after wear

CHAPTER 5
EVALUATION OF FRICTION WEAR OF DUCTILE MATERIAL

5.1 FRICTION WEAR

When two nominally flat surfaces are placed in contact under load, the contact takes place at the tips of the asperities and the load is supported by the deformation of contacting asperities, and the discrete contact spots (junctions) are formed. When these two surfaces move relative to each other, a lateral force is required to overcome adhesion. This force is referred to as adhesion friction. The adhesion strength depends upon the mechanical properties and the physical and chemical interaction of the contacting bodies. The adhesion strength is reduced by reducing surface interactions at the interface. The resistance to motion whenever one solid slide over another solid is known as friction wear.

Wear is a process of removal of material from one to another when in contact. As the wear is surface removal phenomena and occurs mostly at outer surface, it is more appropriate and economical to make surface modification of existing alloy than using the wear resistance alloy.

5.1.1 Experimental Procedure for Friction Wear

Dry sliding wear test for different number of specimen was conducted with the help of pin on disc machine (Model: Wear and Friction monitor TR-20) made by the DUCOM, as shown in the figure 5.1. The pin was held against the counter surface of sliding disc (EN 32 steel disc) with wear track of diameter 60mm. The pin was loaded against the disc through a dead weight load system. The wear test of specimen (Steel 304 and Grey cast iron) was treated under the load of 2 kg, 3 kg, 4 kg, 5 kg, and at a speed of 200, 400, 600, 800 rpm. The sample used was of 8mm dia. and 3.75cm in length. The surface of the pin was slide against the emery paper of grit size (80) prior to test in order to ensure effective contact of fresh and flat surface with the steel disc. The samples and wear track was cleaned with the help of acetone before experiment. The wear rate was expressed in the terms of weight loss (gm).

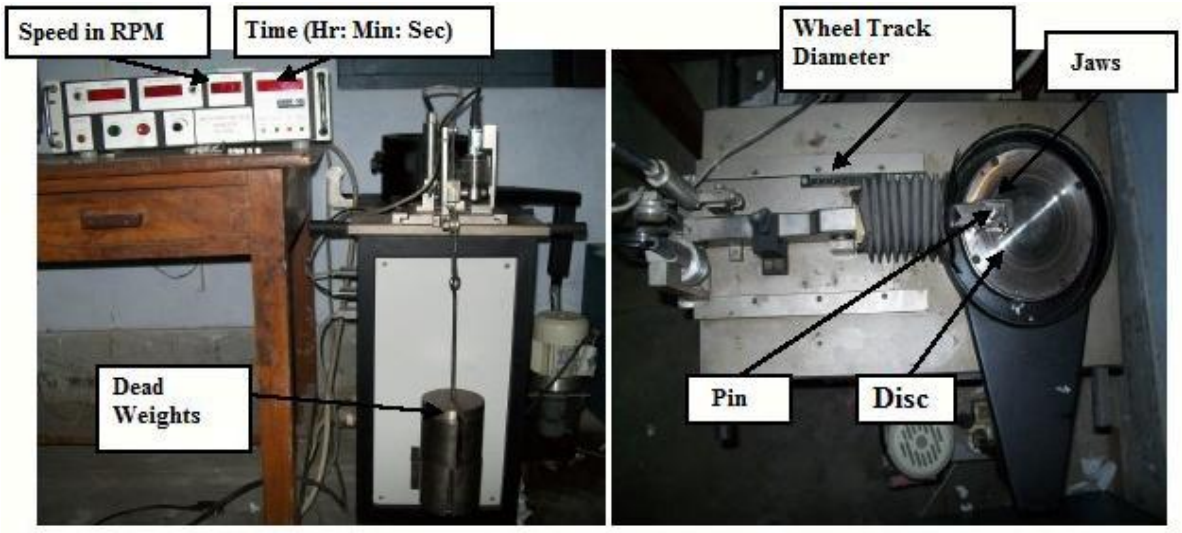

Figure 5.1 Sliding wear apparatus

In this study pin on disc was used to study the tribological characterization. The test procedure is as follow:

- Initially the surface of the pin was made flat such that it will support load over its entire cross section called first stage. This was achieved by surfaces of the pin sample ground using emery paper (80 grit size) prior to test.
- Run in wear was performed in the next stage / second stage. This stage avoids initial turbulent period associated with friction wear curves,
- Final stage / third stage are the actual testing called constant / steady state wear stage. This stage is the dynamic competition between material transfer processes (transfer of material from pin onto disc and formation of wear debris).
- One of the major precautions taken while performing experiment that both the pin and disc must be cleaned with the acetone and applied load must be in the normal direction.

5.2 PARAMETER AFFECTING SLIDING WEAR

Friction wear affected by no. of parameters, one of them is lubrication as lubricants can drastically change the friction and wear characteristics of sliding system and also capable of altering the nature of surface interaction between contacting solids. The functions of solid lubricants are same as that of liquids, that is, separation of surfaces and provision of shear path within the interface. Under extreme pressure conditions, the lubricant film can become

thin enough to allow direct contact between solids. In boundary lubrication, any separation of surfaces depends on molecules adhered to the surface rather than on a continuous oil film.

Second parameter affecting the friction wear is load. Load is directly related to the weld junction as load increases the area of weld junction increase it results in adhesion. As load increases physical failure of metal occurs at the interface due to bulk failure. In general, at low velocities and load friction increases with an increase of speed and it decreases at high speeds and loads. With hard materials such as steel, friction increases with an increase of roughness and load whereas, for soft materials such as rubber, fibre and nylon friction decreases with an increase of load.

Third parameter is sliding speed they control the degree of adhesion (metallic intimacy), sub-surface damage, thermo-mechanical effects on the sliding surface. As more sliding speed more frictional heat will generate results in tendency to break the oxide film. With increase in sliding speed and load wear rate increases it may show either linear or non-linear behaviour.

5.3 EVALUATION OF FRICTION WEAR

The most common methods of studying the wear consists of examination of sliding material before and after the test, any difference in material is attributed to wear. The detection of wear generally uses one or the other techniques of weighing, mechanical gauging, and examination of surface and sub-surface features and wear debris. Wear rate can be determined by one of the simplest method is weighing technique in which specimen is weighed before and after running, using weighing balances of accuracy 0.1 mg and weight loss is calculated to get wear rate. Second method is gauging in this method wear is measured by decrease in dimensions i.e. length using venire calliper or electrical system based on linear variable displacement transducer (LVDT) principle of resolution limit about 10^{-5} m. Third one method is optical technique in this method make small micro-hardness indentation on a surface where it slides and to study how its size is reduced during the sliding.

5.3.1. Evaluation of friction wear of steel 304

A pin on disc tribometer is used to perform the wear experiment. The wear tracks, alloy and specimen is cleaned with acetone before performing the experiment. Each specimen is weighted using a digital weighing balance having an accuracy of 0.0001gm. For experiments we have used parameters: speed 200, 400, 600, 800 rpm, weights: 2, 3, 4, 5 kg. And time: 15, 20, 25, 30min. under room temperature.

From figure 5.2-5.5 observed that friction wear of steel 304 increases with time of operation 15 to 30 minutes and between 25 to 30 minute rate of friction wear increases very slowly as compared to time of operation between 15 to 25 minutes. It is also observed that rate of friction wear increases with the changing the load and with changing the speed.

From figure 5.2 seen that at 200 rpm speed rate of friction wear in the terms of weight loss increase 94.33% from 15 minutes to 30 minutes of the operation for handling 2kg weight, similarly weight loss increases 79.94% for handling 3kg weight, similarly weight loss increases 93.36% for handling 4kg weight and similarly weight loss increases 85.54% for handling 5kg weight.

From figure 5.3 observed that at 400 rpm speed rate of friction wear in the terms of weight loss increase 96.28% from 15 minutes to 30 minutes of the operation for handling 2kg weight, similarly weight loss increases 59.74% for handling 3kg weight, similarly weight loss increases 53.17% for handling 4kg weight and similarly weight loss increases 46.10% for handling 5kg weight

From figure 5.4 seen that at 600 rpm speed rate of friction wear in the terms of weight loss increase 51.99% from 15 minutes to 30 minutes of the operation for handling 2kg weight, similarly weight loss increases 45.61% for handling 3kg weight, similarly weight loss increases 51.29% for handling 4kg weight and similarly weight loss increases 48% for handling 5kg weight.

From figure 5.5 noted that at 800 rpm speed rate of friction wear in the terms of weight loss increase 69.04% from 15 minutes to 30 minutes of the operation for handling 2kg weight, similarly weight loss increases 59.56% for handling 3kg weight, similarly weight loss increases 60.73% for handling 4kg weight and similarly weight loss increases 67.72% for handling 5kg weight

The results reveal that at lower weight with variation of time of the operation more weight loss occurring as compared to higher weight.

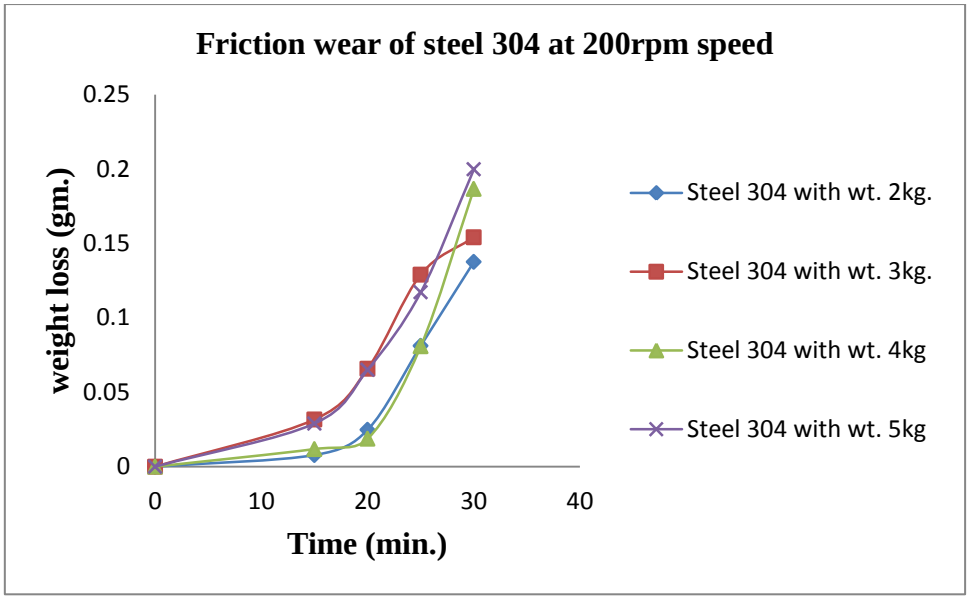

Figure 5.2 Friction wear of steel 304 at 200 rpm speed

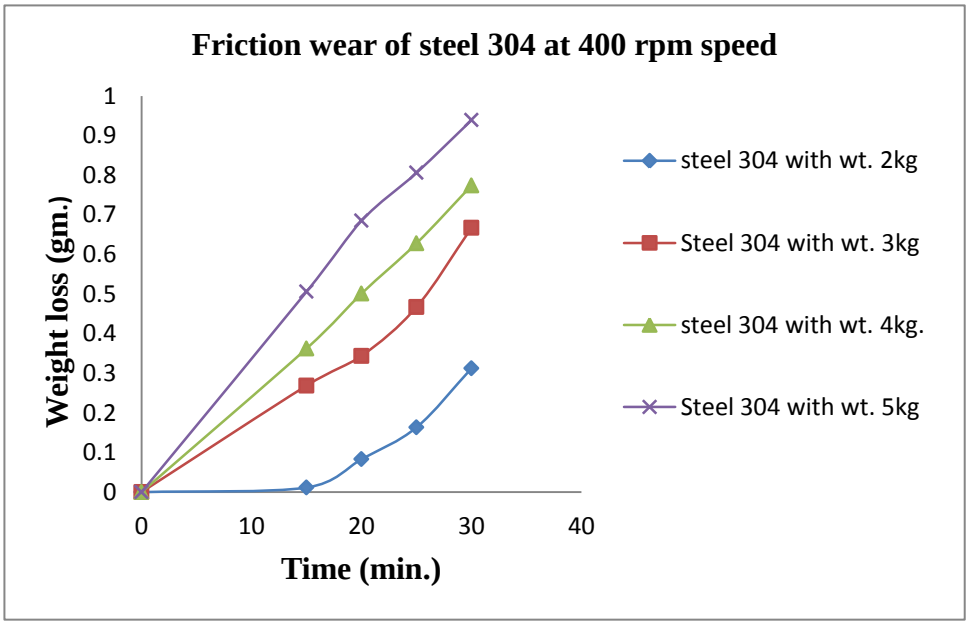

Figure 5.3 Friction wear of steel 304 at 400 rpm speed

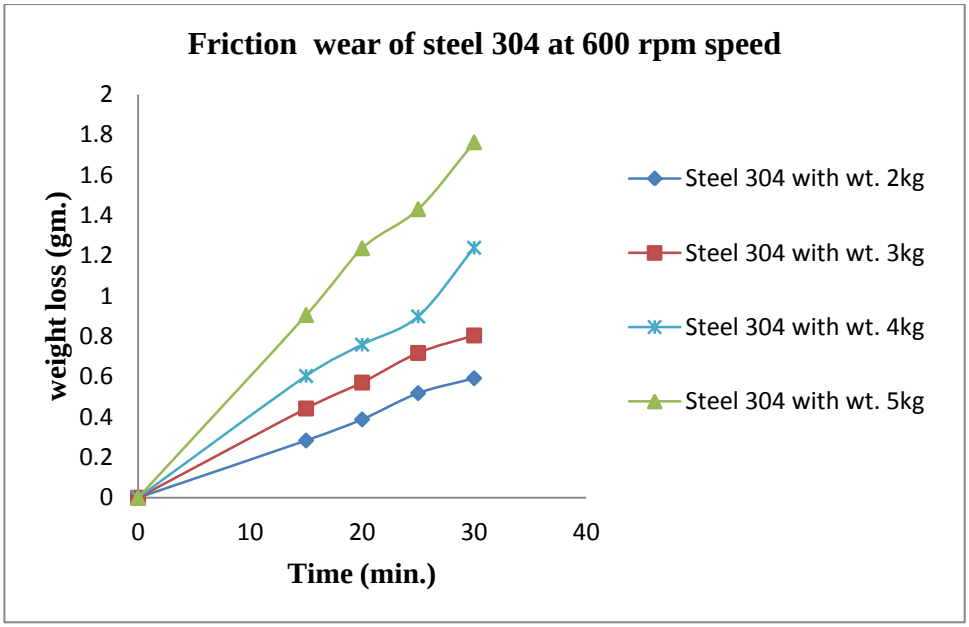

Figure 5.4 Friction wear of steel 304 at 600 rpm speed

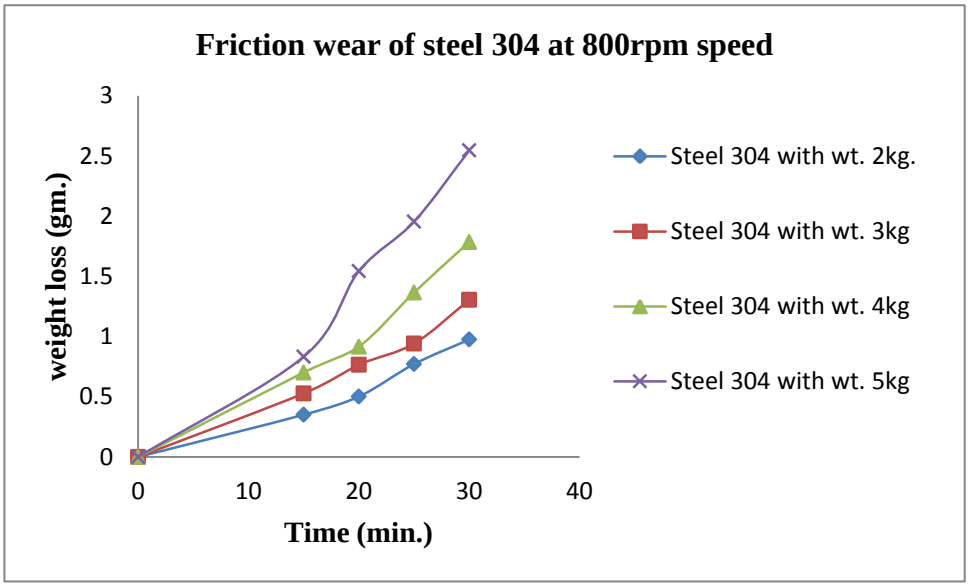

Figure 5.5 Friction wear of steel 304 at 800 rpm speed

5.3.2 Evaluation of friction wear of grey cast iron

Friction wear behaviour of grey cast iron was calculated on the pin on disc apparatus. Each specimen is weighted before and after the test using a digital weighing balance having an accuracy of 0.0001gm. The wear tracks, alloy and specimen are cleaned with acetone before performing the

experiment. For experiments we have used parameters: speed 200, 400, 600, 800rpm, weights: 2, 3, 4, 5 kg. And time: 15, 20, 25, 30min. under room temperature.

From figure 5.6-5.9 observed that friction wear of grey cast iron increases with time of operation 15 to 30 minutes and between 25 to 30 minute rate of friction wear increases very slowly as compared to time of operation between 15 to 25 minutes. It is also observed that rate of friction wear increases with the changing the load and with changing the speed.

From figure 5.6 seen that at 200 rpm speed rate of friction wear in the terms of weight loss increase 26.3% from 15 minutes to 30 minutes of the operation for handling 2kg weight, similarly weight loss increases 55.2% for handling 3kg weight, similarly weight loss increases 53.8% for handling 4kg weight and similarly weight loss increases 48.54% for handling 5kg weight.

From figure 5.7 noted that at 400 rpm speed rate of friction wear in the terms of weight loss increase 18.3% from 15 minutes to 30 minutes of the operation for handling 2kg weight, similarly weight loss increases 36.5% for handling 3kg weight, similarly weight loss increases 29.74% for handling 4kg weight and similarly weight loss increases 40% for handling 5kg weight

From figure 5.8 seen that at 600 rpm speed rate of friction wear in the terms of weight loss increase 24 from 15 minutes to 30 minutes of the operation for handling 2kg weight, similarly weight loss increases 20.8% for handling 3kg weight, similarly weight loss increases 37.7% for handling 4kg weight and similarly weight loss increases 55% for handling 5kg weight.

From figure 5.9 observed that at 800 rpm speed rate of friction wear in the terms of weight loss increase 34.4% from 15 minutes to 30 minutes of the operation for handling 2kg weight, similarly weight loss increases 50.4% for handling 3kg weight, similarly weight loss increases 34.4% for handling 4kg weight and similarly weight loss increases 42.2% for handling 5kg weight

The results reveal that at lower weight with variation of time of the operation less weight loss occurring as compared to higher weight.

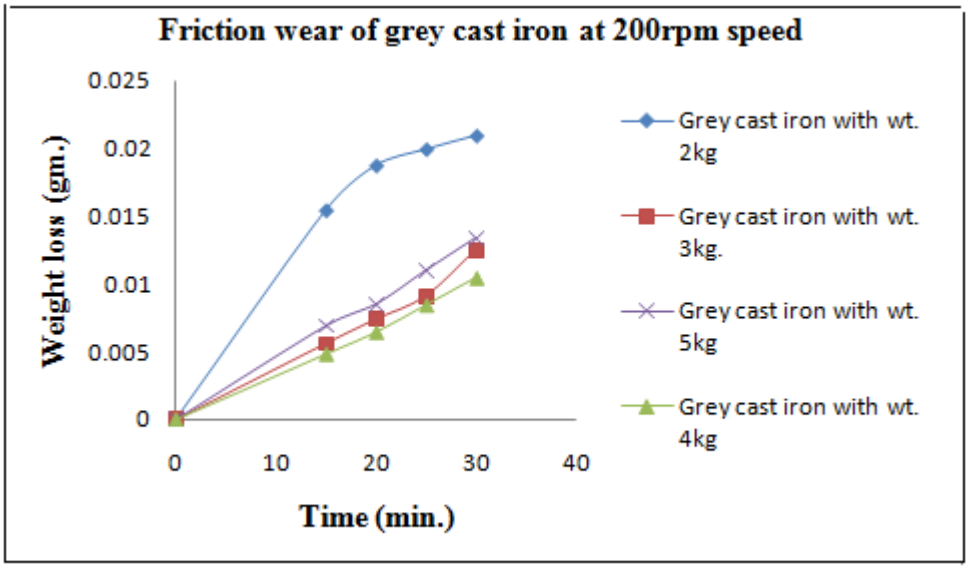

Figure 5.6 Friction wear of grey cast iron at 200 rpm speed

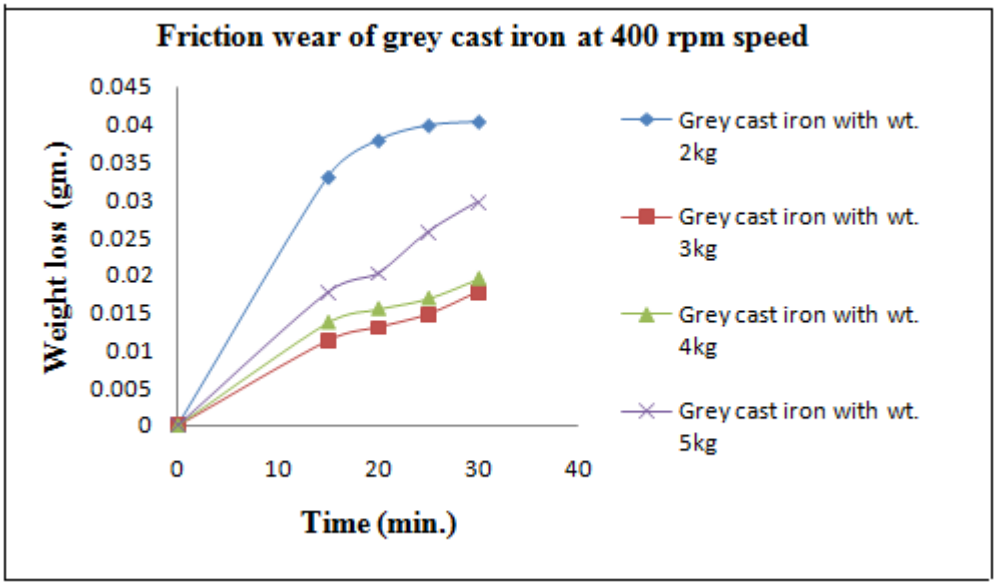

Figure 5.7 Friction wear of grey cast iron at 400 rpm speed

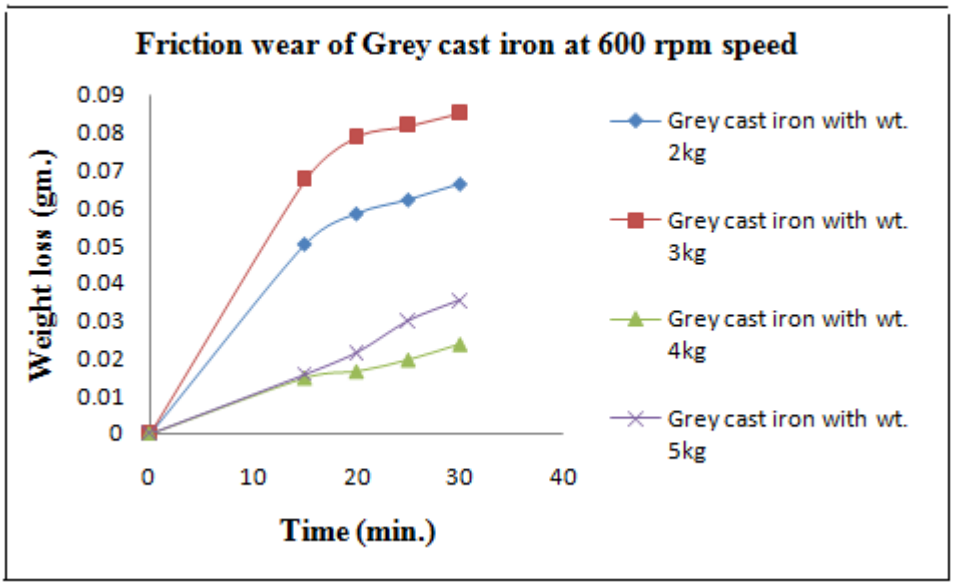

Figure 5.8 Friction wear of grey cast iron at 600 rpm speed

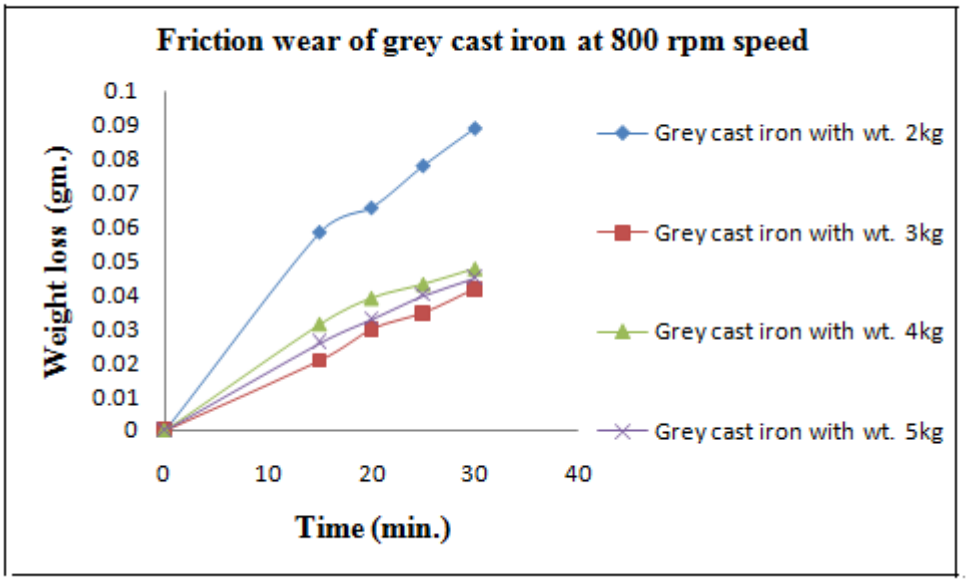

Figure 5.9 Friction wear of grey cast iron at speed 800 rpm

5.3.3 SEM of steel 304 and grey cast iron

Figure 5.10-5.13 shows the SEM of steel 304 and grey cast iron before and after friction wear.

From figure 5.11 observed that after friction wear at 800 rpm speed with 5kg load deep wear tracks formed on the surface of steel 304, indicates removal of the material. From figure 5.13 observed wear tracks indication of removal of graphite structure from the grey cast iron.

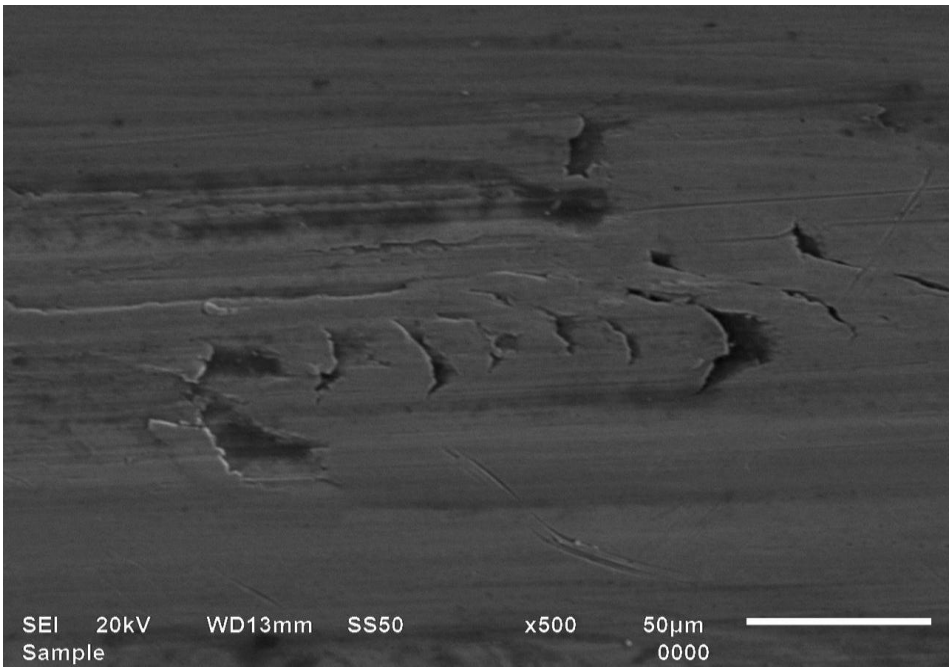

Figure 5.10 SEM of steel 304 before friction wear

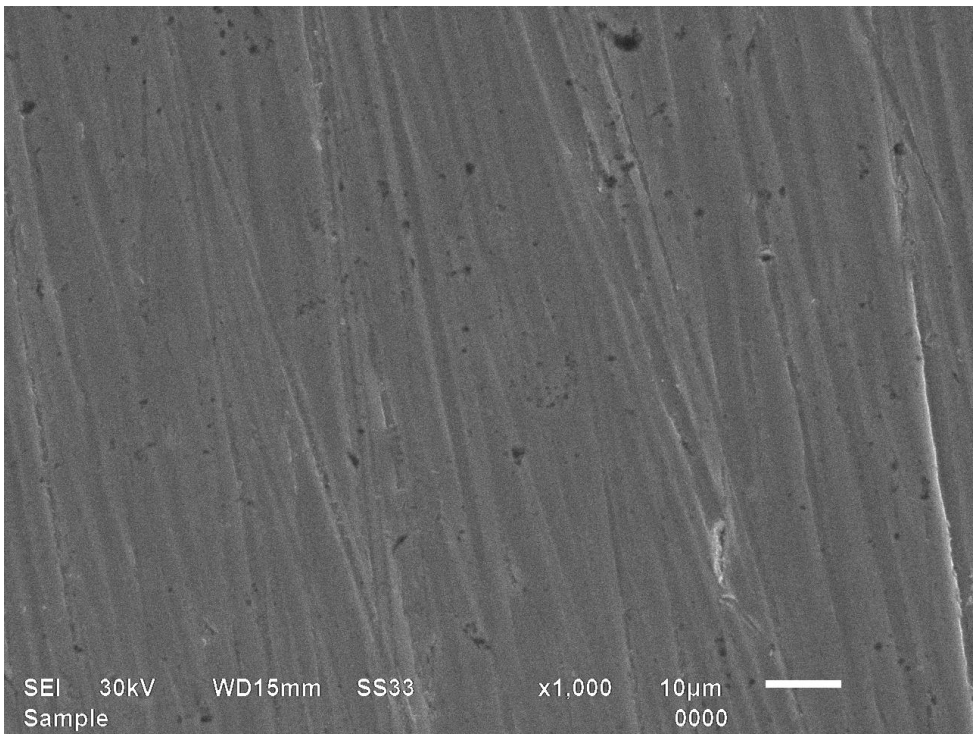

Figure 5.11 SEM of steel 304 after friction wear at 800 rpm speed

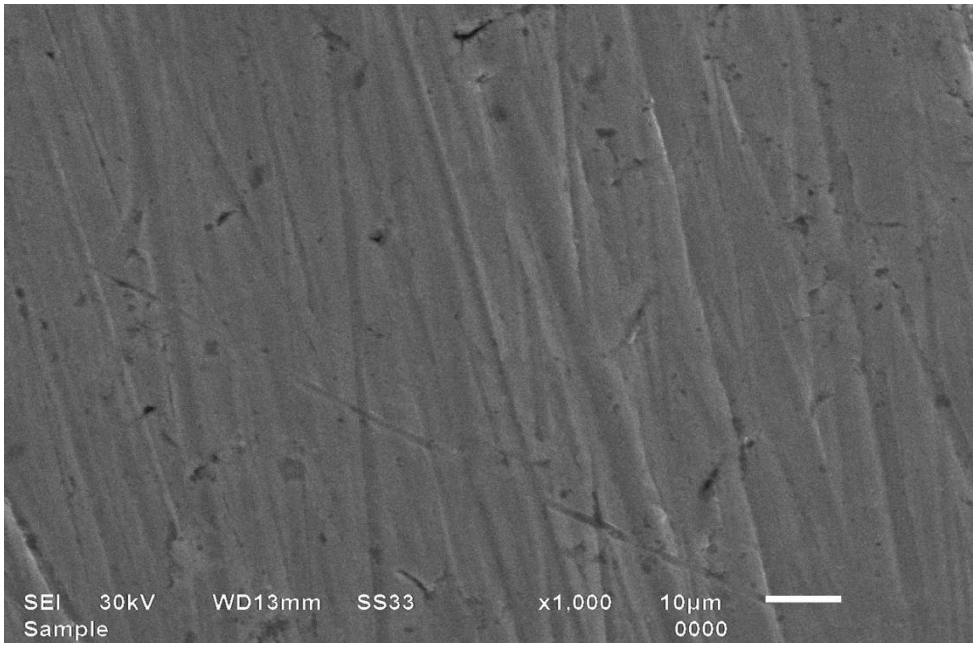

Figure 5.12 SEM of grey cast iron before friction wear

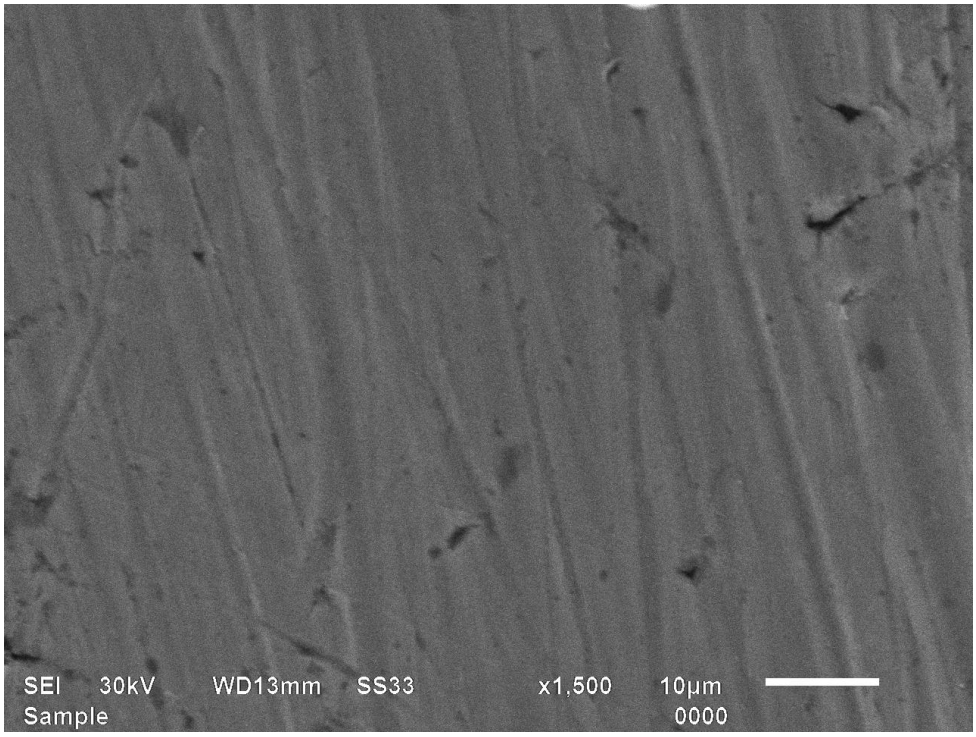

Figure 5.13 SEM of grey cast iron after friction wear at 800 rpm speed

CONCLUSION

- Erosion wear is a serious problem in slurry pumps and slurry transportation pipe line and friction wear is in ball bearing, cylinder head and piston. The choice of new material for working elements firstly considers improvement in its construction and needs to investigate its working life. The grey cast iron and steel 304 selected as a base material for pumps, pipes, and ball bearing. The electroplating technique is used for coating of chromium hard as a base material. From the experiment it is observed that erosion pot tester TR-41 used for the evaluation of the erosion wear of material in terms of loss of material by weight.
- From the experiment evaluation it is observed that erosion wear of ductile material (steel 304 and grey cast iron) is a function of time of operation, speed of evaluation and concentration of the bottom and fly ash slurry.
- It is also observed that friction wear of ductile material (steel 304 and grey cast iron) is a function of time of operation, speed of evaluation and weight of the load. It is also reveals that with coating (chromium hard) on the ductile materials rate of erosion wear decreases rapidly.
- Chromium coated steel shows approximately 1.5 times better performance than uncoated steel. Similarly chromium coated grey cast iron shows approximately 2.5 times better performance than uncoated grey cast iron.

FUTURE SCOPE

- The erosion wear studies can be performed with other coating techniques.
- The computational approach can be used to simulate the similar work with different operating conditions.
- The effect of erosion wear of pump impeller of ash disposal system can be studied.
- The similar erosion wear studies can be extended by using other types of pot tester and different slurry concentration.
- The friction wear studies can be performed on other type of testers at different parameters.

REFERENCES

1. M. Panayotova, (2000), “Deposition of Fe–C alloy on structural steel and cast iron for repair of worn machine parts”. Surface and Coatings Technology, vol. 124, pp. 266–271.

2. Harry H. Tian and Graeme R. Addie, (2005), “Experimental study on erosive wear of some metallic materials using Coriolis wear testing approach”, Wear, vol.258, pp. 458–469.

3. LI Xiao-yan and LU Tao, (2005), “Analysis of corrosion behaviour of petrochemical pipe elbow”. Journal of central south university technology, vol.12, pp. 119-123.

4. Shimizu, T. Naruse, Y. Xinba and K. Kimura, (2006), “Erosive wear properties of high V–Cr–Ni stainless spheroidal carbides cast iron at high temperature”. Wear, vol.267, pp. 104–109.

5. T. Manisekaran, M. Kamaraj, S.M. Sharrif and S.V. Joshi, (2006), “Slurry Erosion Studies on Surface Modified 13Cr-4Ni Steels”. Effect of Angle of Impingement and Particle Size ASM International, vol. 35, pp. 1059-9495.

6. B.S. Mann, VivekArya, A.K. Maiti, M.U.B. Rao, (2006), “Corrosion and erosion performance of HVOF/TiAlN PVD coatings and candidate materials for high pressure gate valve application”. Wear, vol. 260, pp. 75-82.

7. K. Yıldızlı, M.B. Karamıs and F. Nair, (2006), “Erosion mechanisms of nodular and gray cast irons at different impact angles”. Wear, Vol. 261, pp. 622–633.

8. Harpreet Singh, Buta Singh Sidhu and D.Puri, (2007), “Wear and oxidation behaviour of shrouded plasma sprayed fly ash coatings” .Tribology International, vol.40, pp.800–808.

9. Girish R. Desale, Bhupendra K. Gandhi and S.C. Jain, (2008), “Slurry erosion of ductile materials under normal impact condition”. Wear, vol.264, pp.322–330.

10. M.N. Noui-Mehidi , L.J.W. Graham, J. Wu, B.V. Nguyen and S. Smith,(2008), "Study of erosion behaviour of paint layers for multilayer paint technique applications in slurry erosion", Wear, vol. 264, pp. 737–743.

11. S.C.Mishra, S.Prahara and AlokSatpathy, (2009), "Evaluation of erosion wear of a ceramic coating with Taguchi approach". Manufacturing Engineering, vol.4, pp.234-244.

12. Narendra M. Dube, Anirudh Dube and Deepak H. Veeregowd, (2009), "Experimental technique to analyse the slurry erosion wear due to turbulence". Wear, vol. 267, pp. 259–263.

13. R. Keshavamurthy and B. Venkataraman, (2011), "Slurry erosive wear behaviour of thermally sprayed Inconel-718 coatings by APS process". Wear, vol.271, pp.1365– 1371.

14. A. K. Jha, R. Batham, M. Ahmed and A. K. Majumdar, (2011), "Effect of impinging angle and rotating speed on erosion behaviour of aluminium". Non ferrous Meto. Society china, vol. 21, pp. 32-38.

15. A.P. Harsha, (2011), "An investigation on low stress abrasive wear characteristics of high performance engineering thermoplastic polymers". Wear, vol. 271, pp.942-951.

16. VinayPratap Singh, AnjanSil and R. Jayaganthan, (2011), "A study on sliding and erosive wear behaviour of atmospheric plasma sprayed conventional and nanostructure alumina coatings". Materials and Design, vol. 32, pp. 584–591.

17. N. Krishnamurthy and M.S. Muralib, (2012) "Characterization and solid particle erosion behaviour of plasma sprayed alumina and calcia-stabilized zirconia coatings on Al-6061 substrate". Wear, vol. 274-275, pp.15-27.

18.ShujiangGeng, Shaojun Qi, Dong Xiang, Shenglong Zhu and Fuhui Wang , (2012),"Oxidation and electrical behaviour of ferritic stainless steel interconnect with Fe-Co-Ni coating by electroplating". Journal of Power Sources, vol.15725, pp. 40-50.

19. J.C. Caicedo, G. Cabrera, W. Aperador, H.H. Caicedo and A. Mejia, (2012), "Determination of the best behaviour among AISI D3 steel, 304 stainless steel and CrN/AlN coatings under erosive-corrosive effect". Vacuum, vol. 5770, pp. 1-23.

20. Hung-Kuk Oh, Kyu-Hyun Yeon and Hak Yun Kim, (1999), "The influence of atmospheric humidity on the friction and wear of carbon steels". Journal of Materials Processing Technology, vol. 95, pp. 10-16.

21. E. Fernandez , M. Cadenas, R. Gonzalez , C. Navas, R. Fernandez and J. de Damborenea, (2006), "Wear behaviour of laser clad NiCrBSi coating". Wear, vol.259, pp. 870–875.

22.M. Reza Bateni , J.A. Szpunar , X. Wang and D.Y. Li, (2006), "Wear and corrosion wear of medium carbon steel and 304 stainless steel". Wear, vol.260, pp. 116–122.

23. W. Grzesik, Z. Zalisz, S. Krol and P. Nieslony, (2006), "Investigations on friction and wear mechanisms of the PVD-TiAlN coated carbide in dry sliding against steels and cast iron". Wear, vol. 261, pp. 1191–1200.

24. Morteza Zandrahimi, M. Reza bateni, A. Poladi and Jerzy A. Szpunar, (2007), "The formation of martensite during wear of AISI 304 stainless steel". Wear, vol.263, pp. 674–678

25. MengHuaXichengWei and Jian Li, (2008), "Friction and wear behaviour of SUS 304 austenitic stainless steel against Al_2O_3 ceramic ball under relative high load". Wear, vol. 265, pp. 799–810.

26. SukruTaktak, SukruUlker and Ibrahim Gunes, (2008), "High temperature wear and friction properties of duplex surface treated bearing steels". Surface & Coatings Technology, vol. 202, pp. 3367–3377.

27. A. Cruzad., M. Hartelt, R. Wasche, M.A. Urchegui and X. Gomez, (2010), "Fretting wear of thin steel wires. Part 1: Influence of contact pressure". Wear, vol. 268, pp.1409–1416.

28. B. K. Prasad, S. Rathod, M. S. Yadav and O. P. Modi (2010), "The Influence of Lead Suspension in Oil Lubricant on the Sliding Wear Behaviour of Cast Iron". TribolLett, vol. 37, pp.289–299.

29. Manoj Masanta, S.M. Shariff and A. Roy Choudhury, (2011), "A comparative study of the tribological performances of laser clad TiB_2–TiC–Al_2O_3 composite coatings on AISI 1020 and AISI 304 substrates". Wear, vol.271, pp. 1124– 1133.

30. B.K. Prasad, (2011), "Sliding wear response of a grey cast iron: Effects of some experimental parameters". Tribology International, vol.44 pp. 660–667.

31. You Wang, Zhaoyi Pan, Zheng Wang, Xiaoguang Sun and Liang Wang,(2011), "Sliding wear behaviour of Cr–Mo–Cu alloy cast irons with and without nano-additives". Wear, vol. 271, pp. 2953– 2962.

33. J.J. Coronado, (2011), "Effect of load and carbide orientation on abrasive wear resistance of white cast iron". Wear, vol. 270, pp. 823–827.

34. G.M. Balamurugan, Muthukannan Duraiselvam and V. Anandakrishnan, (2012), "Comparison of high temperature wear behaviour of plasma sprayed WC–Co coated and hard chromium plated AISI 304 austenitic stainless steel". Materials and Design, vol. 35, pp.640–646.

35. M.X. Weib, S.Q. Wang and X.H. Cui, (2012), "Comparative research on wear characteristics of spheroidal graphite cast iron and carbon steel". Wear, vol. 274– 275, pp. 84– 93.

APPENDIX

Table 1.Variation of weight loss v/s time of steel 304 at 700rpm speed

Weight loss (gm) / Time (min.)	At 20% C_w by wt.		At 40% C_w by wt.		At 60% C_w by wt.	
	Bottom ash	Fly ash	Bottom ash	Fly ash	Bottom ash	Fly ash
60	0.0114	0.0069	0.0232	0.0099	0.0374	0.0176
90	0.0192	0.0083	0.0305	0.0117	0.0424	0.0209
150	0.0221	0.0131	0.0379	0.0153	0.0501	0.0231
120	0.0271	0.0154	0.0389	0.0194	0.0523	0.0271

Table 2.Variation of weight loss v/s time of steel 304 at 1000rpm speed

Weight loss (gm) / Time (min.)	At 20% C_w by wt.		At 40% C_w by wt.		At 60% C_w by wt.	
	Bottom ash	Fly ash	Bottom ash	Fly ash	Bottom ash	Fly ash
60	0.0201	0.0097	0.0557	0.0237	0.1162	0.0404
90	0.0331	0.0126	0.0608	0.0357	0.1451	0.0464
150	0.0475	0.0172	0.0852	0.0402	0.1558	0.0512
120	0.0577	0.0142	0.0992	0.0392	0.1992	0.0492

Table 3.Variation of weight loss v/s time of steel 304 at 1400rpm speed

Weight loss (gm) / Time (min.)	At 20% C_w by wt.		At 40% C_w by wt.		At 60% C_w by wt.	
	Bottom ash	Fly ash	Bottom ash	Fly ash	Bottom ash	Fly ash
60	0.0462	0.0204	0.0945	0.0255	0.1554	0.0465
90	0.0594	0.0264	0.1054	0.0386	0.1712	0.0571
150	0.0852	0.0294	0.1401	0.0492	0.2158	0.0631
120	0.0890	0.0373	0.1447	0.0522	0.2209	0.0721

Table 4.Variation of weight loss v/s time of coated and uncoated steel 304 at 700rpm speed

Weight loss (gm) / Time (min.)	At 20% C_w by wt. Bottom ash		At 40% C_w by wt. Bottom ash		At 60% C_w by wt. Bottom ash	
	Uncoated	Coated	Uncoated	Coated	Uncoated	Coated
60	0.0114	0.0084	0.0232	0.0132	0.0374	0.0274
90	0.0192	0.102	0.0305	0.0223	0.0424	0.0324
150	0.0221	0.0121	0.0379	0.293	0.0501	0.0401
120	0.0271	0.0171	0.0389	0.0312	0.0523	0.0423

Table 5.Variation of weight loss v/s time of coated and uncoated steel 304 at 1000rpm speed

Weight loss (gm) / Time (min.)	At 20% C_w by wt. Bottom ash		At 40% C_w by wt. Bottom ash		At 60% C_w by wt. Bottom ash	
	Uncoated	Coated	Uncoated	Coated	Uncoated	Coated
60	0.0201	0.0101	0.0357	0.0257	0.1162	0.0946
90	0.0301	0.0201	0.0608	0.0308	0.1451	0.1158
150	0.0475	0.0305	0.0852	0.0571	0.1558	0.1260
120	0.0577	0.0377	0.0992	0.0737	0.1992	0.1532

Table 6.Variation of weight loss v/s time of coated and uncoated steel 304 at 1400rpm speed

Weight loss (gm) / Time (min.)	At 20% C_w by wt. Bottom ash		At 40% C_w by wt. Bottom ash		At 60% C_w by wt. Bottom ash	
	Uncoated	Coated	Uncoated	Coated	Uncoated	Coated
60	0.0462	0.0323	0.0945	0.0756	0.1554	0.1280
90	0.0594	0.0412	0.1054	0.0845	0.1712	0.1430
150	0.0852	0.0672	0.1401	0.1134	0.2158	0.1876
120	0.0890	0.0701	0.1447	0.1250	0.2209	0.1932

Table 7.Variation of weight loss v/s time of Grey cast iron at 700rpm speed

Weight loss (gm) / Time (min.)	At 20% C_w by wt.		At 40% C_w by wt.		At 60% C_w by wt.	
	Bottom ash	Fly ash	Bottom ash	Fly ash	Bottom ash	Fly ash
60	0.0689	0.0187	0.0751	0.0277	0.0871	0.0318
90	0.0855	0.0267	0.0986	0.0303	0.1135	0.0391
150	0.0967	0.0322	0.1265	0.0363	0.1435	0.0432
120	0.1123	0.0407	0.1304	0.0465	0.1532	0.0499

Table 8.Variation of weight loss v/s time of Grey cast iron at 1000rpm speed

Weight loss (gm) / Time (min.)	At 20% C_w by wt.		At 40% C_w by wt.		At 60% C_w by wt.	
	Bottom ash	Fly ash	Bottom ash	Fly ash	Bottom ash	Fly ash
60	0.0775	0.0357	0.0897	0.0421	0.1034	0.0588
90	0.0983	0.0422	0.1065	0.0482	0.1265	0.0632
150	0.1165	0.0478	0.1238	0.0532	0.1421	0.0673
120	0.1197	0.0525	0.1478	0.0593	0.1554	0.0703

Table 9.Variation of weight loss v/s time of Grey cast iron at 1400rpm speed

Weight loss (gm) / Time (min.)	At 20% C_w by wt.		At 40% C_w by wt.		At 60% C_w by wt.	
	Bottom ash	Fly ash	Bottom ash	Fly ash	Bottom ash	Fly ash
60	0.1083	0.0498	0.1267	0.0587	0.1375	0.0656
90	0.1183	0.0536	0.1363	0.0658	0.1423	0.0699
150	0.1256	0.0586	0.1432	0.0684	0.1476	0.0726
120	0.1287	0.0637	0.1478	0.0737	0.1523	0.0774

Table 10.Variation of weight loss v/s time of coated and uncoated Grey cast iron at 700rpm speed

Weight loss (gm) / Time (min.)	At 20% C_w by wt. Bottom ash		At 40% C_w by wt. Bottom ash		At 60% C_w by wt. Bottom ash	
	Uncoated	Coated	Uncoated	Coated	Uncoated	Coated
60	0.0689	0.0037	0.0751	0.0067	0.0871	0.0103
90	0.0855	0.0087	0.0986	0.0107	0.1135	0.0176
150	0.0967	0.0122	0.1265	0.0136	0.1435	0.0218
120	0.1123	0.0156	0.1304	0.0175	0.1532	0.0258

Table 11.Variation of weight loss v/s time of coated and uncoated Grey cast iron at 1000 rpm speed

Weight loss (gm) / Time (min.)	At 20% C_w by wt. Bottom ash		At 40% C_w by wt. Bottom ash		At 60% C_w by wt. Bottom ash	
	Uncoated	Coated	Uncoated	Coated	Uncoated	Coated
60	0.0775	0.0087	0.0897	0.0107	0.1034	0.0187
90	0.0983	0.0102	0.1065	0.0147	0.1265	0.0259
150	0.1165	0.0145	0.1238	0.0197	0.1421	0.0306
120	0.1197	0.0198	0.1478	0.0242	0.1554	0.0345

Table 12.Variation of weight loss v/s time of coated and uncoated grey cast iron at 1400rpm speed

Weight loss (gm) / Time (min.)	At 20% C_w by wt. Bottom ash		At 40% C_w by wt. Bottom ash		At 60% C_w by wt. Bottom ash	
	Uncoated	Coated	Uncoated	Coated	Uncoated	Coated
60	0.1083	0.0257	0.1267	0.0375	0.1375	0.0452
90	0.1183	0.0363	0.1363	0.0456	0.1425	0.0568
150	0.1256	0.0428	0.1432	0.051	0.1476	0.0657
120	0.1287	0.0502	0.1478	0.0579	0.1532	0.0745

Table 13.Variation of weight loss v/s time of Grey cast iron at 200rpm speed

Weight loss (gm) / Time (min.)	At 2kg wt.	At 3kg wt.	At 4kg wt.	At 5kg wt.
15	0.0154	0.0056	0.0048	0.0069
20	0.0187	0.0074	0.0064	0.0085
25	0.0199	0.0091	0.0084	0.011
30	0.0209	0.0125	0.0104	0.0134

Table 14.Variation of weight loss v/s time of Grey cast iron at 400rpm speed

Weight loss (gm) / Time (min.)	At 2kg wt.	At 3kg wt.	At 4kg wt.	At 5kg wt.
15	0.033	0.0113	0.0157	0.0177
20	0.0379	0.0131	0.0155	0.0202
25	0.0399	0.0148	0.0169	0.0257
30	0.0404	0.0178	0.0195	0.0297

Table 15.Variation of weight loss v/s time of Grey cast iron at 600rpm speed

Weight loss (gm) / Time (min.)	At 2kg wt.	At 3kg wt.	At 4kg wt.	At 5kg wt.
15	0.0504	0.0674	0.0147	0.0153
20	0.0585	0.0789	0.0164	0.0215
25	0.0622	0.0818	0.0195	0.0299
30	0.0699	0.0852	0.0236	0.0353

Table 16.Variation of weight loss v/s time of Grey cast iron at 800rpm speed

Weight loss (gm) / Time (min.)	At 2kg wt.	At 3kg wt.	At 4kg wt.	At 5kg wt.
15	0.0583	0.02077	0.0314	0.0259
20	0.0655	0.0299	0.0391	0.0329
25	0.0799	0.0347	0.0432	0.0399
30	0.0899	0.0418	0.0478	0.0451

Table 17.Variation of weight loss v/s time of Steel 304 at 200rpm speed

Weight loss (gm) / Time (min.)	At 2kg wt.	At 3kg wt.	At 4kg wt.	At 5kg wt.
15	0.0078	0.0317	0.0118	0.0290
20	0.0248	0.0658	0.0188	0.0651
25	0.0812	0.1290	0.0809	0.1172
30	0.1376	0.1541	0.1866	0.1998

Table 18.Variation of weight loss v/s time of Steel 304 at 400rpm speed

Weight loss (gm) / Time (min.)	At 2kg wt.	At 3kg wt.	At 4kg wt.	At 5kg wt.
15	0.0116	0.2687	0.3624	0.5062
20	0.0833	0.3437	0.5012	0.6853
25	0.1635	0.4672	0.628	0.8063
30	0.3125	0.6672	0.774	0.4393

Table 19.Variation of weight loss v/s time of Steel 304 at 600rpm speed

Weight loss (gm) / Time (min.)	At 2kg wt.	At 3kg wt.	At 4kg wt.	At 5kg wt.
15	0.2834	0.4426	0.6039	0.9060
20	0.3886	0.5713	0.7592	1.2372
25	0.5187	0.7181	0.8992	1.4312
30	0.5925	0.8050	1.2398	1.7631

Table 20.Variation of weight loss v/s time of Steel 304 at 800rpm speed

Weight loss (gm) / Time (min.)	At 2kg wt.	At 3kg wt.	At 4kg wt.	At 5kg wt.
15	0.3511	0.5728	0.7010	0.8331
20	0.5021	0.7659	0.9156	1.5441
25	0.7721	0.9420	1.3655	1.955
30	0.9765	1.3054	1.7852	2.5471

Figure 1 Chemical composition of grey cast iron

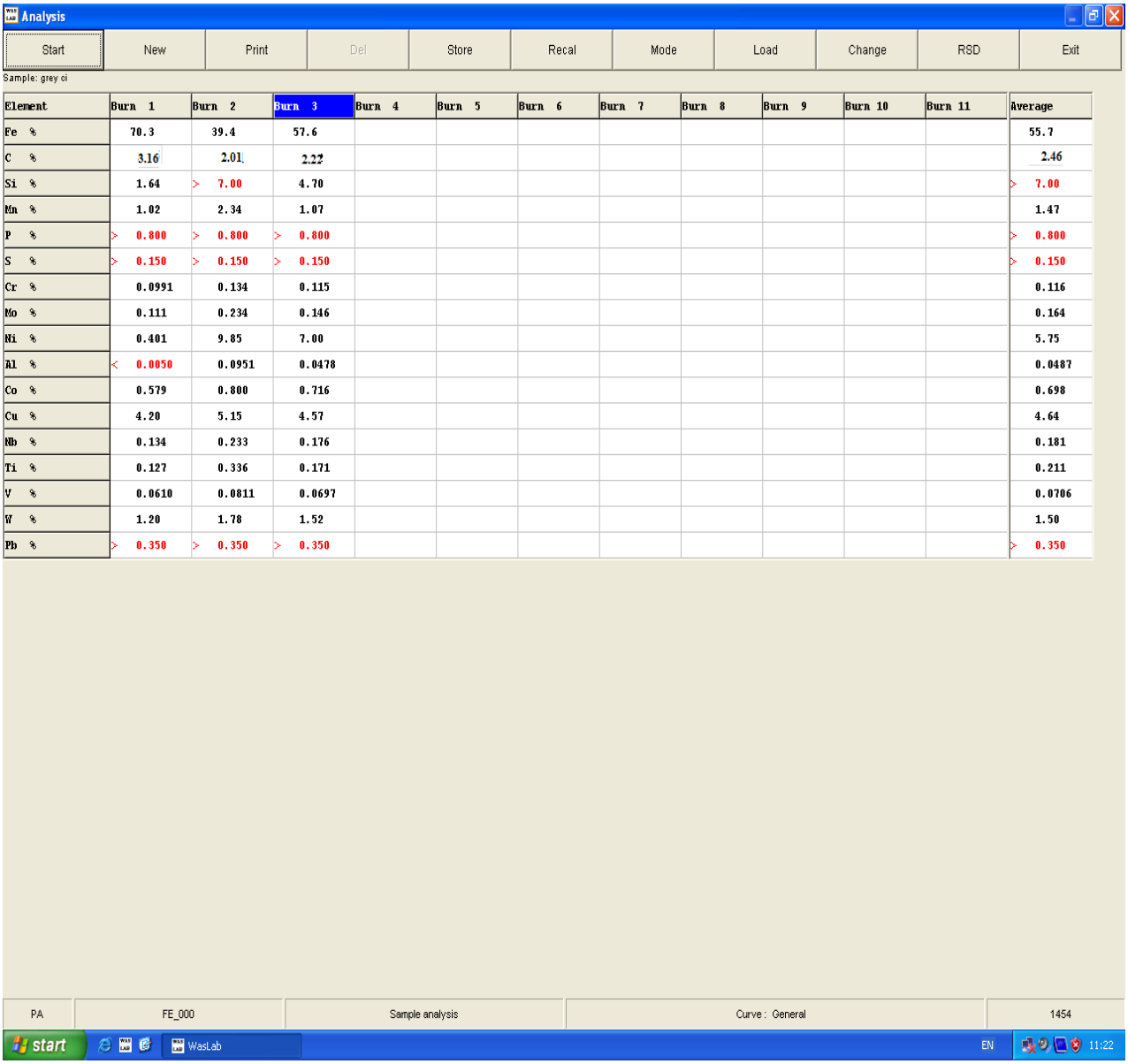

Element	Burn 1	Burn 2	Burn 3	Burn 4	Burn 5	Burn 6	Burn 7	Burn 8	Burn 9	Burn 10	Burn 11	Average
Fe %	70.3	39.4	57.6									55.7
C %	3.16	2.01	2.22									2.46
Si %	1.64	> 7.00	4.70									> 7.00
Mn %	1.02	2.34	1.07									1.47
P %	> 0.800	> 0.800	> 0.800									> 0.800
S %	> 0.150	> 0.150	> 0.150									> 0.150
Cr %	0.0991	0.134	0.115									0.116
Mo %	0.111	0.234	0.146									0.164
Ni %	0.401	9.85	7.00									5.75
Al %	< 0.0050	0.0951	0.0478									0.0487
Co %	0.579	0.800	0.716									0.698
Cu %	4.20	5.15	4.57									4.64
Nb %	0.134	0.233	0.176									0.181
Ti %	0.127	0.336	0.171									0.211
V %	0.0610	0.0811	0.0697									0.0706
W %	1.20	1.78	1.52									1.50
Pb %	> 0.350	> 0.350	> 0.350									> 0.350

Figure 2 Chemical composition of steel 304

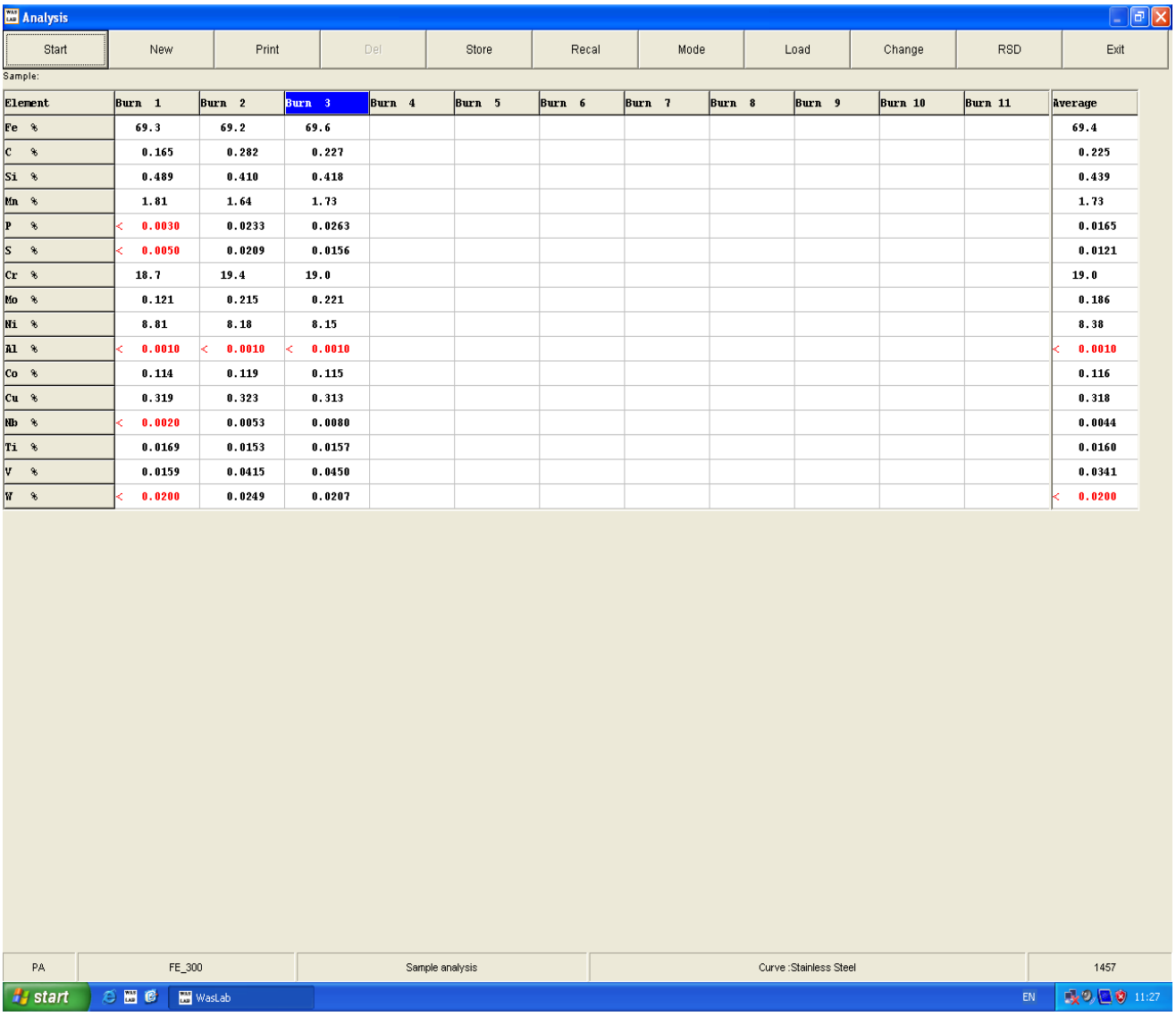

Element	Burn 1	Burn 2	Burn 3	Burn 4	Burn 5	Burn 6	Burn 7	Burn 8	Burn 9	Burn 10	Burn 11	Average
Fe %	69.3	69.2	69.6									69.4
C %	0.165	0.282	0.227									0.225
Si %	0.489	0.410	0.418									0.439
Mn %	1.81	1.64	1.73									1.73
P %	< 0.0030	0.0233	0.0263									0.0165
S %	< 0.0050	0.0209	0.0156									0.0121
Cr %	18.7	19.4	19.0									19.0
Mo %	0.121	0.215	0.221									0.186
Ni %	8.81	8.18	8.15									8.38
Al %	< 0.0010	< 0.0010	< 0.0010									< 0.0010
Co %	0.114	0.119	0.115									0.116
Cu %	0.319	0.323	0.313									0.318
Nb %	< 0.0020	0.0053	0.0080									0.0044
Ti %	0.0169	0.0153	0.0157									0.0160
V %	0.0159	0.0415	0.0450									0.0341
W %	< 0.0200	0.0249	0.0207									< 0.0200

REFERENCES

1. M. Panayotova, (2000), “Deposition of Fe–C alloy on structural steel and cast iron for repair of worn machine parts”. Surface and Coatings Technology, vol. 124, pp. 266–271.

2. Harry H. Tian and Graeme R. Addie, (2005), “Experimental study on erosive wear of some metallic materials using Coriolis wear testing approach”, Wear, vol.258, pp. 458–469.

3. LI Xiao-yan, and LU Tao, (2005), “Analysis of corrosion behaviour of petrochemical pipe elbow”. Journal of central south university technology, vol.12, pp. 119-123.

4. Shimizu, T. Naruse, Y. Xinb and K. Kimura, (2006), “Erosive wear properties of high V–Cr–Ni stainless spheroidal carbides cast iron at high temperature”. Wear, vol.267, pp. 104–109.

5. T. Manisekaran, M. Kamaraj, S.M. Sharrif and S.V. Joshi, (2006), “Slurry Erosion Studies on Surface Modified 13Cr-4Ni Steels”. Effect of Angle of Impingement and Particle Size ASM International, vol. 35, pp. 1059-9495.

6. B.S. Mann, VivekArya, A.K. Maiti and M.U.B. Rao, (2006), “Corrosion and erosion performance of HVOF/TiAlN PVD coatings and candidate materials for high pressure gate valve application”. Wear, vol. 260, pp. 75-82.

7. K. Yıldızlı, M.B. Karamıs and F. Nair, (2006), “Erosion mechanisms of nodular and gray cast irons at different impact angles”. Wear, Vol. 261, pp. 622–633.

8. Harpreet Singh, Buta Singh Sidhu and D.Puri, (2007), “Wear and oxidation behaviour of shrouded plasma sprayed fly ash coatings” .Tribology International, vol.40, pp.800–808.

9. Girish R. Desale, Bhupendra K. Gandhi and S.C. Jain, (2008), “Slurry erosion of ductile materials under normal impact condition”. Wear, vol.264, pp.322–330.

10. M.N. Noui-Mehidi , L.J.W. Graham, J. Wu, B.V. Nguyen and S. Smith,(2008), “Study of erosion behaviour of paint layers for multilayer paint technique applications in slurry erosion”, Wear, vol. 264, pp. 737–743.

11. S.C.Mishra, S.Praharaj and AlokSatpathy, (2009), “Evaluation of erosion wear of a ceramic coating with Taguchi approach”. Manufacturing Engineering, vol.4, pp.234-244.

12. Narendra M. Dube, Anirudh Dube and Deepak H. Veeregowd, (2009), “Experimental technique to analyse the slurry erosion wear due to turbulence”. Wear, vol. 267, pp. 259–263.

13. R. Keshavamurthy and B. Venkataraman, (2011), “Slurry erosive wear behaviour of thermally sprayed Inconel-718 coatings by APS process”. Wear, vol.271, pp.1365– 1371.

14. A. K. Jha, R. Batham, M. Ahmed and A. K. Majumdar, (2011), “Effect of impinging angle and rotating speed on erosion behaviour of aluminium”. Non ferrous Meto. Society china, vol. 21, pp. 32-38.

15. A.P. Harsha, (2011), “An investigation on low stress abrasive wear characteristics of high performance engineering thermoplastic polymers”. Wear, vol. 271, pp.942-951.

16. VinayPratap Singh, AnjanSil and R. Jayaganthan, (2011), “A study on sliding and erosive wear behaviour of atmospheric plasma sprayed conventional and nanostructure alumina coatings”. Materials and Design, vol. 32, pp. 584–591.

17. N. Krishnamurthy and M.S. Muralib, (2012) “Characterization and solid particle erosion behaviour of plasma sprayed alumina and calcia-stabilized zirconia coatings on Al-6061 substrate”. Wear, vol. 274-275, pp.15-27.

18.ShujiangGeng, Shaojun Qi, Dong Xiang, Shenglong Zhu and Fuhui Wang , (2012),”Oxidation and electrical behaviour of ferritic stainless steel interconnect with Fe-Co-Ni coating by electroplating”. Journal of Power Sources, vol.15725, pp. 40-50.

19. J.C. Caicedo, G. Cabrera, W. Aperador, H.H. Caicedo and A. Mejia, (2012), “Determination of the best behaviour among AISI D3 steel, 304 stainless steel and CrN/AlN coatings under erosive-corrosive effect”. Vacuum, vol. 5770, pp. 1-23.

20. Hung-Kuk Oh, Kyu-Hyun Yeon and Hak Yun Kim, (1999), “The influence of atmospheric humidity on the friction and wear of carbon steels”. Journal of Materials Processing Technology, vol. 95, pp. 10-16.

21. E. Fernandez , M. Cadenas, R. Gonzalez , C. Navas, R. Fernandez and J. de Damborenea, (2006), “Wear behaviour of laser clad NiCrBSi coating”. Wear, vol.259, pp. 870–875.

22.M. Reza Bateni , J.A. Szpunar , X. Wang and D.Y. Li, (2006), “Wear and corrosion wear of medium carbon steel and 304 stainless steel”. Wear, vol.260, pp. 116–122.

23. W. Grzesik, Z. Zalisz, S. Krol and P. Nieslony, (2006), “Investigations on friction and wear mechanisms of the PVD-TiAlN coated carbide in dry sliding against steels and cast iron”. Wear, vol. 261, pp. 1191–1200.

24. MortezaZandrahimi, M. Reza bateni, A. Poladi and Jerzy A. Szpunar, (2007), “The formation of martensite during wear of AISI 304 stainless steel”. Wear, vol.263, pp. 674–678

25. MengHuaXichengWei and Jian Li, (2008), “Friction and wear behaviour of SUS 304 austenitic stainless steel against Al2O3 ceramic ball under relative high load”. Wear, vol. 265, pp. 799–810.

26. SukruTaktak, SukruUlker and Ibrahim Gunes, (2008), “High temperature wear and friction properties of duplex surface treated bearing steels”. Surface & Coatings Technology, vol. 202, pp. 3367–3377.

27. A. Cruzad., M. Hartelt, R. Wasche, M.A. Urchegu and X. Gomez, (2010), “Fretting wear of thin steel wires. Part 1: Influence of contact pressure”. Wear, vol. 268, pp.1409–1416.

28. B. K. Prasad, S. Rathod, M. S. Yadav and O. P. Modi (2010), “The Influence of Lead Suspension in Oil Lubricant on the Sliding Wear Behaviour of Cast Iron”. TribolLett, vol. 37, pp.289–299.

29. Manoj Masanta, S.M. Sharif and A. Roy Choudhury, (2011), “A comparative study of the tribological performances of laser clad TiB_2–TiC–Al_2O_3 composite coatings on AISI 1020 and AISI 304 substrates”. Wear, vol.271, pp. 1124– 1133.

30. B.K. Prasad, (2011), “Sliding wear response of a grey cast iron: Effects of some experimental parameters”. Tribology International, vol.44 pp. 660–667.

31. You Wang, Zhaoyi Pan, Zheng Wang, Xiaoguang Sun and Liang Wang,(2011), “Sliding wear behaviour of Cr–Mo–Cu alloy cast irons with and without nano-additives”. Wear, vol. 271, pp. 2953– 2962.

33. J.J. Coronado, (2011), “Effect of load and carbide orientation on abrasive wear resistance of white cast iron”. Wear, vol. 270, pp. 823–827.

34. G.M. Balamurugan, Muthukannan Duraiselva and V. Anandakrishnan,(2012), “Comparison of high temperature wear behaviour of plasma sprayed WC–Co coated and hard chromium plated AISI 304 austenitic stainless steel”. Materials and Design, vol. 35, pp.640–646.

35.M.X. Weib, S.Q. Wang and X.H. Cuib, (2012), “Comparative research on wear characteristics of spheroidal graphite cast iron and carbon steel”. Wear, vol. 274– 275, pp. 84– 93.